HOLOCENE PALEOENVIRONMENTAL RECONSTRUCTION OF DEPOSITIONAL ENVIRONMENTS ON THE SUNDA SHELF, SOUTHWEST SOUTH CHINA SEA, USING A MULTIDISCIPLINARY APPROACH

By

Michael R. Twarog

August 2018

Directors of Thesis: Dr. Eduardo Leorri and Dr. Stephen Culver
Major Department: Geological Sciences

Abstract

The last glacial maximum, ca. 21,000 years ago, caused a fall in eustatic sea level of ca. 120 m below present. The low-gradient, shallow Sunda Shelf, Southeast Asia was subaerially exposed during this sea-level lowstand and experienced rising sea level thereafter. Sea level rose to a +1.3–5 m highstand ca. 6,500 cal yr BP, and then fell to modern sea level. The objective of this research is to characterize environmental change on the Sunda Shelf in response to the post-glacial rising eustatic sea level. To address this objective, six gravity cores were collected along a transect crossing the paleo-Chao Phraya incised river valley complex between peninsular Malaysia and southern Vietnam. Thirteen AMS radiocarbon samples, 130 bulk sediment magnetic susceptibility samples (BMS), 66 X-ray fluorescence spectrometry (XRF) samples, and 54 samples for the analysis of foraminiferal assemblages were used to characterize change in the depositional environments of the cored sediments.

BMS, XRF, and foraminiferal analysis distinguish two main units. Unit 1 is found in the lower part of the cores and typically contains more terrestrial material than sediments further up-core as shown by higher BMS values, higher % Ti, % Al, % Fe, and lower indicators of marine influence, for example, lower % Ca, % planktonic foraminifera, and percentages of deeper water

benthic foraminifera such as *Heterolepa dutemplei*. Unit 2 is characterized by a significant increase in % Ca, % *Heterolepa dutemplei* and % planktonic foraminifera ca. 6,500 cal yr BP.

Unit 1 is consistent with shallower water depths and is part of a transgressive systems tract (TST, ca. 1 m thick) that terminates ca. 6,500 cal yr BP. Unit 2 represents the overlying highstand systems tract (HST, ca. 1 m thick) and is characterized by an increase in % planktonics, % Ca, and shifts in benthic foraminiferal assemblages, indicating deeper water conditions than the sediments below. This shift from a TST to a HST ca. 6500 cal yr BP is consistent with the Sunda Shelf sea-level record.

HOLOCENE PALEOENVIRONMENTAL RECONSTRUCTION OF DEPOSITIONAL ENVIRONMENTS ON THE SUNDA SHELF, SOUTHWEST SOUTH CHINA SEA, USING A MULTIDISCIPLINARY APPROACH

A Thesis

Presented to the faculty of the Department of Geological Sciences

East Carolina University

In Partial Fulfillment of the Requirement for the Degree

Master of Science in Geology

by

Michael R. Twarog

HOLOCENE PALEOENVIRONMENTAL RECONSTRUCTION OF DEPOSITIONAL ENVIRONMENTS ON THE SUNDA SHELF, SOUTHWEST SOUTH CHINA SEA, USING A MULTIDISCIPLINARY APPROACH

By

Michael R. Twarog

APPROVED BY:

CO-DIRECTOR OF THESIS: _____
Eduardo Leorri, PhD

CO-DIRECTOR OF THESIS: _____
Stephen Culver, PhD, DSc

COMMITTEE MEMBER: _____
David Mallinson, PhD

COMMITTEE MEMBER: _____
Peter Parham, PhD

CHAIR OF THE DEPARTMENT OF
GEOLOGICAL SCIENCES: _____
Stephen Culver, PhD, DSc

DEAN OF THE
GRADUATE SCHOOL: _____
Paul J. Gemperline, PhD

ACKNOWLEDGEMENTS

I would like to thank my advisors, Dr. Steve Culver and Dr. Edu Leorri for their constant support, patience and guidance throughout this entire project. I would also like to thank Dr. Dave Mallinson, Dr. Peter Parham, and Dr. Eric Horsman for all their support and input. Without these four people I would have certainly been lost.

I would like to thank John Woods, Jim Watson, Kim West, Dare Merritt, and the rest of the faculty and staff in the Department of Geological Sciences for all their kindness and support during my time here. A huge thank you goes to the crew of the *RV Discovery*, to the students at UMT for lab support, and to all of those in the Malaysia lab group: Haley Hindes, Devon Reed, C.J. Whitley, Sam Martin, Emily Harrison, and Bailey Donovan. A special thank you to Nina Shmorhun.

I thank Dr. David Menier for sharing the results of his geophysical surveys off Kuala Terengganu. I would like to acknowledge the funding from National Science Foundation Grant OISE-1157222 to Dr. Stephen Culver, without which this project would have not been possible.

Finally, I would also like to thank family and especially my parents. They have never once let me down and I could never have hoped to complete this impossible task without their love and unyielding support.

Table of Contents

List of Tables

List of Figures

List of Appendices

Introduction

The shallow-gradient Sunda Shelf (Fig. 1) is one of the most extensive continental shelves in the world, however, characterization of late Quaternary sediments on the shelf is limited to a transect of cores collected along the paleo-North Sunda River incised valley (Hanebuth et al., 2000, 2011; Hanebuth and Stattegger, 2003). This study seeks to further extend the understanding of late Quaternary stratigraphic architecture and evolution of the Sunda Shelf using sediment cores taken across the paleo-Chao Phraya River incised valley (north of the paleo-North Sunda River incised valley) and along the trends of the paleo-Marang and paleo-Terengganu river incised valleys, two of the tributaries to the paleo-Chao Phraya. Characterization of the Quaternary sediment veneer on the Sunda Shelf provides insight into the environmental response, and resultant stratigraphic record, to late Pleistocene and Holocene rising sea level and hydro-isostasy.

The Sunda shelf and southwestern South China Sea (SCS) are located north of the equator, south of Indochina and to the west of the deep SCS basin (Fig. 1). During the last glacial maximum (LGM), ca. 21 ka (Fairbanks et al., 1989; Hanebuth et al., 2011), the Sunda Shelf was subaerially exposed as a result of a sea-level lowstand (ca. 120 m below present sea level) (Figs. 1A, 2) (Fairbanks et al., 1989; Hanebuth et al., 2009). Rivers drained across and incised the subaerially exposed shelf, eventually feeding into the semi-enclosed SCS (Hanebuth et al., 2000). Sea level rose after the LGM, and the incised river valleys provided greater accommodation space than the adjacent shelf for post-LGM sediment accumulation. Alqahtani et al. (2015) posited the existence of a ca. 16-meter-thick Holocene sediment record within the incised valley of the paleo-Chao Phraya River. Seismic data suggest that this incised valley

trended southeast across the Gulf of Thailand before turning to the northeast, off Kuala Terengganu, Malaysia (Alqahtani et al., 2015) (Figs. 1A, B).

The purpose of this research is to investigate whether the thick Holocene sediment record (Fig. 1C) within the main trunk of the incised valley of the paleo-Chao Phraya River (Fig. 1B) exists and, if so, to characterize the sediments within. Gravity cores collected along the trends of the paleo-Terengganu and paleo-Marang incised river valleys (tributaries to the paleo-Chao Phraya River) indicate Holocene sediment records on the order of 1–2 m thickness (Hindes, 2016; Reed, 2016; Harrison, 2017; Donovan, 2017) (Fig 1B). Hanebuth et al. (2011) summarized the Holocene veneer of seafloor sediments on the open Sunda Shelf as typically carbonate mud less than 1 m thick, but with several meters in channels.

The objectives of this research are: (1) to characterize the post-LGM cored sediments collected in this study and interpret paleodepositional conditions within the channel of the paleo-Chao Phraya River; (2) to document down-core benthic foraminiferal assemblages and compare them to modern, surficial benthic foraminiferal assemblages on the Sunda Shelf; (3) to compare the post-LGM sediments and foraminiferal assemblages of this study (from the paleo-Chao Phraya River incised valley) to those in cores collected along the trend of the incised paleo-Terengganu River and paleo-Marang River incised valleys; and (4) to provide a summary sequence stratigraphic interpretation of the post-LGM infill of the paleo-Chao Phraya River and its tributaries using sedimentologic and foraminiferal data.

To address these objectives, six gravity cores were collected in May 2016 to complement the nine cores collected along the trends of the incised paleo-Terengganu River and paleo-Marang River incised valleys. Five of the cores were collected within the boundaries of the main trunk of the paleo-Chao Phraya River incised valley, and one was collected to the west,

immediately outside of the incised valley (Fig. 1B). Several analytical approaches were used. Bulk sediment magnetic susceptibility and X-ray fluorescence spectrometry of 19 elements (both major and minor) were used to characterize the source of the cored sediments (e.g., terrestrial or marine). Benthic foraminiferal assemblages were documented in all six cores and compared to surficial (modern) benthic assemblages documented by Szarek et al. (2006), Minhat et al. (2016), Suriadi (2017) and Martin et al. (2018) and down-core benthic assemblages documented by Harrison (2017) and Donovan (2017) (Fig. 1B). The geochronological framework of the gravity cores was determined using AMS radiocarbon dating methods.

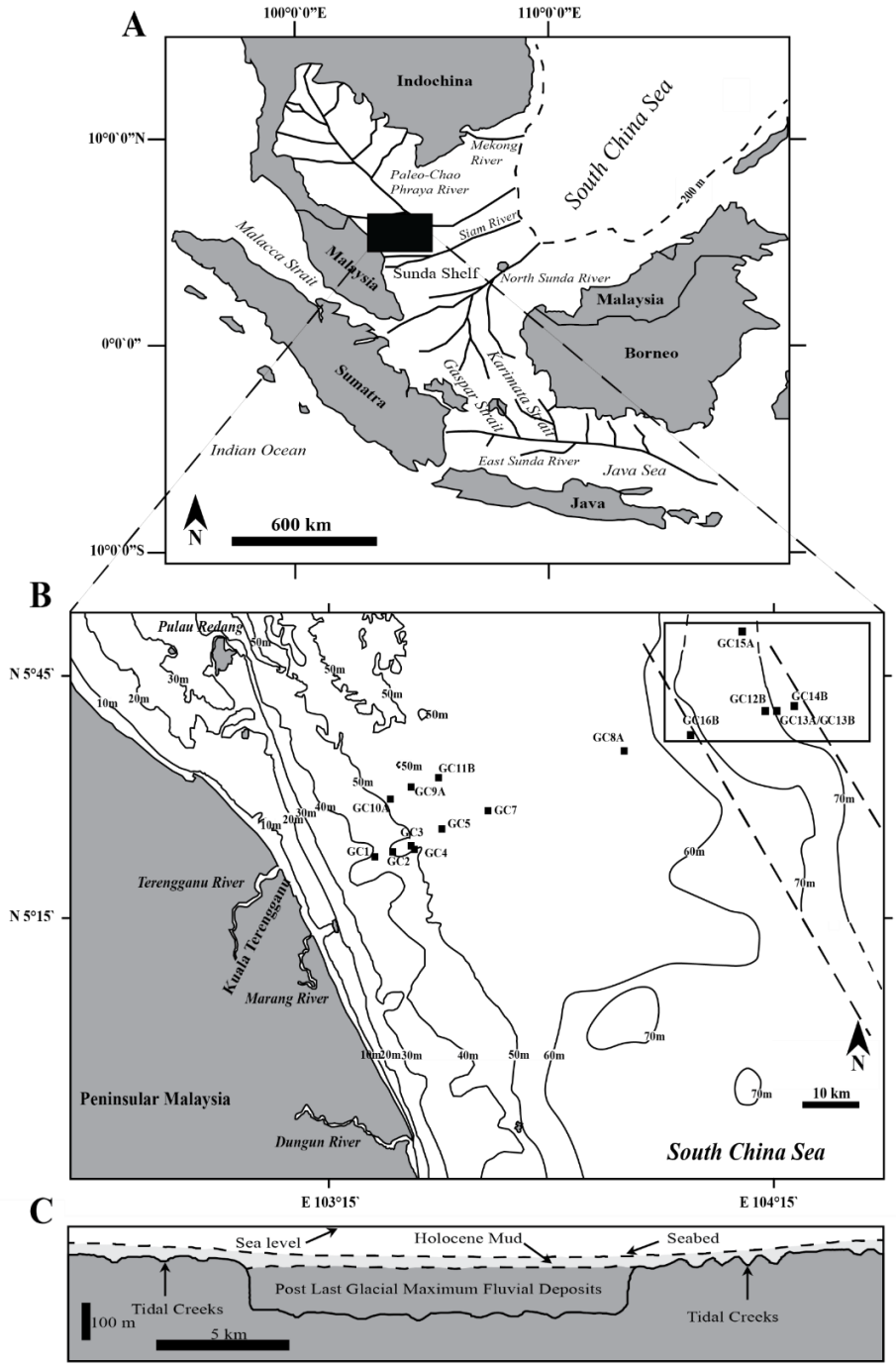

Figure 1: A: Location of the study area (black rectangle) on the Sunda Shelf, southern SCS. The edge of the SCS continental shelf is indicated by dashed line. **B**: Bathymetric map of the shelf off Kuala Terengganu showing locations of cores studied by Hindes (2016) (GC5, 7), Reed (2016) (GC1, 2, 3, 4), Harrison (2017) (GC9A, 10A) and Donovan (2017) (GC8A, 11B) along trends of the paleo-Terengganu and paleo-Marang River systems (tributaries of the paleo-Chao Phraya River). The rectangle outlines the suite of gravity cores used in this study. The dashed lines indicate the boundaries of the paleo-Chao Phraya River incised valley (from Alqahtani et al., 2015). **C**: Cross-sectional depositional model of the paleo-Chao Phraya River incised valley (modified from Alqahtani et al., 2015). Vertical scale is approximated. Holocene sediment was interpreted to be ca. 16 m thick within the paleo-valley (Alqahtani et al., 2015).

Background

Geologic setting

At ca. 125,000 km^2, the Sunda Shelf is one of the largest epicontinental shelves in the world (Hanebuth et al., 2000; Alqahtani et al., 2015). This shallow-gradient shelf (1:9000) has an average water depth of 70 to 80 m, and is connected to the Java Sea to the south through the Karimata Strait and Gaspar Strait, and to the Indian Ocean through the Malacca Strait. It is open to the deep SCS basin to the northeast (Pelejero at al., 1999; Woodson et al., 2017) (Fig. 1A, B). When sea level fell during the last glacial maximum (ca. 21 ka Hanebuth et al., 2011) (Fig. 2) the shelf was subaerially exposed and dissected by the paleo-river systems of the Mekong, Siam, North Sunda, East Sunda, and the Chao Phraya (Fig. 1A). The main trunk of the incised paleo-Chao Phraya River drained across the Gulf of Thailand and into the SCS, southeast of Indochina (Molengraaff, 1921; Molengraaff and Weber, 1921; Dickerson, 1941; Alqahtani et al., 2015). The incised valleys of the paleo-Terengganu and paleo-Marang rivers (Hindes, 2016; Reed, 2016; Harrison, 2017; Donovan, 2017) drained east-northeast across the Sunda Shelf off the coast of Kuala Terengganu, into the paleo-Chao Phraya River (Fig. 1B).

The near-surface Quaternary stratigraphy of the Sunda Shelf has been divided into three units: a Pleistocene regressive/lowstand unit, a late Pleistocene transgressive unit, and a surficial Holocene unit (Emmel and Curray, 1982; Evans et al., 1982; Hanebuth and Stattegger, 2003). These units accumulated in response to three major drivers: a change in sea level that prompted a response in sediment deposition; the extent and topography of the Sunda Shelf (i.e., the low relief of the shelf and development of channel structures as a result of fluvial incision); and terrestrial sediment supply (Hanebuth and Stattegger, 2003).

The regressive/lowstand unit was formed between 50 ka (or older) and 23 ka (Hanebuth and Stattegger, 2003). This unit formed as a result of a sea-level fall and the subsequent LGM sea-level lowstand, during large-scale exposure and fluvial incision on the shelf (Hanebuth and Stattegger, 2003; Figs. 1A, 2A). This unit was determined to be at least 40 m thick on average and is composed of marine regressive deposits overlain by terrestrial facies (Hanebuth and Stattegger, 2003). Similar regressive deposits were described by Emmel and Curray (1982) in deltas near the Malacca Strait where they are characterized by prograding delta foresets.

The transgressive unit encompasses a progression of terrestrial to coastal to marine deposits that increase in thickness with present water depth. Age estimates from this unit range from 20.5–13 ka, therefore, it formed during post-LGM sea-level rise (Hanebuth and Stattegger, 2003; Fig 2A). Evans et al. (1995) defined a similar unit that largely consists of channel-fill, resulting from flooding of incised valleys off southwest peninsular Malaysia. The base of this unit represents a subaerial to submarine disconformity (Hanebuth and Stattegger, 2003).

The surficial Holocene unit on the Sunda Shelf is generally <1 m thick and is subject to reworking. This unit, with age estimates ranging from 10–4 ka, is composed of foraminiferal-rich muds (Hanebuth and Stattegger, 2003). A discontinuity separates this unit from the underlying transgressive unit. Similar Holocene units have been described as thin sediment veneers underlain by discontinuities (e.g., Emmel and Curray, 1982 and Evans et al., 1995).

Past and Modern Environmental Setting

The last glacial maximum (LGM), ca. 21 ka, exhibited a ca. 120 m fall in sea level in the Sunda Shelf region (Fig. 2A) (Fairbanks et al., 1989; Hanebuth et al., 2009). After the LGM, sea level rose at variable rates, due to the addition of glacial meltwater into the world's oceans, until ca. 7,000 to 6,500 cal yr BP when the rate of sea-level rise slowed and the region experienced a

mid-Holocene relative sea-level (RSL) highstand of as much as 5 m above present mean sea level (Geyh et al., 1979; Hanebuth et al., 2011; Fig. 2 A, B), although other researchers have suggested a highstand on the order of +1.3 to +3 m (Hesp et al., 1998; Bird et al., 2007; Mallinson et al., 2014; Parham et al., 2014). For the purposes of this study, a midrange value of +3 m is used. After the mid-Holocene highstand, RSL fell with several possible stillstands in the later Holocene (<5,000 cal yr BP; Mallinson et al., 2014; Bradley et al., 2016). Horton et al. (2005) suggested a RSL fall from 4,000 to 2,000 cal yr BP, likely as a result of hydro-isostatic adjustments. Mallinson et al. (2014) reported similar findings with a RSL fall or still-stand interpreted from ca. 3,000 to 1,900 cal yr BP. After 1,900 cal yr BP, RSL possibly underwent minor oscillations (Mallinson et al., 2014). Yu and Chen (2009) also reported late Holocene oscillations and indicated that RSL was ca. 1.2 meters higher than present at 1,200 cal yr BP. Approximately 300 cal yr BP, RSL began to rise forming the modern, transgressive system (Hanebuth et al., 2011; Culver et al., 2015; Bradley et al., 2016).

In the study area and surrounding regions, annual RSL variations are a response to seasonal changes in the East Asian Monsoon (Luu et al., 2015). Sea-level anomalies on decadal scales are likely driven by El Niño-Southern Oscillation (ENSO) variations (Luu et al., 2015). ENSO is a phenomenon in which atmospheric pressure over the Pacific decreases in association with warming over the equatorial Pacific Ocean and an easterly shift of atmospheric advection (Brijker et al., 2007). ENSO events affect the East Asian Monsoon and result in droughts in the Malay Peninsula and nearby areas (Brijker et al., 2007). ENSO's counterpart, La Niña, conversely results in high precipitation in the Malay region (Brijker et al., 2007). Millennial sea-level variation is primarily driven by the advance and retreat of glacial ice, associated climatic conditions and vertical land movements (Clark et al., 1978; Bradley et al., 2016).

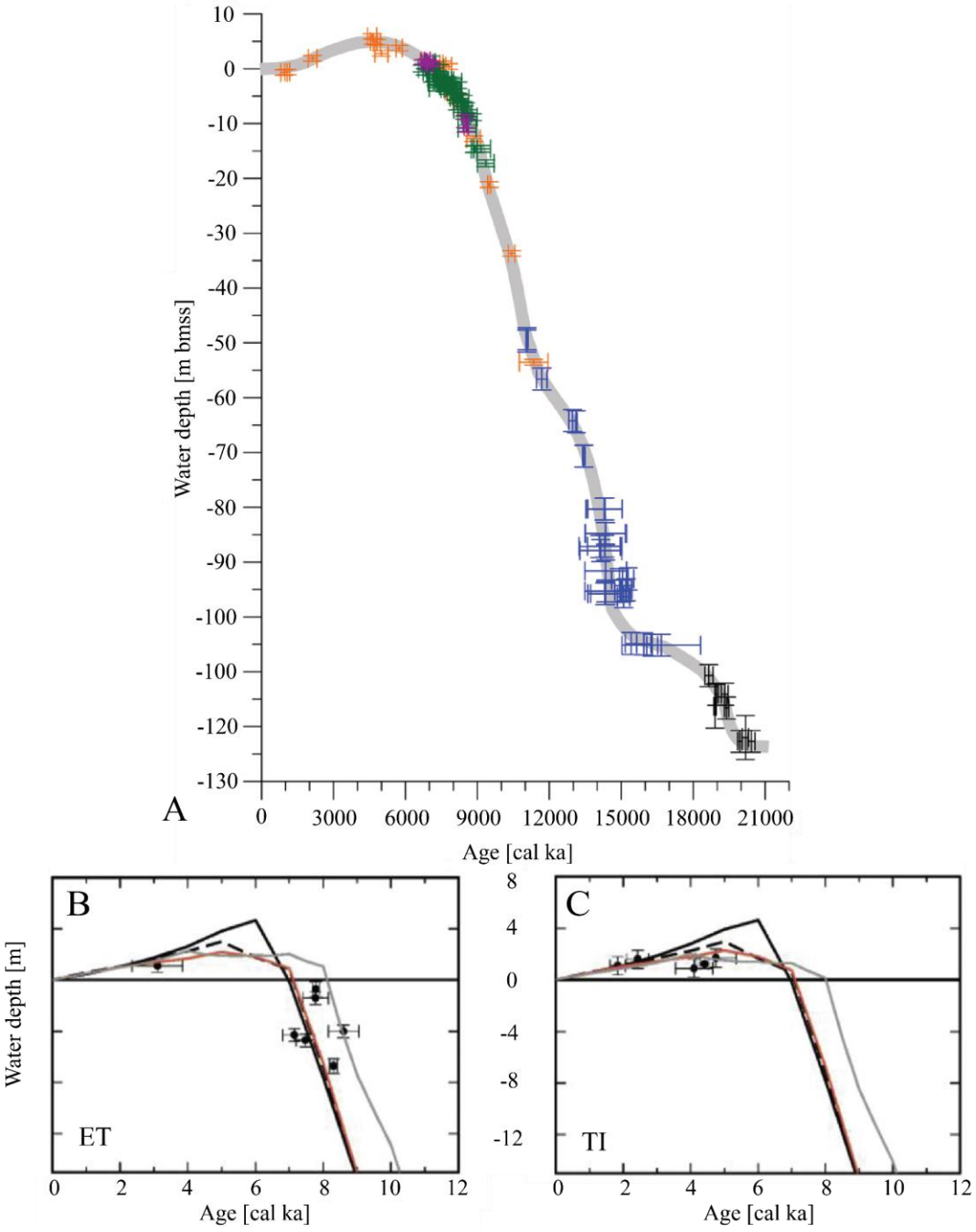

Figure 2: A: Sea-level curve for the Sunda Shelf, modified from Hanebuth et al. (2011). Data for this curve were collected from Geyh et al. (1979), Hesp et al. (1998), Hanebuth et al. (2000), Bird et al. (2007), and Hanebuth et al. (2009). **B & C**: modeled ice-volume equivalent sea level curves for the Malay Peninsula from Bradley et al. (2016). The several lines represent adjustments for various lithosphere thickness and upper mantle viscosity parameters. ET indicates the eastern coast of Thailand and TI indicates Tiomin Island, near southeastern peninsular Malaysia.

Several oceanic currents are featured in the southern SCS off the eastern coastline of peninsular Malaysia. The southern SCS (Fig. 1A) contains a complex current structure (both at the surface and in the subsurface) that is both seasonally and annually variable (Fig. 3) (Fang et al., 2012; Ke et al., 2014). Geostrophic currents, formed by pressure gradient forces and the Coriolis effect, are common in the SCS and can attain velocities of 50–110 cm/s (Fang et al., 1998; Liu et al., 2004). The wind-driven SCS southwestern coastal boundary current is strongest in winter and flows from off the eastern coast of Indochina, into the SCS off the coast of peninsular Malaysia, and ultimately into the Java Sea (Fig 1A). This current undergoes a seasonal reversal, flowing southwest in the winter (ca. January; Fig. 3A) and northeast in the summer (ca. July; Fig. 3B), when the current is weaker (Fang et al., 2012).

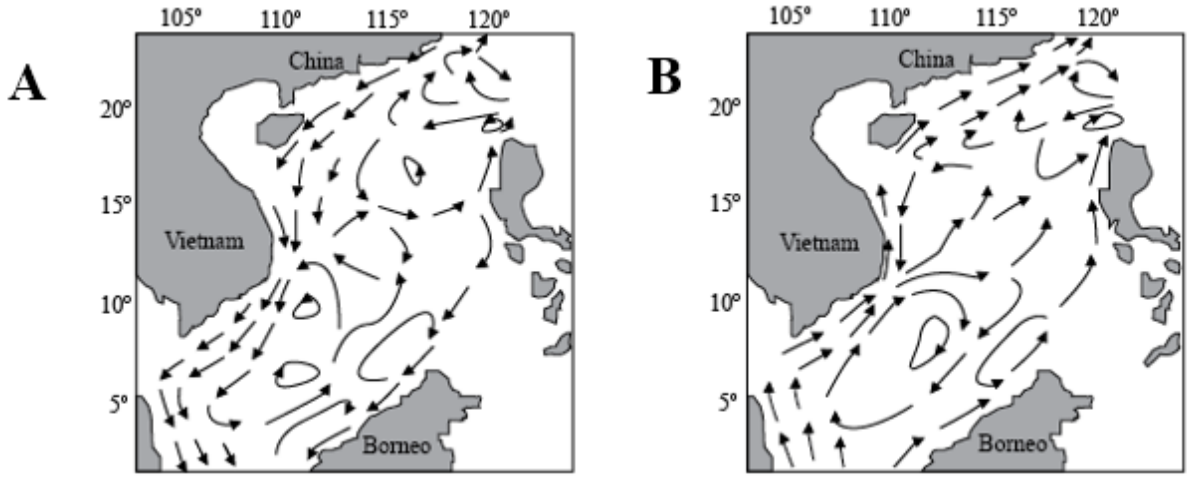

Figure 3: A, winter and **B**, summer flow of the SCS southwestern coastal boundary current (off the eastern coasts of peninsular Malaysia and Vietnam) (from Fang et al., 1998, 2012) showing seasonal reversal.

Foraminifera of the Sunda Shelf

The distribution of foraminifera on the Sunda Shelf is predominantly related to environmental variables that are dependent on water depth and distance from shore (e.g., primary productivity, grain size distribution, calcium carbonate content, salinity and total organic carbon; Szarek et al., 2006, Minhat et al., 2016, and Martin et al., 2018). Several depth zones have been defined on the basis of foraminiferal assemblages (Table 1). The 0–20 m depth interval is characterized by sandy sediments and by *Amphistegina* spp., with several abundant subsidiary taxa (CGT2) off Kuala Terengganu (Fig. 4; Table 1; Martin et al., 2018). In contrast, the waters less than 20 m in depth are characterized by *Elphidium, Pararotalia*, and *Ammonia* off the southern tip of peninsular Malaysia (Fig 4; Table 1; Minhat et al., 2016). Martin et al. (2018) recognized three zones from 20–60 m water depth, the two shallower zones (CGT2 and CGT3) are characterized by sandy sediment and strongly dominated by larger benthic foraminifera (Table 1). From ca. 40–60 m water depth, sediments are increasingly muddy and the assemblage (CGT4) is dominated by *Heterolepa dutemplei* and *Asterorotalia milletti* (Fig 4; Table 1; Martin et al., 2018). In contrast, the assemblage from >20 m water depth, recorded by Minhat et al. (2016), was characterized by agglutinated taxa (e.g., *Bigenerina nodosaria*) in muddy sand substrates (Table 1). Off Sabah, Borneo (Fig. 4), Biswas (1976) documented abundant larger foraminifera from 20–60 m water depth, similar to

Table 1: Foraminiferal assemblages on the Sunda Shelf.

Zonation (water depth)	Biswas (1976) (>63μ)	Szarek et al. (2006) (>150μ)	Martin et al. (2018) (>150μ)	Minhat et al. (2016) (>63μ)
0 to 20 m	• No Planktonics • Benthic species richness 33 • *Quinqueloculina semistriata* • *Elpidium cripsum* • *Ammonia beccarii* • *Calcarina hispida*		**8 to 14 m water depth (CGT1)** • Total number of taxa 49 • *Amphistegina radiata (10%)* • *Amphistegina lessonii (7%)* • *Planorbulina acervalis (6%)* • *Sahulia conica (6%)* • *Millettiana millettii (5%)*	**<20m water depth** • *Elphidium* species • *Pararotalia nipponica* • *Pararotalia* sp. 1 • *Ammonia tepida*
20 to 60 m	• Benthic species richness increases from ca. 50 to ca. 78 • Planktonic foraminifera 5 to 10% • *Quinqueloculina seminulum* • *Pseudorotalia schroeterianus* • *Cellanthus craticulatus* • *Amphistegina lessonii* • *Operculina ammonoides* • *Operculina venosa*		**21 to 22 m water depth (CGT2)** • Total number of taxa 33 • *Amphistegina lessonii* (54%) • *Amphistegina radiata* (31%) • *Cellanthus craticulatus* (8%) **32 to 41 m water depth (CGT3)** • Total number of taxa 46 • *Assilina ammonoides* (15%) • *Amphistegina radiata* (13%) • *Discorbinella bertheloti* (9%) • *Amphistegina lessonii* (7%) • *Millettiana millettii* (5%) **water depths <60 m (CGT4)** • Total number of taxa 50 • *Heterolepa dutemplei* (16%) • *Asterorotalia milletti* (16%) • *Elphidium advenum* (9%) • *Ammonia supera* (8%) • *Textularia* sp. A (7%).	**>20 m water depth** • *Textularia pseudosolita* • *Textularia foliacea* • *Textularia agglutinans* • *Bigenerina nodosaria* **(0 to 40 m water depth)** • *Asterorotalia pulchella* • *Cavarotalia annectens* • *Pseudorotalia schroeteriana* • *Eponides repandus*
60 to 120 m	• Benthic species richness 85 • Planktonic foraminifera 40% • *Spiroloculina communis* • *Cibicides margaritiferus* • *Cibicides praecinctus* • *Cancris indicus*	**Inner shelf (60 to 109 m water depth)** • *Ammomassilina alveoliniformis* • *Asterorotalia pulchella* • *Neouvigerina proboscidea* • *Islandiella japonica* • *Hanzawaia nipponica* • *Pseudogaudryina pacifica* • *Fijinonion fijiense* • <7,500 individuals/ 10cc **Inner shelf-high energy zone biofacies (80 to 107m)** • *Heterolepa dutemplei* • *Textularia lythostrota* • *Asterorotalia gaimardii* • *Quinqueloculina seminulum* • *Ammonia beccarii* • *Hanzawaia grossepunctata* • *Spirotextularia floridana* • *Elphidium advenum* • *Agglutinella agglutinans* • *Spiroplectinella higuchii* • >20,000 individuals/ 10cc **Outer shelf-high energy zone biofacies (106 to 121 m)** • *Cibicidoides pachyderma* • *Textularia bocki* • *Operculina ammonoides* • *Poroepistominella decoratiformis* • *Uvigerina schwageri* • *Hoeglundina elegans*, • *Spiroloculina communis* • Ca. 20,000 individuals/ 10cc	**60 m water depth (CGT5)** • Total number of taxa 56 • *Heterolepa dutemplei* (18%) • *Assilina ammonoides* (9%) • *Textularia* sp. A (7%) • *Hanzawaia grossepunctata* (6%) • *Elphidium advenum* (6%)	
>120 m	**120 to 200 m** • 65 to 80% planktonic foraminifera • Benthic species richness of 107 • Dominant benthic *Uvigerina schwageri*	**Outer shelf biofacies (109 to 226 m)** • *Facetocochlea pulchra* • *Bulimina marginata* • *Cibicides deprimus* • *Bolivina spathulata*. • <6,000 individuals/ 10cc		

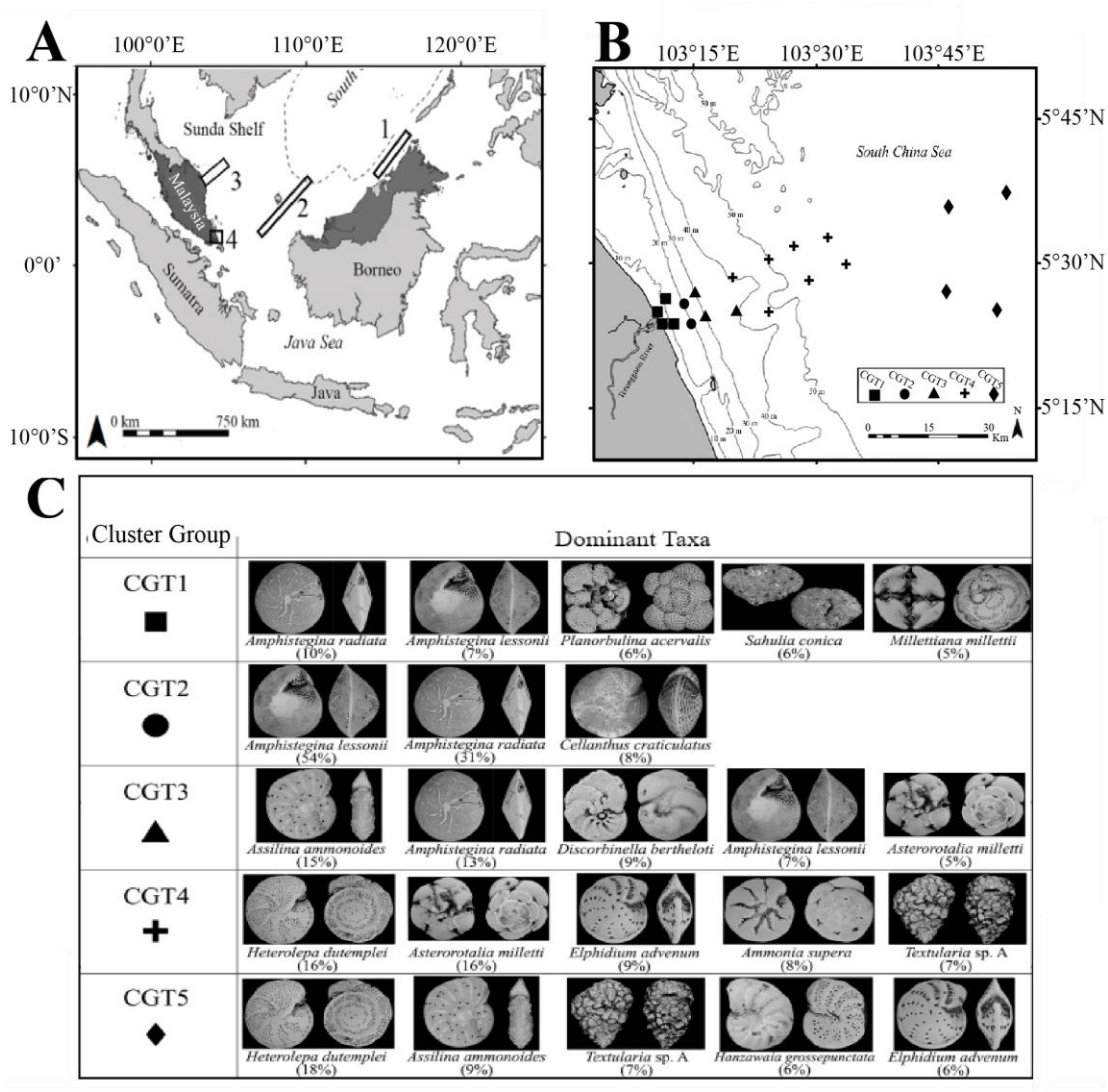

Figure 4. A: locations of published foraminiferal studies on the Sunda Shelf. (1) Biswas (1976), (2) Szarek et al. (2006), (3) Martin et al., 2018, (4) Minhat et al. (2016). **B:** distribution of biofacies (cluster groups 1–5) off the coast of peninsular Malaysia (Martin et al., 2018). **C:** dominant taxa in each biofacies (Martin et al., 2018).

assemblages off Kuala Terengganu (Table 1). The deepest assemblage (CGT5) recorded by Martin et al. (2018), like CGT4, is dominated by *Heterolepa dutemplei* but also contains relatively abundant specimens of the larger foraminifer, *Assilina ammonoides* (which is absent from CGT4). The substrate of these locations is muddy, shell-rich sand. Martin et al. (2018) suggested that this assemblage was likely a mix of modern specimens with older Quaternary specimens (including *Assilina ammonoides)* reworked from underlying sediment. Biswas (1976) recorded two assemblages and Szarek et al. (2006) recorded four assemblages from 60–200 m water depth that were not recorded in the shallower water off Kuala Terengganu (Martin et al., 2018) and the southern tip of peninsular Malaysia (Minhat et al., 2016). Biswas (1976) recorded no planktonic foraminifera from 0–20 m water depth and then an increase in planktonic foraminifera with depth (5–10% to 65–80% of assemblages); benthic species richness also increased with depth (50–107) (Table 1). Szarek et al. (2006) similarly noted both increasing diversity of benthic foraminifera and planktonic to benthic ratios with increased water depth and distance from shoreline (Table 1). Martin et al. (2018) reported planktonic foraminifera present in water depths exceeding 30 m and the planktonic foraminifera percentage increased with both distance from shoreline and water depth. Benthic species richness also increased with depth after an initially high value in the shallowest biofacies (CGT1) (8–14 m water depth). Minhat et al. (2016) reported that numbers of species were higher in deeper water than shallower water but their study only documented foraminifera in waters <40 m in depth.

Methods

Core collection, logging and sampling

In May 2016, six 1.25–2.2 m gravity cores were collected using the *RV Discovery* (Universiti Malaysia Terengganu) at water depths ranging 68–77 m along a transect crossing the trend of the paleo-Chao Phraya river incised valley (Fig. 1; Table 2). The weighted, steel core barrels with plastic (7 cm diameter) liners were lowered slowly through the water column and allowed to free-fall from ca. 5 m above the seafloor in an attempt to minimize disturbance of the surface sediment. No core-catcher was used in order to maximize penetration and recovery. Coring locations were selected using maps in Alqhatani et al. (2015).

The cores were cut in half lengthwise and logged at Universiti Malaysia Terengganu. The gravity coring process disturbed the upper portions (ca. 25–50 cm) of each core (Table 2). The extent of each disturbed portion (typically wet, unconsolidated mud) was noted in preliminary core logs and these sections of core were discarded. The remaining sections of each core were cut into 1 cm contiguous samples. The outer ca. 1 mm of sediment was scraped from each sample with a clean spatula because the outer rim of material adjacent to the core liner is often smeared downward during the coring process. Burrowed sediments were not sampled wherever possible. Samples were dried in an oven at ca. 50 ^{o}C and placed in labeled plastic bags.

From the first undisturbed sample downwards, samples were selected at 10 cm intervals for analysis of bulk sediment magnetic susceptibility (BMS), at 15 cm intervals for elemental analysis by means of x-ray fluorescence spectrometry (XRF), and at 20 cm intervals for analysis of foraminiferal assemblages. Sampling the six cores yielded totals of 130 BMS samples, 66 XRF samples, and 54 foraminiferal samples. For samples selected for BMS, 5.5 cc of powdered sediment was measured using a ceramic crucible and saved for analysis. XRF samples were also

weighed, powdered, then mixed in a ball mill with 20% PB-100 pellet binder for eight minutes (final weights ranging 6.1646–7.9772 g) to ensure homogeneity and finally compressed in a pellet press at forty-five psi for four minutes.

Table 2. Location (decimal degrees), water depth, core length, distance from shoreline, and interval of sediment disturbed by coring. Location and water depth were recorded using the satellite navigation and depth sounding instruments onboard the *RV Discovery*. Distance from shoreline was measured using Google Earth.

Core ID	Core Location	Water Depth (m)	Core Length (cm)	Dist. from shore (km)	Interval of disturbed sediment
GC16B	5.6163°, 104.0658°	71	215	106	0–46 cm
GC12B	5.6663°, 104.235°	75	182	126	0–48 cm
GC13A	5.6666°, 104.2605°	73	194	130	0–43 cm
GC13B	5.6666°, 104.2605°	73	190	130	0–35 cm
GC14B	5.6771°, 104.3006°	68	135	134	0–26 cm
GC15A	5.8320°, 104.1839°	77	224	127	0–26 cm

Sediment Analysis

Bulk Sediment Magnetic Susceptibility

Samples were analyzed using a Kappabridge MFK-A produced by Advanced Geoscience Instruments Company (AGICO). A 5.5 cc crucible was used to standardize the volume of sediment used. Each sample was analyzed five times at an induced magnetic field of 200 A/m and a frequency of 976 HZ. Results from the Kappabridge were averaged to produce a mean value of magnetic susceptibility. The MFK1-A was calibrated using a reference sample of known magnetic response, provided by AGICO, at the beginning and end of each sample run. A reference sample (TER15-GC5, 19.2–20.5 cm; Hindes, 2016) was also run at the beginning and end of analyzing each core to account for any machine drift. The error for this analysis is considered to be the standard deviation from the averaged value for the reference sample ($4.84 \times 10^{-5} \pm 1.91 \times 10^{-6}$; error <5%).

X-Ray Fluorescence Spectrometry

Each sample was analyzed for 19 major and trace elements (wt. %) through a wavelength dispersive X-ray fluorescence spectrometer by Axios (PANanalytical). The application used for analysis was constructed using 21 standards from distributors such as the National Institute of Standards and Technology and the United States Geological Survey. A reference sample (XLSC REF 10.2) was run at the beginning and end of analyzing each core to ensure replicability. The error (wt. %) for this analysis is considered to be the application's root mean square for the calibration of each channel (Table 3). The equation for which is $\text{RMS}=\sqrt{\frac{1}{n-1} * \sum_{i=1}^{N}(Xi - \overline{X})^2}$ where *Xi* is any valid measurement, N represents the number of valid measurements, $\overline{X}$ represents the average of valid measurements.

Table 3. The channel. root mean square (RMS), and minimum lower limit of detection (min LLD) of each element used in XRF.

Channel	RMS (wt. %)	Min LLD (ppm)
Al	1.34	Not calculated
Br	0.00042	2.84
Ca	0.24	2.07
Cu3	0.00116	1.28
Fe	0.51	9.84
K	0.14	7.97
Mg	0.47	17.65
Mn	0.025	3.15
Na	0.25	19.61
Ni	0.0019	0.70
P	0.025	1.49
S	0.038	0.55
Si	1.55	Not calculated
Ti	0.067	Not calculated
Zn	0.0027	1.05
Zr4	0.008	Not calculated
Sr	0.005	0.45
Pb	0.00087	1.38
As	0.00055	0.83

Foraminifera

Foraminiferal samples were weighed and disaggregated by soaking overnight in ca. 150 ml of distilled water with <1 g each of sodium hexametaphosphate and sodium hydroxide to aid in disaggregation. Samples were washed over a nest of 1000, 150, and 63μ sieves to remove the mud fraction and to separate the sand-sized fraction, in which foraminifera were concentrated, from the coarser-sediment fraction. The three sediment aliquots were dried in an oven at 50°C and stored in glass vials. To provide data comparable to that in Szarek et al. (2006) and Martin et al. (2018), the 150–1000 micron aliquot was split using a microsplitter to provide manageable quantities of sediment for picking. Splits were spread evenly on a 45-square picking tray and a random numbers table was used to select grid squares to be picked. All specimens were picked from selected squares until approximately 300 specimens were selected and transferred to 60 square microslides. Benthic foraminifera were identified to the species level by comparison with illustrations in foraminiferal studies from the South China Sea region (e.g., Graham and Militante, 1959; Whittaker and Hodgkinson, 1979; Haig, 1988; Loeblich and Tappan, 1981, 1994; Jones, 1994; Szarek, 2001; Culver et al., 2012, 2015; Martin et al., 2018). Planktonic foraminifera were counted but not identified. Identifications were confirmed by reference to type and comparative material located at the National Museum of Natural History, Smithsonian Institution, Washington, D.C.

Geochronology

Thirteen samples were sent to National Ocean Sciences Accelerator Mass Spectrometry (NOSAMS) in Woods Hole, MA for C-14 AMS radiocarbon dating. Eleven samples consisted of the benthic foraminifer *Pseudorotalia indopacifica* whenever specimens were abundant enough to provide at least 4 mg of material required for processing. In two cases, articulated bivalves

were dated due to low numbers of *P. indopacifica*. Age estimates were calibrated using the Marine13 calibration curve through CALIB 7.1 (Stuiver et al., 2017). A delta R of -45 with an uncertainty of 49 was used to adjust for regional marine reservoir affects (Southon et al., 2002).

Data Analysis

Regression analyses were used to determine correlations both between and within BMS and XRF data to aid in paleoenvironmental interpretation. Al wt. % values were plotted against other elemental data (and against BMS data) because Al is retained in terrestrial weathering products such as kaolinite, typically unaltered by contaminants and diagenetic activity, and reflects grain-size related compositional changes (Skowronek et al., 1994; Bahr et al., 2005; Cearreta et al., 2013; Leorri et al., 2014).

Relative abundances calculated from foraminiferal census data were plotted to exhibit trends of foraminifera in the cores. Species richness (number of species in a sample), Fisher's alpha, and percent Rotaliina, Miliolina, Textulariina were determined for each sample.

Q-mode hierarchical cluster analysis (Mello and Buzas, 1968; Martin et al., 2018) was used to distinguish groups within the benthic foraminiferal relative abundance data. Only those species represented by 2% or more of the assemblage in one or more samples were included in the cluster analysis dataset. Relative abundance data were transformed prior to analysis using the equation, 2 arc sin $\sqrt{p_i}$ (Buzas, 1979), where p_i is equal to the fraction of the ith species. All core samples were analyzed together using Ward's linkage and Euclidean distances in SYSTAT 13 (Systat Software Inc., Chicago, Illinois).

An SPSS (International Business Machines, version 23) multivariate discriminant data file constructed by Martin et al. (2018) distinguished five modern benthic foraminiferal biofacies

(defined by cluster analysis) that occur in order, from shallow to deep along two transects, on the Sunda Shelf in the vicinity of and to the west of the current study (Fig. 4); 1 (8–14 m water depth), 2 (21–22 m), 3 (32–41 m), 4 (44–59 m), 5 (60m) (see Table 4). A discriminant analysis was run to classify core samples within the five modern biofacies. If species recorded in Martin et al. (2018) were also found in this study, their abundances in core samples were entered into the SPSS file whether or not they comprised greater than 2% or more of the assemblage in any one core sample.

Results

BMS, Elemental, Radiocarbon and Foraminiferal Data

Figures 5 to 10 illustrate radiocarbon, BMS, elemental, and abundant foraminiferal data for each core. Unit boundaries, based upon these data, are indicated as inferred discontinuities.

Core GC16B is composed almost entirely of mud with an upper sandy mud unit from 30–45 cm core depth (Fig. 5). The percent mud decreases from ca. 100%–85% between 85 cm and 65 cm (Fig. 11). A radiocarbon age estimate from 167–168 cm was 12,577–12,814 cal yr BP. A second age estimate from 49 to 50 cm was 5,562–5,313 cal yr BP. Thus, the Pleistocene/ Holocene boundary (11,700 cal yr BP) is between the two depths (Table 4).

Core GC14B is composed of two lithologic units: a lower, black organic-rich, burrowed mud unit overlain by a greenish-brown shelly mud unit that contains a higher percentage of sand-sized material (Figs. 6, 11). The boundary between the two is a burrowed sharp contact (erosional surface). A sample from 70–71 cm from the lower unit yielded a radiocarbon age estimate of 11,051–11,332 cal yr BP. A sample from 35–36 cm, from the sandy mud unit above the erosional contact, yielded an age estimate of 3,590–3,880 cal yr BP (Table 4).

Cores GC12B, GC13A, GC13B, and GC15A are composed of a green-grey to brown shelly mud with variably decreasing percent mud up-core (Fig. 11). The top two samples in GC13B are from an overlying sandy mud (Figs. 9, 11) Two radiocarbon age estimates each from cores GC12B, GC13A, GC13B and three from core GC15A were all within the Holocene (Fig. 7–10; Table 4), ranging from 9,380–9,600 cal yr BP (GC15A; Fig. 10) to 1,005–1,254 cal yr BP (GC15A; Fig. 10).

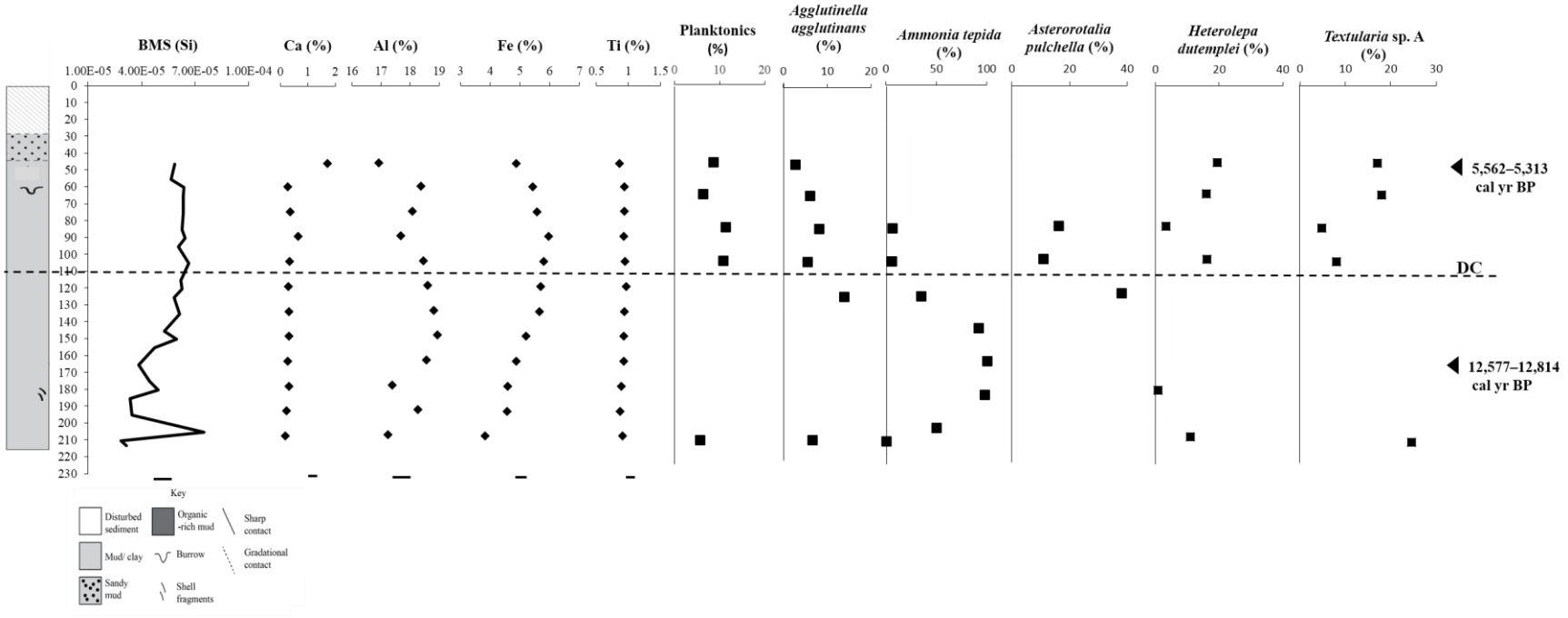

Figure 5: Lithologic log for core GC16B with the range for calibrated radiocarbon age estimates (black arrowheads), BMS, Ca, Al, Fe, and Ti trends, percent planktonics and trends of relative abundance (percent) for the five most abundant benthic species. Note changes of scale. DC indicates an interpreted discontinuity. Core collected in 71 m water depth. Error ranges are indicated beneath plots.

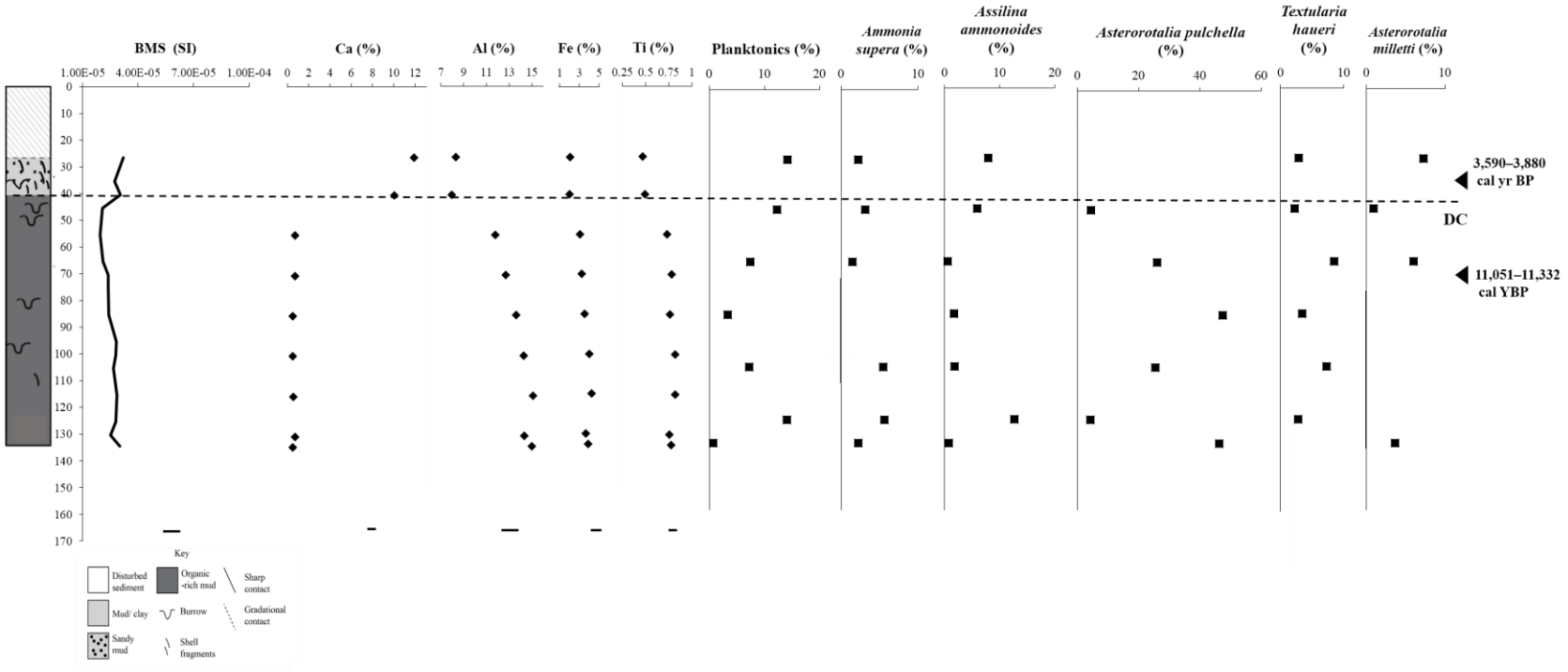

Figure 6: Lithologic log for core GC14B with the range for calibrated radiocarbon age estimates (black arrowheads), BMS, Ca, Al, Fe, and Ti trends, percent planktonics and trends of relative abundance (percent) for the five most abundant benthic species. Note changes of scale. DC indicates a discontinuity (burrowed, erosional, irregular surface). Core collected in 68 m water depth. Error ranges are indicated beneath plots.

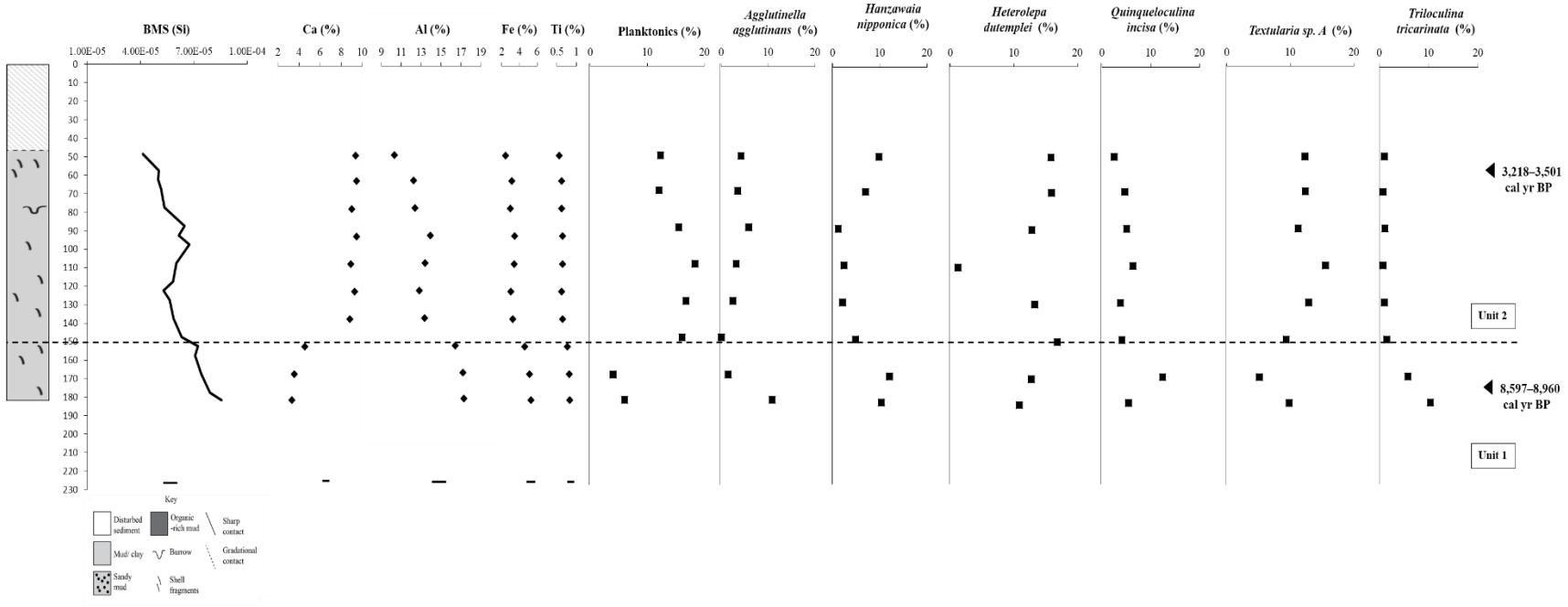

Figure 7: Lithologic log for core GC12B with the range for calibrated radiocarbon age estimates (black arrowheads), BMS, Ca, Al, Fe, and Ti trends, percent planktonics and trends of relative abundance (percent) for the six most abundant benthic species. Note changes of scale. Core collected in 75 m water depth. Error ranges are indicated beneath plots.

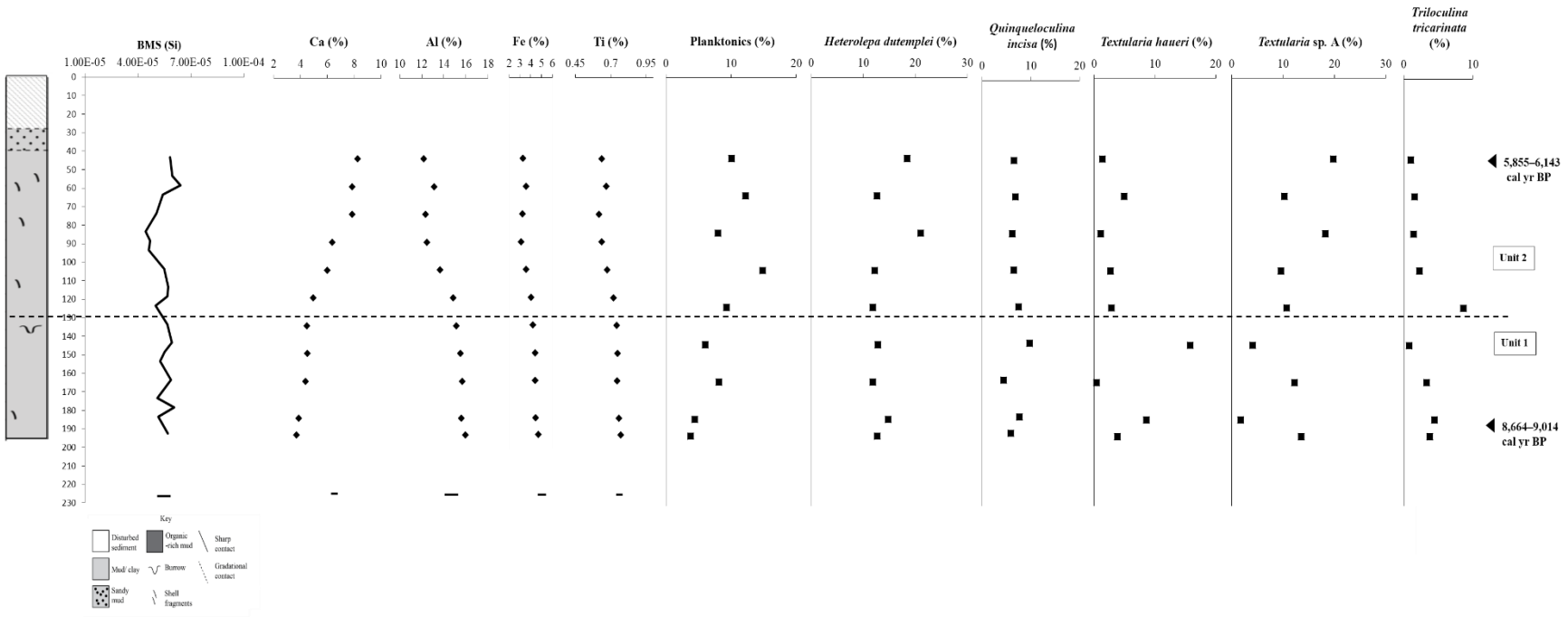

Figure 8: Lithologic log for core GC13A with the range for calibrated radiocarbon age estimates (black arrowheads), BMS, Ca, Al, Fe, and Ti trends, percent planktonics and trends of relative abundance (percent) for the five most abundant benthic species. Note changes of scale. Core collected 73 m water depth. Error ranges are indicated beneath plots.

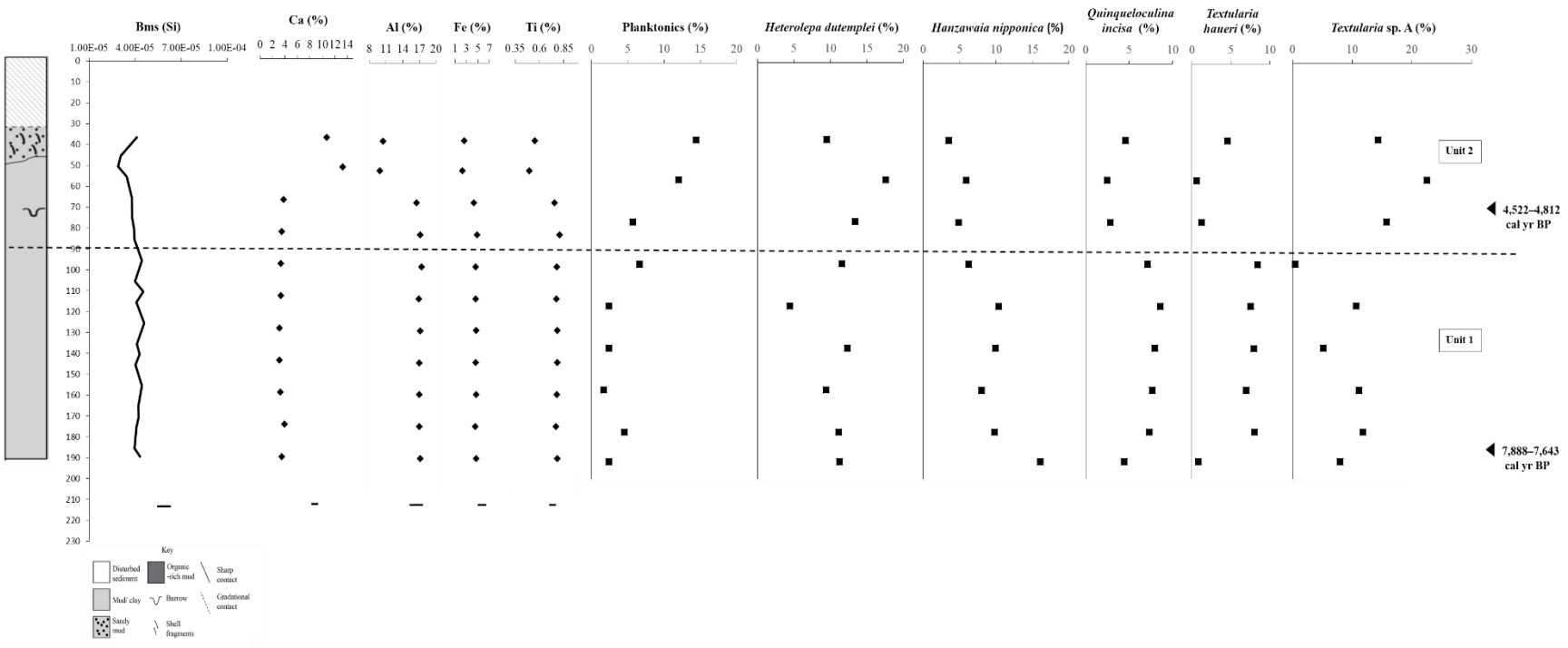

Figure 9: Lithologic log for core GC13B with the range for calibrated radiocarbon age estimates (black arrows), BMS, Ca, Al, Fe, and Ti trends, percent planktonics and trends of relative abundance (percent) for the five most abundant benthic species. Note the changes of scale. Core collected in 73 m water depth. Error ranges are indicated beneath plots.

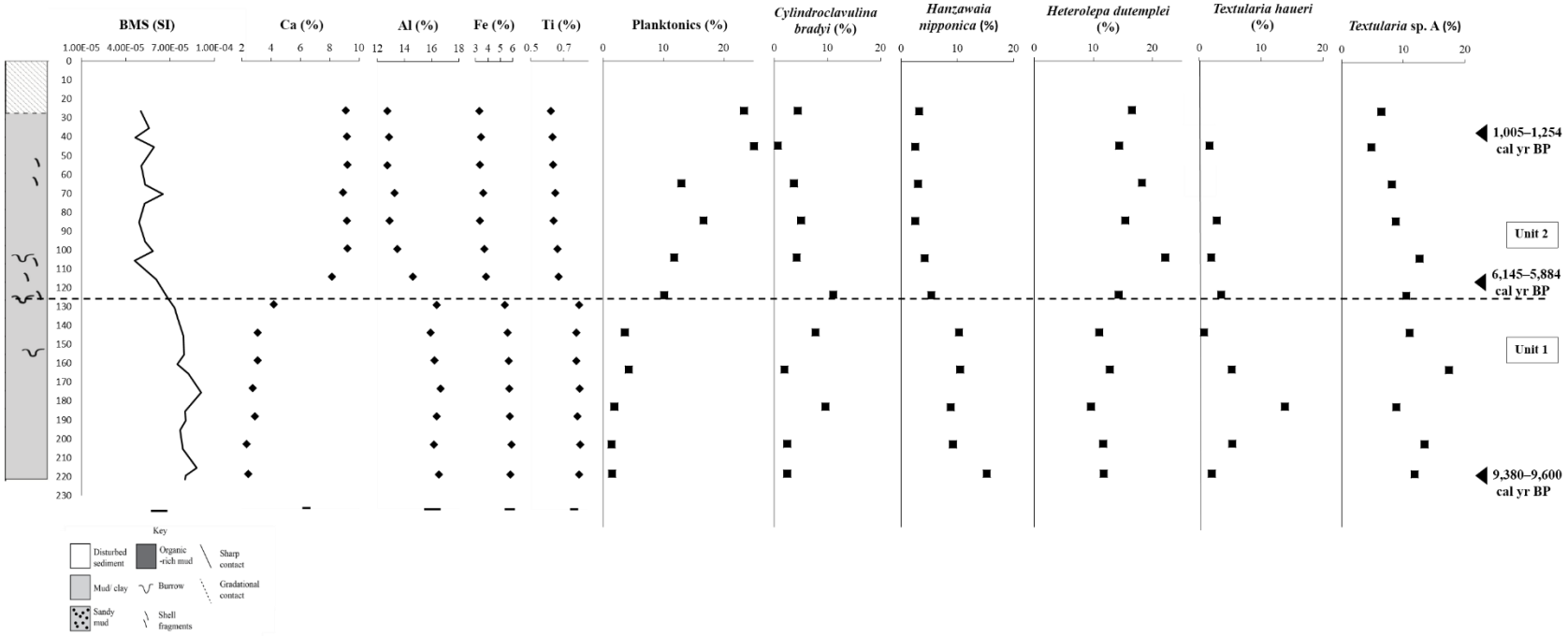

Figure 10: Lithologic log for core GC15A with the range for calibrated radiocarbon age estimates (black arrowheads), BMS, Ca, Al, Fe, and Ti trends, percent planktonics and trends of relative abundance (percent) for the five most abundant benthic species. Note changes of scale. Core collected in 77 m water depth. Error ranges are indicated beneath plots.

Table 4: AMS Radiocarbon age estimates from NOSAMS with associated data and values used in calibration. The ages referred to in the text and on figures are the midpoint ages from the range of calibrated years before present.

SAMPLE ID	REPORTED AGES	CAL. YEARS BP	MIDRANGE CAL. YR BP	% AGE CERTAINTY	δ13C	Δ R	Δ R UNCERTAINTY	TYPE
GC16B, 49-50cm	5,040	5,562-5,313	5,440	95.4	NA	-45	49	Foraminifera
GC16B, 167-168cm	11,150	12,577-12,814	12,700	95.4	-7.88	-45	49	Mollusc
GC12B, 59-60cm	3,440	3,218-3,501	3,360	95.4	-0.38	-45	49	Foraminifera
GC12B, 174-175cm	8,200	8,597-8,960	8,780	95.4	-0.7	-45	49	Foraminifera
GC13A, 48-49cm	5,530	5,855-6,143	6,000	95.4	-0.24	-45	49	Foraminifera
GC13A, 189-190cm	8,270	8,664-9,014	8,840	95.4	-0.71	-45	49	Foraminifera
GC13B, 70-71cm	4,440	4,522-4,812	4,670	95.4	-0.38	-45	49	Foraminifera
GC13B, 188-189cm	7,250	7,888-7,643	7,770	95.4	NA	-45	49	Foraminifera
GC14B, 35-36cm	3,750	3,590-3,880	3,740	95.4	-0.04	-45	49	Foraminifera
GC14B, 70-71cm	10,150	11,051-11,332	11,190	95.4	-11.39	-45	49	Mollusc
GC15A, 39-41cm	1,530	1,005-1,254	1,130	95.4	-0.32	-45	49	Foraminifera
GC15A, 118-119cm	5,550	6,145-5,884	6,010	95.4	NA	-45	49	Foraminifera
GC15A, 219-221	8,780	9,380-9,600	9,490	95.4	-1.11	-45	49	Foraminifera

Core GC16B exhibits an initial increase in BMS values followed by an immediate decrease (Fig. 5). Above the increase, values increase again from ca. 180 cm to 110 cm and then stabilize. Core GC14B exhibits a near vertical BMS profile, although values are lower than in GC16B (Fig. 6). The elemental profiles for these two cores are generally uniform until the upper segments of the sampled intervals (Figs. 5, 6), although Al wt. % and Fe wt. % are both greater in GC16B. At ca. 50 cm in GC16B and 40 cm in GC14B, there are increases in % Ca and decreases in wt. % Al, Fe, and Ti (Figs. 5, 6).

Cores GC12B, GC13A, GC13B, and GC15A vary from the other two cores in this study in terms of BMS and elemental data. The BMS data in GC13A and GC13B do not show significant changes when compared to error bars. Cores GC12B and GC15A exhibit variably upward-decreasing BMS profiles throughout the cores. All four of these cores exhibit similar

elemental profiles (Figs. 7–10). Ca generally increases up-core, whereas Al, Fe, and Ti, generally decrease up-core (Figs. 7–10).

The foraminiferal assemblages in cores GC16B and GC14B differ from those of the other four cores. In core GC16B, the number of species/number of calculated specimens in 1 g is lower in the majority of samples (Table 5). *Agglutinella agglutinans, Ammonia tepida* and *Asterorotalia pulchella* are the three most dominant benthic species in this core (Fig. 5). Core GC14B exhibits comparably low numbers of species/ number of calculated specimens in 1 g, although values are greater than in GC16B (Table 5). *Ammonia supera, Assilina ammonoides,* and *Asterorotalia pulchella* are the three most dominant benthic foraminifera (Fig. 6).

Cores GC12B, GC13A, GC13B, and GC15A vary from the other two cores. Planktonic foraminifera exhibit greater values and increasing trends up-core (Figs. 7–10). Numbers of species for these cores are both greater and more consistent (Table 5). *Heterolepa dutemplei, Hanzawaia nipponica, Quinqueloculina incisa*, and *Textularia* sp. A are some of the more dominant benthic foraminifera in these cores (Figs. 7–10).

The cores can be divided into two groups based upon geochronology, stratigraphy, lithology, and foraminifera. Cores GC16B and GC14B can be grouped together. They both contain disconformities between late Pleistocene and Holocene lithologic units. Core GC16B, although lithologically similar to GC12B, GC13A, GC13B, and GC15A, differs in its foraminiferal assemblages, its BMS signal and elemental trends. The bulk of this core is characterized by generally homogenous values of BMS, percent Ca, Al, Fe and Ti (Fig. 5). This section of core has a foraminiferal assemblage dominated by *Ammonia tepida,* which does not occur in other cores, and low calculated numbers of tests in 1 g of sediment (Table 5). Planktonic foraminifera are not present where *A. tepida* is abundant (Fig. 5). The bottom sample and top two

samples contain radiocarbon age estimates, foraminiferal assemblages, BMS signals, and percent Ca, Al, Fe, and Ti similar to those of the upper unit in GC12B, GC13A, GC13B, and GC15A (Figs. 5, 7–10).

GC14B contains a black organic-rich mud unit overlain by shelly greenish-brown mud unit, separated by a burrowed erosional contact (Fig. 6). This core differs from GC12B, GC13A, GC13B, and GC15A in both lithology and radiocarbon age, i.e., older age estimates and presence of organic-rich mud. The foraminiferal assemblage of the organic-rich mud unit is dominated by *Asterorotalia pulchella* and *Ammonia supera,* and low calculated numbers of tests in 1 g of sediment (Fig 6; Table 5). Planktonic foraminifera and *A. pulchella* exhibit a negative correlation in this unit (Fig. 6). Above the erosional contact, Ca content reaches its greatest percentage within the core and, conversely, Al, Fe, and Ti exhibit the lowest percentages (Fig. 6). The greenish-brown mud unit contains greater percentages of planktonic foraminifera and higher abundance of *Assilina ammonoides* than other lithofacies (Fig. 6).

GC12B, GC13A, GC13B, and GC15A can be grouped together due to similar lithologic and foraminiferal characteristics and geochronology. The entirety of these cores is Holocene in age. Two units are distinguishable.

Unit 1 occurs at the base of these cores and, in contrast to the overlying Unit 2, is characterized by greater BMS values, greater percent mud, and greater Al, Fe, and Ti and by greater percent *Hanzawaia nipponica* than the overlying unit (Figs. 7–11; Table 6). Unit 1 is also characterized by lower wt. % Ca, lower percent planktonic foraminifera, lower calculated numbers of tests in 1 g of sediment and lower percent *Heterolepa dutemplei* (Figs. 7–10; Table 6).

Unit 2 is located above Unit 1 in these four cores and is distinguished by increased percent planktonics, increased percent Ca content, lower BMS signal, lower percent mud, and lower percent Al, Fe, and Ti (Figs. 7–11; Table 6). This unit is also characterized by higher percent *Heterolepa dutemplei*, lower percent *Hanzawaia nipponica,* and higher calculated numbers of tests in 1 g of sediment (Figs. 7–10; Table 5). Unit 1 transitions to Unit 2 ca. 6,500 cal yr BP (Figs. 7–10).

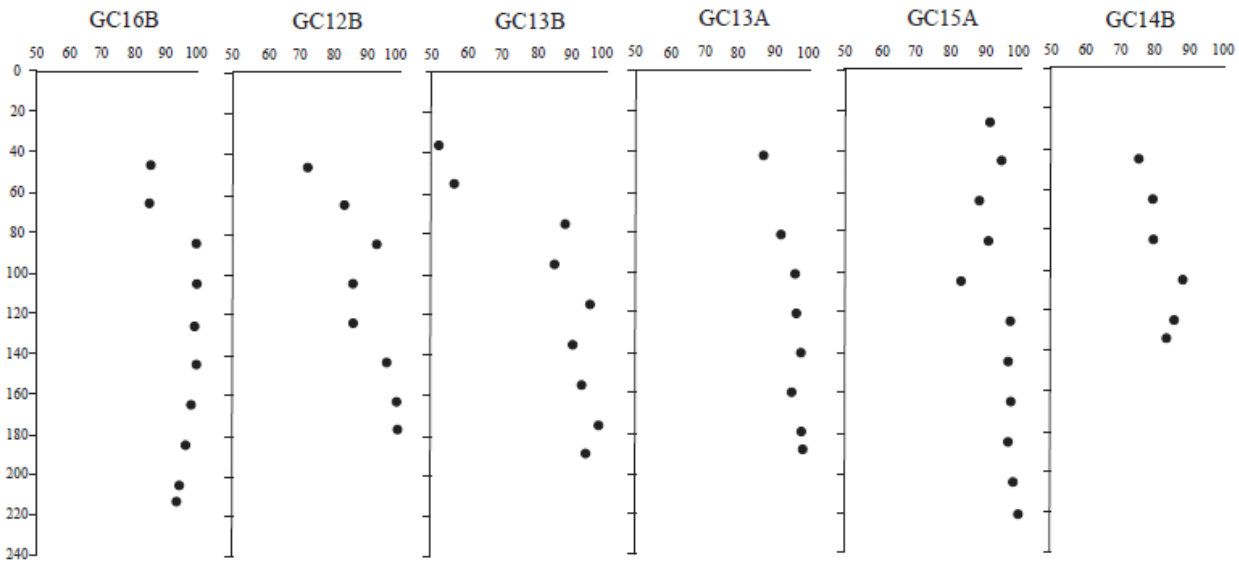

Figure 11: Percent mud content for each core, calculated from wet-sieving of foraminiferal samples. Except for GC15A (see Fig. 1), cores are ordered from left to right, west to east.

Table 5: Summary foraminiferal data for 54 samples from all six cores.

Sample ID, Sample Depth	no. specimens	no. species (S)	Calc. no. tests/ 1 g	Fisher's alpha	% planktonics	% textulariid	% miliolid	% rotaliid
GC15A 26-27	248	41	175	13.9	23.39	15.73	12.50	48.39
GC15A 45-46	312	49	2013	16.4	25.00	11.86	16.35	46.79
GC15A 65-66	269	47	2690	16.4	13.01	17.84	16.36	52.79
GC15A 85-86	318	55	4818	19.1	16.67	23.90	19.18	40.25
GC15A 105-106	262	37	32750	11.8	11.83	26.34	14.50	47.33
GC15A 125-126	315	43	2864	13.4	10.16	34.92	15.56	39.37
GC15A 145-146	272	40	1537	13	3.68	28.68	26.10	41.54
GC15A 165-166	304	38	1143	11.5	4.28	30.26	18.42	47.04
GC15A 185-186	260	43	1677	14.7	1.92	38.08	20.00	40.00
GC15A 205-206	282	48	605	16.7	1.42	28.37	21.99	48.23
GC15A 221-222	203	39	832	14.5	1.48	23.65	24.14	50.74
GC14B 26-27	316	42	1090	13	14.24	14.24	13.92	57.59
GC14B 45-46	220	50	2650	20.2	12.27	17.73	10.00	60.00
GC14B 65-66	200	37	8	13.4	7.50	22.50	10.00	60.00
GC14B 85-86	59	20	2	10.5	3.39	10.17	6.78	79.66
GC14B 105-106	55	20	4	11.3	7.27	16.36	1.82	74.55
GC14B 125-126	71	26	3	15	14.08	4.23	12.68	69.01
GC14B 134-135	136	29	5	11.3	0.74	16.18	8.09	75.00
GC13B 36-37	285	49	95335	17.1	14.39	27.37	14.39	43.86
GC13B 55-56	324	45	38896	14.3	12.04	37.65	9.26	41.05
GC13B 75-76	247	46	1594	16.6	5.67	25.91	20.24	48.18
GC13B 95-96	225	49	1621	19.3	6.67	16.44	20.44	56.44
GC13B 115-116	291	48	936	16.4	2.41	25.43	27.15	45.02
GC13B 135-136	252	45	1335	16	2.38	24.21	23.41	50.00
GC13B 155-156	287	50	923	17.6	1.74	29.27	17.77	51.22
GC13B 175-176	287	44	1852	14.5	4.53	25.09	20.91	49.48
GC13B 189-190	249	43	2360	15	2.41	23.69	18.88	55.02
GC13A 43-44	288	45	8727	15	10.07	31.25	14.24	44.44
GC13A 63-64	262	48	3403	17.3	12.21	29.39	16.41	41.98
GC13A 83-84	276	46	8364	15.8	7.97	30.43	14.49	47.10
GC13A 103-104	262	54	3970	20.7	14.89	23.28	23.28	38.55
GC13A 123-124	279	51	1800	18.3	9.32	20.43	30.11	40.14
GC13A 143-144	266	51	855	18.7	6.02	29.32	21.43	43.23
GC13A 163-164	270	46	8182	15.9	8.15	27.04	19.26	45.56
GC13A 183-184	339	57	1389	19.6	4.42	18.88	23.60	53.10
GC13A 192-193	236	40	1180	13.4	3.81	28.81	16.10	51.27
GC12B 48-49	274	37	16506	11.5	12.77	29.20	7.66	50.36
GC12B 67-68	258	37	15542	11.8	12.02	32.17	14.34	41.47
GC12B 87-88	258	38	3909	12.3	15.50	35.66	14.73	34.11
GC12B 107-108	251	43	4564	15	18.33	33.47	19.52	28.69
GC12B 127-128	287	44	17289	14.4	16.72	27.87	13.94	41.46
GC12B 147-148	268	51	10141	18.6	16.04	20.52	17.16	46.27
GC12B 167-168	274	42	881	13.8	4.01	20.44	24.09	51.46
GC12B 181-182	184	31	1187	10.7	5.98	28.80	20.11	45.11
GC16B 46-47	257	38	11682	12.3	8.56	30.35	9.34	51.75
GC16B 65-66	300	49	9090	16.6	6.33	33.00	12.00	48.67
GC16B 85-86	62	20	3	10.5	11.29	19.35	4.84	64.52
GC16B 105-106	37	16	1	NA	10.81	18.92	0.00	70.27
GC16B 125-126	29	7	1	NA	0.00	17.24	0.00	82.76
GC16B 145-146	12	2	0.03	NA	0.00	8.33	0.00	91.67
GC16B 165-166	30	1	2	NA	0.00	0.00	0.00	100.00
GC16B 185-186	130	4	4	0.8	0.00	0.00	0.00	100.00
GC16B 205-206	2	2	0.05	NA	0.00	0.00	50.00	50.00
GC16B 213-214	211	37	6	13	5.69	50.71	9.95	33.65

Table 6: Summary data for Unit 1 vs. Unit 2 in cores GC12B, GC13A, GC13B, and GC15A.

		BMS (Si)	Al %	Fe%	Ti%	Ca%	Planktonics %	*Hanzawaia nipponica* %	*Heterolepa dutemplei* %
Unit 2	Mean	5.32E-05	12.725	3.269	0.628	8.746	14.33	3.45	14.73
	Standard Dev.	8.90E-06	1.230	0.425	0.047	1.650	4.44	2.31	4.57
Unit 1	Mean	5.99E-05	16.512	4.942	0.780	3.470	3.94	8.64	11.46
	Standard Dev.	1.75E-05	0.645	0.552	0.021	0.624	1.97	4.05	2.16

Cluster Analysis of Foraminiferal Relative Abundance Data

The Q-mode cluster dendrogram is shown in Figure 12. The 54 samples cluster into four groups (G1A, G1B, G2A, G2B) at a Euclidean distance of 0.4. G1A is composed of six samples and 18 taxa (Table 7) with *Ammonia tepida* (63.38%) dominating, and *Asterorotalia pulchella* (9.01%), *Quinqueloculina adiazeta* (8.33%), and *Cribroelphidium* cf. *C. detense* (4.30 %) also abundant. G1B is composed of eight samples and 53 taxa with *Asterorotalia pulchella* (20.60%), *Heterolepa dutemplei* (10.63 %), *Textularia* sp. A (5.69%), and *Assilina ammonoides* (4.58%) as the most abundant taxa (Table 6). G2A is composed of 24 samples and 57 taxa with *Heterolepa dutemplei* (14.65%), *Textularia* sp. A (13.26%), *Quinqueloculina incisa* (4.65%), and *Cylindroclavulina bradyi* (4.12%) dominating (Table 6). G2B is composed of 16 samples and 55 taxa with *Heterolepa dutemplei* (11.31%), *Hanzawia nipponica* (9.26%), *Textularia* sp. A (9.02%), and *Quinqueloculina incisa* (6.88%) as the most abundant taxa (Table 6). The distribution of the cluster groups is shown on the lithologic logs of Figure 14.

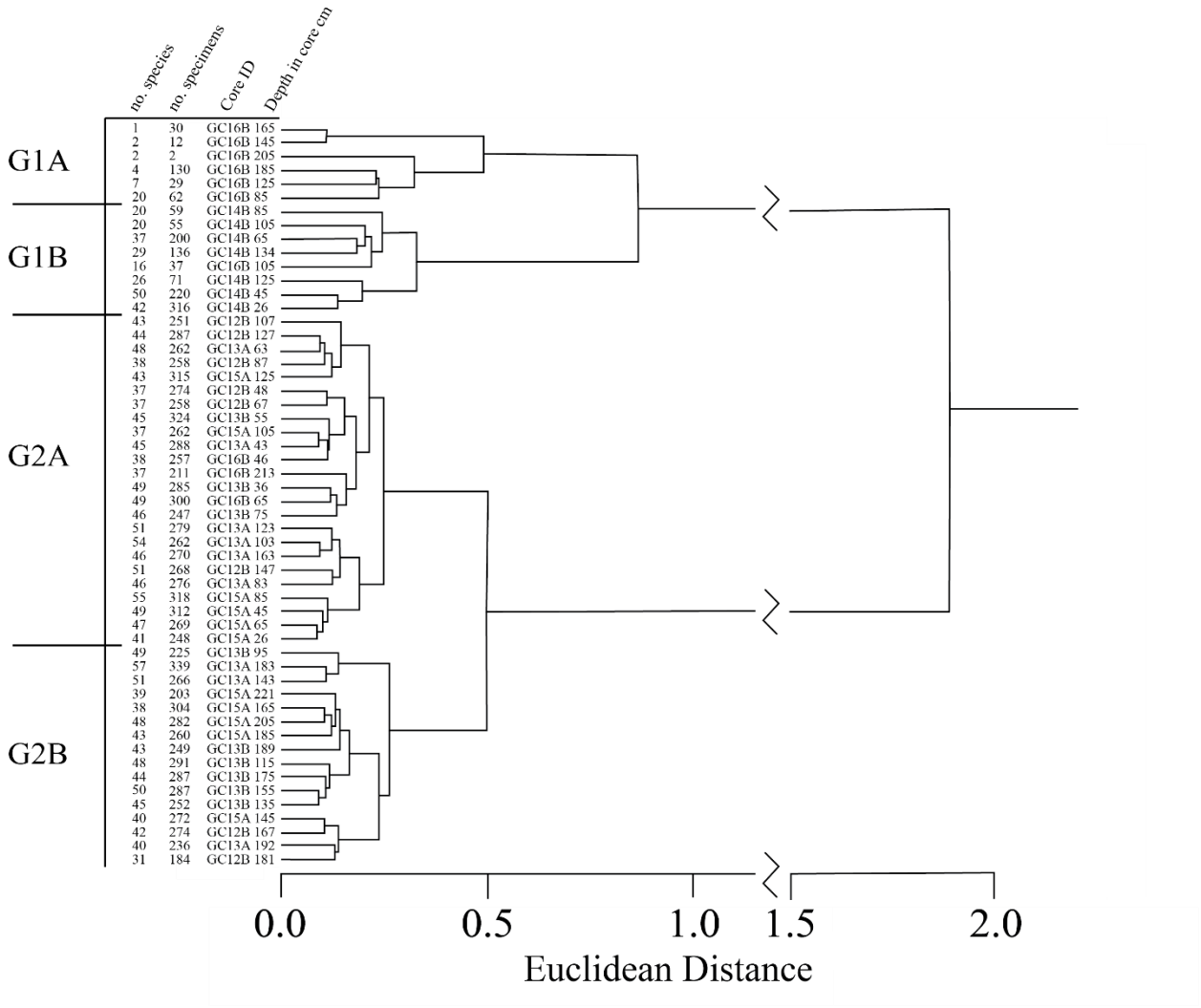

Figure 12: Cluster dendrogram for all samples in six cores along with numer of specimens picked per sample and number of species per sample.

Table 7: Cluster analysis of all core samples: mean percent of species within each cluster group (see Fig. 12).

G1A	Mean	Range	G1B	Mean	Range	G2A	Mean	Range	G2B	Mean	Range
6 Samples, 18 Taxa	**%**	**%**	**8 Samples, 53 Taxa**	**%**	**%**	**24 Samples, 57 Taxa**	**%**	**%**	**16 Samples, 55 Taxa**	**%**	**%**
Ammonia tepida	63.38	6.45—100.00	*Asterorotalia pulchella*	20.60	0—47.46	*Heterolepa dutemplei*	14.65	1.20—22.14	*Heterolepa dutemplei*	11.31	4.46—14.75
Asterorotalia pulchella	9.01	0—37.93	*Heterolepa dutemplei*	10.63	0—18.64	*Textularia* sp. A	13.26	4.81—24.64	*Hanzawaia nipponica*	9.26	0.75—16.04
Quinqueloculina adiazeta	8.33	0—50.00	*Textularia* sp. A	5.69	0—9.09	*Quinqueloculina incisa*	4.65	0.33—7.53	*Textularia* sp. A	9.02	0.44—17.43
Cribroelphidium cf. *C. detense*	4.30	0—25.81	*Assiliina ammonoides*	4.58	0—12.68	*Cylindroclavulina bradyi*	4.12	0.64—11.11	*Quinqueloculina incisa*	6.88	2.84—12.01
Agglutinella agglutinans	3.64	0—13.79	*Hanzawaia nipponica*	4.39	0—9.18	*Asterorotalia gaimardi*	3.90	0—6.88	*Textularia haueri*	6.35	0—15.79
Textularia haueri	2.77	0—8.33	*Textularia haueri*	3.39	0—8.5	*Hanzawaia nipponica*	3.52	0.72—9.86	*Triloculina tricarinata*	5.61	0.75—10.32
Textularia sp. A	0.81	0—4.84	*Ammonia supera*	2.52	0—5.63	*Agglutinella agglutinans*	3.18	0—6.64	*Ammonia supera*	5.24	2.46—8.03
Elphidium sp.	0.70	0—3.45	*Parrellina hispidula*	2.39	0—8.11	*Ammonia supera*	2.93	0—5.96	*Cylindroclavulina bradyi*	3.87	1.39—9.62
Heterolepa dutemplei	0.67	0—3.23	*Pseudorotalia schroeteriana*	2.28	0—5.08	*Textularia haueri*	2.45	0—7.58	*Asterorotalia gaimardi*	3.41	0—8.03
Asterorotalia gaimardi	0.57	0—3.45	*Asterorotalia milletti*	2.23	0—7.28	*Bigenerina nodosaria*	2.38	0.81—4.74	*Agglutinella agglutinans*	2.57	0.42—10.87
Paracibicides edomica	0.57	0—3.45	*Agglutinella agglutinans*	2.18	0—5.41	*Triloculina tricarinata*	1.80	0—8.60	*Reussella spinulosa*	2.40	0—6.78
Adelosina littoralis	0.27	0—1.61	*Quinqueloculina* sp.	2.00	0—4.5	*Pseudorotalia indopacifica*	1.74	0—4.76	*Bigenerina nodosaria*	2.34	0—4.37
Ammonia supera	0.27	0—1.61	*Bigenerina nodosaria*	1.84	0—5.41	*Spirotextularia floridana*	1.70	0—3.10	*Pseudorotalia indopacifica*	1.77	0.35—4.00
Bigenerina nodosaria	0.27	0—1.61	*Pseudorotalia indopacifica*	1.76	0—5.41	*Paracibicides edomica*	1.67	0—7.06	*Cancris auriculus*	1.63	0—5.67
Elphidium indicum	0.27	0—1.61	*Asterorotalia gaimardi*	1.71	0—4.23	*Proemassilina arenaria*	1.64	0.35—3.33	*Asterorotalia milletti*	1.33	0—2.71
Planispirinella exigua	0.27	0—1.61	*Ammonia tepida*	1.47	0—5.41	*Quinqueloculina philippinensis*	1.46	0—3.49	*Proemassilina arenaria*	1.09	0—2.71
Quinqueloculina incisa	0.27	0—1.61	*Elphidium* cf. *E. advenum*	1.19	0—5.14	*Asterorotalia milletti*	1.45	0—5.28	*Elphidium* cf. *E. advenum*	1.04	0—2.94
Quinqueloculina laevigata	0.27	0—1.61	*Ammonia convexa*	1.01	0—2.82	*Quinqueloculina* sp.	1.12	0—3.51	*Spirotextularia fistulosa*	1.02	0—4.24
			Massilina cf. *M. planata*	0.93	0—4.23	*Nubeculina divaricata*	1.09	0—4.18	*Quinqueloculina laevigata*	1.02	0—2.78
			Reussella spinulosa	0.88	0—2.85	*Pseudorotalia schroeteriana*	0.92	0—2.46	*Planispirinella exigua*	0.99	0—2.95
			Elphidium indicum	0.85	0—5.45	*Spiroloculina communis*	0.85	0—2.00	*Quinqueloculina philippinensis*	0.97	0—2.46
			Quinqueloculina philippinensis	0.83	0—1.69	*Quinqueloculina laevigata*	0.79	0—3.24	*Ammonia convexa*	0.88	0.34—1.47
			Elphidium jensoni	0.81	0—3.64	*Ammonia convexa*	0.74	0—2.71	*Adelosina littoralis*	0.81	0—2.21
			Heterolepa praecincta	0.81	0—5.08	*Quinqueloculina parvaggluta*	0.68	0—3.33	*Spirotextularia floridana*	0.74	0—1.84
			Paracibicides edomica	0.77	0—5.41	*Reussella spinulosa*	0.67	0—2.22	*Pyrgoella tenuiaperta*	0.71	0—2.96
			Cylindroclavulina bradyi	0.66	0—2.22	*Elphidium* cf. *E. advenum*	0.66	0—2.00	*Triloculinella pseudooblonga*	0.66	0—2.06
			Quinqueloculina incisa	0.64	0—1.82	*Discorbia candeiana*	0.65	0—4.30	*Elphidium indicum*	0.60	0—2.06
			Discorbinella bodjongensis	0.57	0—2.70	*Cancris auriculus*	0.57	0—1.57	*Pseudorotalia schroeteriana*	0.59	0—2.09
			Eponides repandus	0.45	0—1.82	*Eponides repandus*	0.54	0—2.02	*Nubeculina divaricata*	0.51	0—3.76
			Cribroelphidium cf. *C. detense*	0.43	0—3.00	*Adelosina littoralis*	0.49	0—1.59	*Ammonia* cf. *A. takanabensis*	0.48	0—2.06
			Proemassilina arenaria	0.43	0—1.69	*Quinqueloculina lamarckiana*	0.46	0—1.53	*Parrellina hispidula*	0.47	0—1.78
			Heterolepa subhaidingeri	0.42	0—3.39	*Discorbinella bodjongensis*	0.43	0—2.11	*Eponides repandus*	0.47	0—1.37
			Reophax sp.	0.42	0—3.39	*Quinqueloculina bicarinata*	0.41	0—2.22	*Quinqueloculina lamarckiana*	0.46	0—2.13
			Nubeculina divaricata	0.42	0—2.00	*Quinqueloculina adiazeta*	0.39	0—2.22	*Paracibicides edomica*	0.46	0—2.22
			Quinqueloculina adiazeta	0.42	0—1.41	*Spirotextularia fistulosa*	0.38	0—1.15	*Discorbia candeiana*	0.42	0—1.09
			Planispirinella exigua	0.40	0—1.58	*Reophax* sp.	0.32	0—1.91	*Spiroloculina communis*	0.41	0—1.20
			Spirotextularia floridana	0.40	0—1.5	*Pyrgoella tenuiaperta*	0.30	0—1.79	*Quinqueloculina* sp.	0.40	0—1.61
			Quinqueloculina lamarckiana	0.37	0—1.27	*Lobatula*	0.25	0—4.74	*Cibicides* sp.	0.36	0—3.56
			Triloculina tricarinata	0.36	0—1.47	*Quinqueloculina crassicarinata*	0.25	0—2.33	*Triloculina trigonula*	0.33	0—1.48
			Cibicides refulgens	0.35	0—2.82	*Triloculinella pseudooblonga*	0.23	0—1.62	*Quinqueloculina adiazeta*	0.33	0—1.33
			Elphidium sp.	0.34	0—2.70	*Assilina ammonoides*	0.23	0—2.33	*Quinqueloculina parvaggluta*	0.29	0—1.18
			Discorbea candeiana	0.32	0—2.53	*Cibicides* sp.	0.22	0—1.60	*Quinqueloculina bicarinata*	0.29	0—1.27
			Ammonia cf. *A. takanabensis*	0.31	0—2.00	*Ammonia* cf. *A. takanabensis*	0.20	0—2.54	*Discorbinella bodjongensis*	0.27	0—1.39
			Quinqueloculina bicarinata	0.30	0—1.47	*Triloculina trigonula*	0.15	0—2.61	*Asterorotalia pulchella*	0.23	0—1.61
			Reophax scorpiorus	0.28	0—2.21	*Planispirinella exigua*	0.14	0—1.43	*Ammonia tepida*	0.15	0—0.54
			Quinqueloculina parvaggluta	0.27	0—1.69	*Spiroloculina depressa*	0.12	0—2.20	*Massilina* cf. *M. planata*	0.07	0—0.84
			Cibicides sp.	0.24	0—1.41	*Elphidium* sp.	0.11	0—2.72	*Elphidium jensoni*	0.06	0—0.34
			Adelosina littoralis	0.16	0—0.5	*Heterolepa subhaidingeri*	0.11	0—1.05	*Reophax* sp.	0.05	0—0.44
			Quinqueloculina laevigata	0.12	0—0.5	*Massilina* cf. *M. planata*	0.07	0—0.38	*Heterolepa praecincta*	0.03	0—0.40
			Triloculina trigonula	0.12	0—0.5	*Heterolepa praecincta*	0.07	0—0.63	*Assilina ammonoides*	0.02	0—.40
			Lobatula	0.10	0—0.5	*Elphidium indicum*	0.06	0—0.73	*Quinqueloculina crassicarinata*	0.02	0—0.37
			Quinqueloculina crassicarinata	0.06	0—0.45	*Cibicides refulgens*	0.05	0—0.39	*Elphidium* sp.	0.02	0—0.34
			Spirotextularia fistulosa	0.06	0—0.45	*Asterorotalia pulchella*	0.03	0—0.47	*Heterolepa subhaidingeri*	0.02	0—0.34
						Parrellina hispidula	0.03	0—0.35	*Cibicides refulgens*	0.02	0—0.29
						Elphidium jensoni	0.02	0—0.40	*Spiroloculina depressa*	0.02	0—0.29
						Ammonia tepida	0.01	0—0.33			
						Cribroelphidium cf. *C. detense*	0.01	0—0.33			

Comparison of foraminiferal data to those of Harrison (2017) and Donovan (2017)

A second cluster analysis was run to compare the Holocene, down-core, benthic foraminiferal assemblages of Harrison (2017) and Donovan (2017) to the down-core samples collected in this study. The samples from GC11B (Donovan, 2017) clustered in Group 1 but are closer to G1B than G1A (Fig. 13) and are labeled G1C. Samples from Harrison (2017) clustered separately from G1A, G1B, G1C but are closer to those groups than to G2A and G2B (Fig. 13). The mean percent of species in each cluster group are shown in Table 8. The distribution of cluster groups is shown on the lithologic logs in Figure 14.

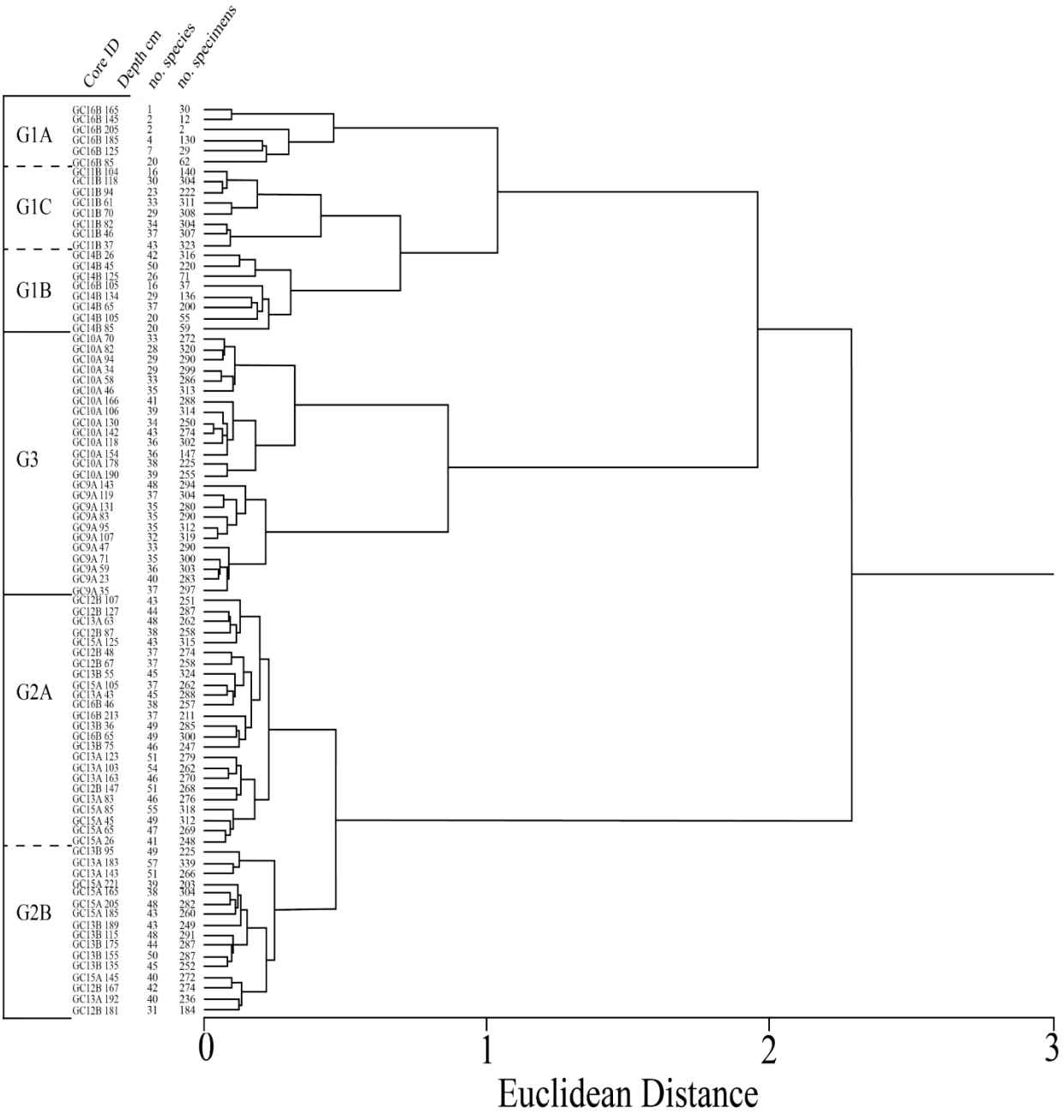

Figure 13. Cluster dendrogram of core samples (G1A, G1B, G2A, G2B) from this study along with Holocene core samples (G3) from Harrison (2017) and Holocene core samples (G1C) from Donovan (2017).

Table 8: Cluster analysis of all core samples including Holocene samples from Harrison (2017), G3 and (Donovan 2017), G1C. Mean percent and range for species within each cluster group are indicated. (see Fig. 14).

G1A	Mean	Range	G1B	Mean	Range	G1C	Mean	Range	G2A	Mean	Range	G2B	Mean	Range	G3	Mean	Range
6 Samples, 18 Taxa	%	%	8 Samples, 53 Taxa	%	%	8 samples, 20 taxa	%	%	24 Samples, 57 Taxa	%	%	16 Samples, 55 Taxa	%	%	25 samples, 26 taxa	%	%
Ammonia tepida	63.38	6.45—100.00	*Asterorotalia pulchella*	20.6	0—47.46	*Asterorotalia pulchella*	30.58	5.21–54.93	*Heterolepa dutemplei*	14.65	1.20—22.14	*Heterolepa dutemplei*	11.31	4.46—14.75	*Heterolepa dutemplei*	13.11	4.74–21.75
Asterorotalia pulchella	9.01	0—37.93	*Heterolepa dutemplei*	10.63	0—18.64	*Textularia* cf. *T. agglutinans*	10.26	2.79–19.28	*Textularia* sp. A	13.26	4.81—24.64	*Hanzawaia nipponica*	9.26	0.75—16.04	*Asterorotalia milletti*	11.73	2.28–21.86
Quinqueloculina adiazeta	8.33	0—50.00	*Textularia* sp. A	5.69	0—9.09	*Hanzawaia nipponica*	8.88	0–28.24	*Quinqueloculina incisa*	4.65	0.33—7.53	*Textularia* sp. A	9.02	0.44—17.43	*Textularia* sp.A	9.36	0–28.57
Cribroelphidium cf. *C. detense*	4.3	0—25.81	*Assiliina ammonoides*	4.58	0—12.68	*Cavarotalia annectens*	7.79	3.62–18.01	*Cylindroclavulina bradyi*	4.12	0.64—11.11	*Quinqueloculina incisa*	6.88	2.84—12.01	*Hanzawaia nipponica*	7.27	4.05–10.39
Agglutinella agglutinans	3.64	0—13.79	*Hanzawaia nipponica*	4.39	0—9.18	*Heterolepa dutemplei*	4.73	0–14.01	*Asterorotalia gaimardi*	3.9	0—6.88	*Textularia haueri*	6.35	0—15.79	*Elphidium* cf. *E. advenum*	3.98	0.72–6.75
Textularia haueri	2.77	0—8.33	*Textularia haueri*	3.39	0—8.5	*Elphidium* cf. *E. advenum*	4.30	1.43–9.32	*Hanzawaia nipponica*	3.52	0.72—9.86	*Triloculina tricarinata*	5.61	0.75—10.32	*Sigmoilopsis schlumbergeri*	2.93	0–6.84
Textularia sp. A	0.81	0—4.84	*Ammonia supera*	2.52	0—5.63	*Bigenerina nodosaria*	3.79	1.62–7.49	*Agglutinella agglutinans*	3.18	0—6.64	*Ammonia supera*	5.24	2.46—8.03	*Bigenerina nodosaria*	2.75	0–8.75
Elphidium sp.	0.7	0—3.45	*Parellina hispidula*	2.39	0—8.11	*Pseudorotalia indopacifica*	2.57	0–8.14	*Ammonia supera*	2.93	0—5.96	*Cylindroclavulina bradyi*	3.87	1.39—9.62	*Pseudorotalia indopacifica*	2.69	0–5.82
Heterolepa dutemplei	0.67	0—3.23	*Pseudorotalia schroeteriana*	2.28	0—5.08	*Pseudorotalia schroeteriana*	2.55	0.90–4.56	*Textularia haueri*	2.45	0—7.58	*Asterorotalia gaimardi*	3.41	0—8.03	*Quinqueloculina incisa*	2.57	0–13.01
Asterorotalia gaimardi	0.57	0—3.45	*Asterorotalia milletti*	2.23	0—7.28	*Quinqueloculina philippinensis*	1.90	0–5.92	*Bigenerina nodosaria*	2.38	0.81—4.74	*Agglutinella agglutinans*	2.57	0.42—10.87	*Ammonia* cf. *A. takanabensis*	2.31	0.62–6.12
Paracibicides edomica	0.57	0—3.45	*Agglutinella agglutinans*	2.18	0—5.41	*Cribroelphidium* cf. *C. detense*	1.87	0.90–5.00	*Triloculina tricarinata*	1.8	0—8.60	*Reussella spinulosa*	2.4	0—6.78	*Quinqueloculina lamarckiana*	1.96	0–4.44
Adelosina littoralis	0.27	0—1.61	*Quinqueloculina* sp.	2	0—4.5	*Triloculina tricarinata*	1.63	0.33–2.86	*Pseudorotalia indopacifica*	1.74	0—4.76	*Bigenerina nodosaria*	2.34	0—4.37	*Triloculina tricarinata*	1.96	0–8.66
Ammonia supera	0.27	0—1.61	*Bigenerina nodosaria*	1.84	0—5.41	*Agglutinella agglutinans*	1.59	0.93–2.14	*Spirotextularia floridana*	1.7	0—3.10	*Pseudorotalia indopacifica*	1.77	0.35—4.00	*Textularia haueri*	1.85	0–4.43
Bigenerina nodosaria	0.27	0—1.61	*Pseudorotalia indopacifica*	1.76	0—5.41	*Quinqueloculina incisa*	1.53	0–3.22	*Paracibicides edomica*	1.67	0—7.06	*Cancris auriculus*	1.63	0—5.67	*Cancris auriculus*	1.82	0–4.69
Elphidium indicum	0.27	0—1.61	*Asterorotalia gaimardi*	1.71	0—4.23	*Cancris auriculus*	1.03	0.31–2.25	*Proemassilina arenaria*	1.64	0.35—3.33	*Asterorotalia milletti*	1.33	0—2.71	*Pseudorotalia schroeteriana*	1.68	0–6.46
Planispirinella exigua	0.27	0—1.61	*Ammonia tepida*	1.47	0—5.41	*Textularia* sp. A	1.01	0–6.81	*Quinqueloculina philippinensis*	1.46	0—3.49	*Proemassilina arenaria*	1.09	0—2.71	*Asterorotalia gaimardi*	1.27	0–5.16
Quinqueloculina incisa	0.27	0—1.61	*Elphidium* cf. *E. advenum*	1.19	0—5.14	*Asterorotalia milletti*	0.96	0–2.96	*Asterorotalia milletti*	1.45	0—5.28	*Elphidium* cf. *E. advenum*	1.04	0—2.94	*Ammonia convexa*	1.2	0–3.25
Quinqueloculina laevigata	0.27	0—1.61	*Ammonia convexa*	1.01	0—2.82	*Heterolepa subhaidingeri*	0.89	0–2.96	*Quinqueloculina* sp.	1.12	0—3.51	*Spirotextularia fistulosa*	1.02	0—4.24	*Nonion japonicum*	1.2	0–5.02
			Massilina cf. *M. planata*	0.93	0—4.23	*Parrellina hispidula*	0.76	0–2.25	*Nubeculina divaricata*	1.09	0—4.18	*Quinqueloculina laevigata*	1.02	0—2.78	*Spirotextularia floridana*	1.04	0–2.96
			Reussella spinulosa	0.88	0—2.85	*Quinqueloculina adiazeta*	0.57	0–2.30	*Pseudorotalia schroeteriana*	0.92	0—2.46	*Planispirinella exigua*	0.99	0—2.95	*Quinqueloculina philippinensis*	1.04	0–3.45
			Elphidium indicum	0.85	0—5.45				*Spiroloculina communis*	0.85	0—2.00	*Quinqueloculina philippinensis*	0.97	0—2.46	*Cavarotalia annectens*	0.91	0–4.18
			Quinqueloculina philippinensis	0.83	0—1.69				*Quinqueloculina laevigata*	0.79	0—3.24	*Ammonia convexa*	0.88	0.34—1.47	*Thurammina* sp. A	0.8	0–7.11
			Elphidium jensoni	0.81	0—3.64				*Ammonia convexa*	0.74	0—2.71	*Adelosina littoralis*	0.81	0—2.21	*Quinqueloculina bicarinata*	0.37	0–2.37
			Heterolepa praecincta	0.81	0—5.08				*Quinqueloculina parvaggluta*	0.68	0—3.33	*Spirotextularia floridana*	0.74	0—1.84	*Spiroloculina manifesta*	0.34	0–2.08
			Paracibicides edomica	0.77	0—5.41				*Reussella spinulosa*	0.67	0—2.22	*Pyrgoella tenuiaperta*	0.71	0—2.96	*Triloculina trigonula*	0.23	0–4.79
			Cylindroclavulina bradyi	0.66	0—2.22				*Elphidium* cf. *E. advenum*	0.66	0—2.00	*Triloculinella pseudooblonga*	0.66	0—2.06	*Nonion subturgidum*	0.19	0–2.17
			Quinqueloculina incisa	0.64	0—1.82				*Discorbia candeiana*	0.65	0—4.30	*Elphidium indicum*	0.6	0—2.06			
			Discorbinella bodjongensis	0.57	0—2.70				*Cancris auriculus*	0.57	0—1.57	*Pseudorotalia schroeteriana*	0.59	0—2.09			
			Eponides repandus	0.45	0—1.82				*Eponides repandus*	0.54	0—2.02	*Nubeculina divaricata*	0.51	0—3.76			
			Cribroelphidium cf. *C. detense*	0.43	0—3.00				*Adelosina littoralis*	0.49	0—1.59	*Ammonia* cf. *A. takanabensis*	0.48	0—2.06			
			Proemassilina arenaria	0.43	0—1.69				*Quinqueloculina lamarckiana*	0.46	0—1.53	*Parrellina hispidula*	0.47	0—1.78			
			Heterolepa subhaidingeri	0.42	0—3.39				*Discorbinella bodjongensis*	0.43	0—2.11	*Eponides repandus*	0.47	0—1.37			
			Reophax sp.	0.42	0—3.39				*Quinqueloculina bicarinata*	0.41	0—2.22	*Quinqueloculina lamarckiana*	0.46	0—2.13			
			Nubeculina divaricata	0.42	0—2.00				*Quinqueloculina adiazeta*	0.39	0—2.22	*Paracibicides edomica*	0.46	0—2.22			
			Quinqueloculina adiazeta	0.42	0—1.41				*Spirotextularia fistulosa*	0.38	0—1.15	*Discorbia candeiana*	0.42	0—1.09			
			Planispirinella exigua	0.4	0—1.58				*Reophax* sp.	0.32	0—1.91	*Spiroloculina communis*	0.41	0—1.20			
			Spirotextularia floridana	0.4	0—1.5				*Pyrgoella tenuiaperta*	0.3	0—1.79	*Quinqueloculina* sp.	0.4	0—1.61			
			Quinqueloculina lamarckiana	0.37	0—1.27				*Lobatula*	0.25	0—4.74	*Cibicides* sp.	0.36	0—3.56			
			Triloculina tricarinata	0.36	0—1.47				*Quinqueloculina crassicarinata*	0.25	0—2.33	*Triloculina trigonula*	0.33	0—1.48			
			Cibicides refulgens	0.35	0—2.82				*Triloculinella pseudooblonga*	0.23	0—1.62	*Quinqueloculina adiazeta*	0.33	0—1.33			
			Elphidium sp.	0.34	0—2.70				*Assilina ammonoides*	0.23	0—2.33	*Quinqueloculina parvaggluta*	0.29	0—1.18			
			Discorbea candeiana	0.32	0—2.53				*Cibicides* sp.	0.22	0—1.60	*Quinqueloculina bicarinata*	0.29	0—1.27			
			Ammonia cf. *A. takanabensis*	0.31	0—2.00				*Ammonia* cf. *A. takanabensis*	0.2	0—2.54	*Discorbinella bodjongensis*	0.27	0—1.39			
			Quinqueloculina bicarinata	0.3	0—1.47				*Triloculina trigonula*	0.15	0—2.61	*Asterorotalia pulchella*	0.23	0—1.61			
			Reophax scorpiorus	0.28	0—2.21				*Planispirinella exigua*	0.14	0—1.43	*Ammonia tepida*	0.15	0—0.54			
			Quinqueloculina parvaggluta	0.27	0—1.69				*Spiroloculina depressa*	0.12	0—2.20	*Massilina* cf. *M. planata*	0.07	0—0.84			
			Cibicides sp.	0.24	0—1.41				*Elphidium* sp.	0.11	0—2.72	*Elphidium jensoni*	0.06	0—0.34			
			Adelosina littoralis	0.16	0—0.5				*Heterolepa subhaidingeri*	0.11	0—1.05	*Reophax* sp.	0.05	0—0.44			
			Quinqueloculina laevigata	0.12	0—0.5				*Massilina* cf. *M. planata*	0.07	0—0.38	*Heterolepa praecincta*	0.03	0—0.40			
			Triloculina trigonula	0.12	0—0.5				*Heterolepa praecincta*	0.07	0—0.63	*Assilina ammonoides*	0.02	0—.40			
			Lobatula	0.1	0—0.5				*Elphidium indicum*	0.06	0—0.73	*Quinqueloculina crassicarinata*	0.02	0—0.37			
			Quinqueloculina crassicarinata	0.06	0—0.45				*Cibicides refulgens*	0.05	0—0.39	*Elphidium* sp.	0.02	0—0.34			
			Spirotextularia fistulosa	0.06	0—0.45				*Asterorotalia pulchella*	0.03	0—0.47	*Heterolepa subhaidingeri*	0.02	0—0.34			
									Parrellina hispidula	0.03	0—0.35	*Cibicides refulgens*	0.02	0—0.29			
									Elphidium jensoni	0.02	0—0.40	*Spiroloculina depressa*	0.02	0—0.29			
									Ammonia tepida	0.01	0—0.33						
									Cribroelphidium cf. *C. detense*	0.01	0—0.33						

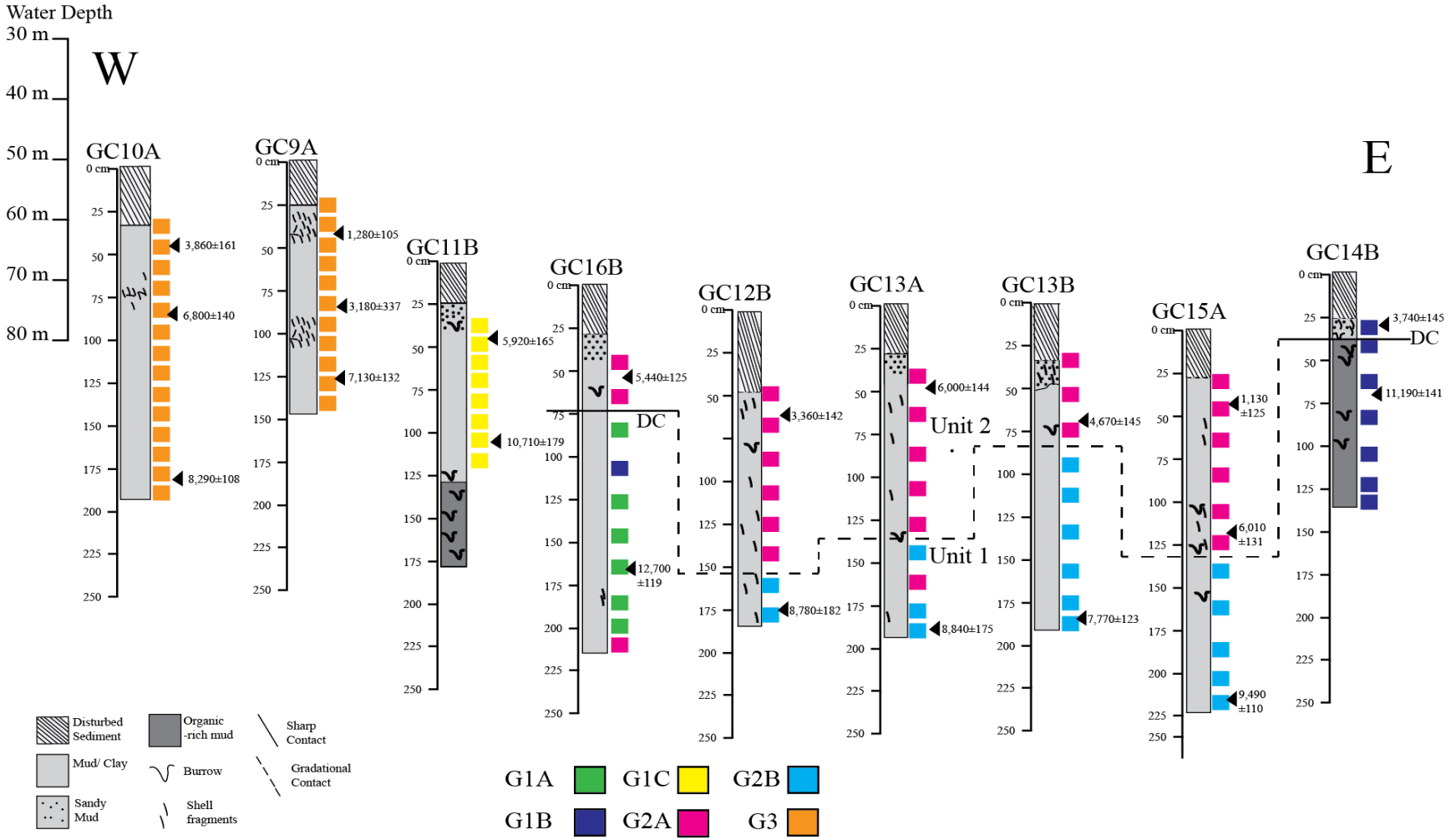

Figure 14: Lithologic logs of six cores (with calibrated radiocarbon age estimates) showing distribution of biofacies (G1A, G1B, G1C, G2A, G2B, G3), plotted against water depth of core collection. Units 1 and 2, defined on the basis of BMS, elements, percent planktonics, and the relative abundance of abundant benthic species, are indicated (dashed correlation line) for cores GC12B, GC13A, GC13B, and GC15A. These units are not present in GC10A, GC9A, GC11B, GC16B (except for 3 samples) and GC14B. UC indicates a discontinuity. The cores are organized from west to east, note that is located approximately 20 km to the north of the rest of the offshore part of the transect.

Discriminant Analysis of Foraminiferal Relative Abundance Data

A discriminant data file constructed by Martin et al. (2018) distinguished five modern benthic foraminiferal biofacies (defined by cluster analysis) that occur in order, with increasing water depth along two transects, on the Sunda Shelf in the vicinity of and to the west of the current study (Fig. 4); 1 (8–14 m water depth), 2 (21–22 m), 3 (32–41 m), 4 (44–59 m), 5 (60m) (see Fig. 4). The depth-related cluster groups were shown to be statistically distinguishable (Tables 9–11). The first three canonical discriminant functions accounted for 93.4% of the variance (Tables 9–11). The species most important for discrimination on CV1, CV2, and CV3 are shown in Table 11. Boxed data indicate the species that have the highest group means for each cluster group. The discriminant data file constructed by Martin et al. (2018) was used as a modern analogue for the classification of the down-core samples of this study.

Foraminiferal samples from the six cores of this study generally plotted between the five *a priori* groups (biofacies) of Martin et al. (2018). The predicted group membership of core samples is shown in (Table 12). Samples from cores GC12B, GC13A, GC13B (Fig. 15), and GC15A (Fig. 16) plotted in a similar location on the graph of CV1 and CV2 (representing 79% of the variance; Table 9) between all *a priori* groups. Samples belonging to cluster groups G2A and G2B were mixed together (except for GC13B) indicating the compositional similarity of the assemblages of these groups (Table 7). Generally, samples near the bottom of cores plotted with shallower *a priori* groups (Table 12).

Samples from core GC14B plotted in a similar location between *a priori* groups (biofacies; Fig. 16), but plotted closest to deeper-water *a priori* groups 3 and 5 (Fig. 16; Table 12). This is supported by classification of group membership (Table 12).

Core GC16B has two groups of samples (Fig. 16; Table 12). The six deepest samples in the core plotted closest to *a priori* groups 1 and 2, towards the left (shallow) side of CV1. Three of four remaining samples plotted between *a priori* groups 3 and 5 (Table 12).

Table 9: Canonical discriminant functions for each eigenvalue for the analysis of five *a priori* groups (biofacies) defined by cluster analysis of modern foraminiferal relative abundance data off Kuala Terengganu. From Martin et al. (2018).

Function	Eigenvalue	% of Variance	Cumulative %
CV1	129.551	52.6	52.6
CV2	63.997	26.0	78.7
CV3	34.551	14.0	92.7

Table 10: Canonical discriminant function scores at group means along three axes (functions) for the analysis of five *a priori* groups (biofacies) from Martin et al. (2018).

Cluster Group	Function		
	CV1	CV2	CV3
CGT1	-19.137	3.531	4.255
CGT2	-10.116	-13.439	-12.446
CGT3	3.831	7.653	-0.519
CGT4	7.655	4.547	-2.691
CGT5	7.926	-10.509	7.066

Table 11: Standardized canonical discriminant function coefficients for the most important species in discrimination along CV1, CV2, and CV3 and their group mean scores. Boxed data indicated the species with highest group means for each cluster group. From Martin et al. (2018).

		Group means				
		CGT1	CGT2	CGT3	CGT4	CGT5
CV1						
1.523	*Assilina ammonoides*	0.13	0.35	0.78	0.14	0.62
0.765	*Heterolepa dutemplei*	0.00	0.00	0.40	0.81	0.88
–0.822	*Peneroplis pertusus*	0.36	0.06	0.03	0.01	0.00
–0.907	*Rosalina globularis*	0.39	0.02	0.05	0.01	0.00
CV2						
2.026	*Cavarotalia annectens*	0.18	0.02	0.17	0.17	0.00
1.972	*Rosalina globularis*	0.39	0.02	0.05	0.01	0.00
–0.960	*Heterolepa praecinta*	0.00	0.00	0.00	0.04	0.26
–1.597	*Discorbinella bodjongensis*	0.19	0.02	0.32	0.26	0.41
CV3						
1.028	*Rupertianella rupertiana*	0.08	0.00	0.00	0.01	0.00
0.720	*Quinqueloculina crassicarinata*	0.09	0.07	0.06	0.01	0.16
–1.283	*Millettiana millettii*	0.36	0.02	0.14	0.02	0.00
–1.573	*Amphistegina lessonii*	0.47	1.65	0.47	0.02	0.00

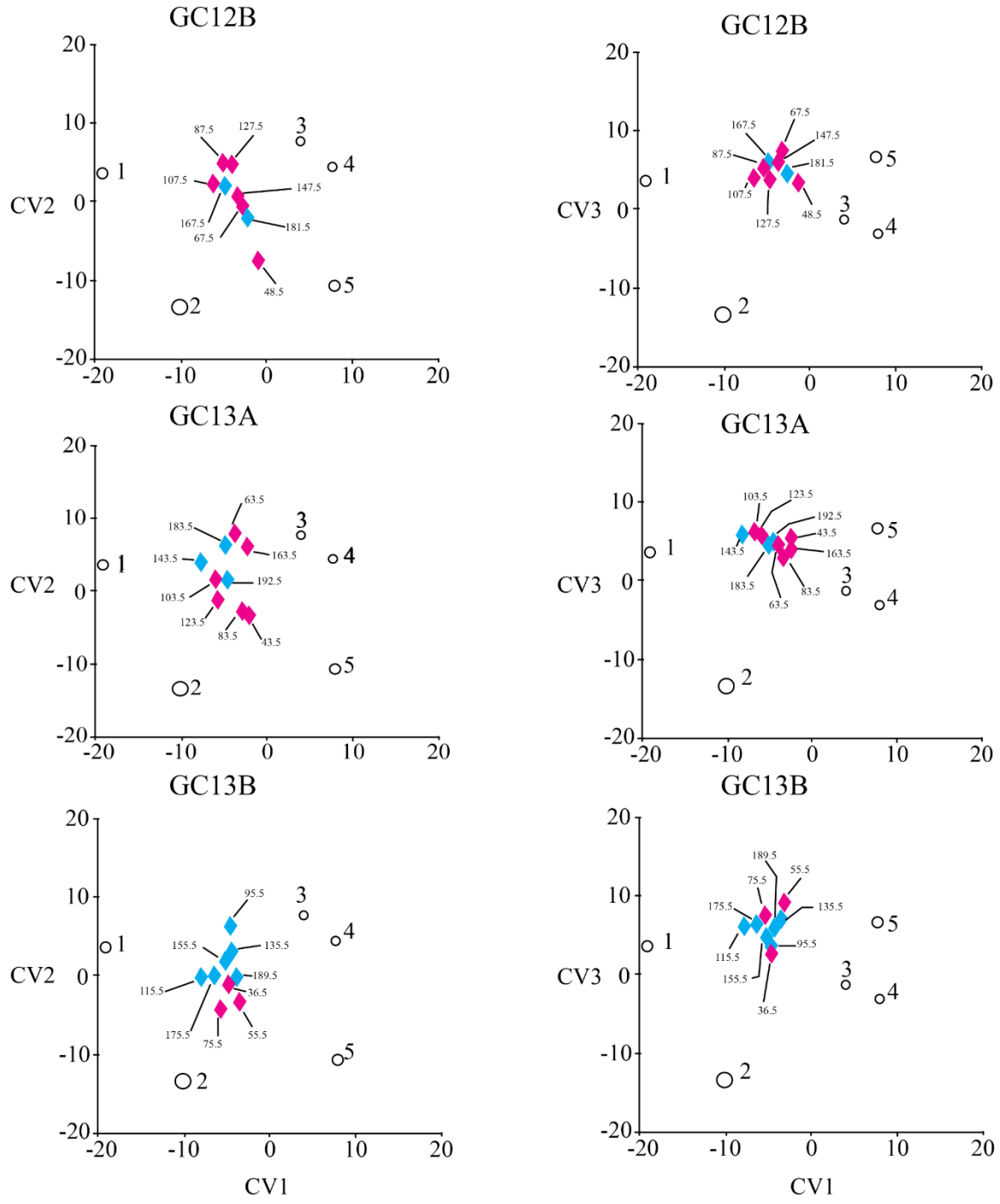

Figure 15: Results of the discriminant analysis between samples collected in this study (diamonds) and the biofacies (CGT 1–5, open circles) of Martin et al. (2018); the area within the circles represents the area of 95% confidence around group centroids. Sample colors are those of cluster groups of Figure 14.

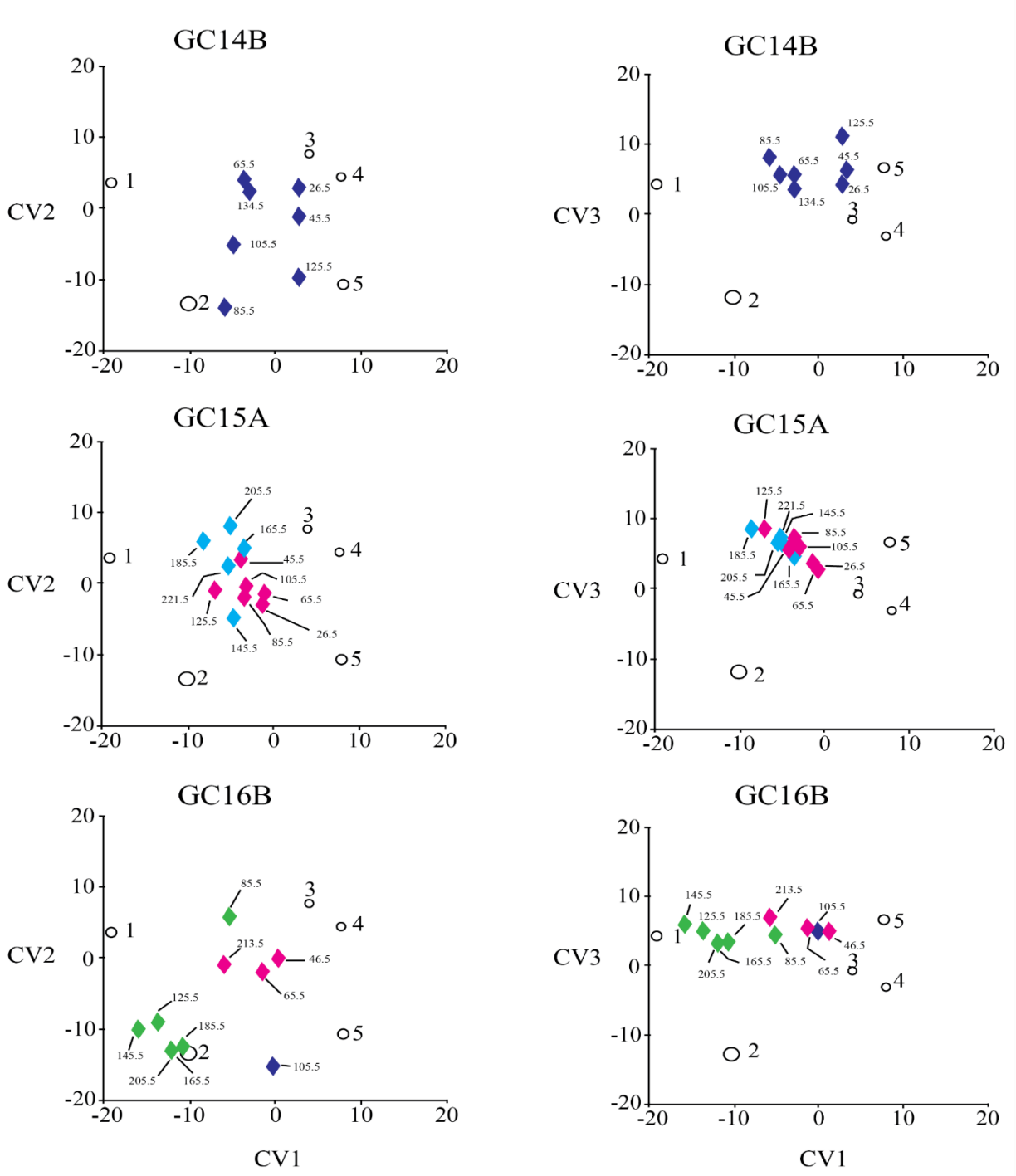

Figure 16: Results of the discriminant analysis between samples collected in this study (diamonds) and the biofacies (CGT 1–5, open circles) of Martin et al. (2018); the area within the circles represents the area of 95% confidence around group centroids. Sample colors are those of cluster groups of Figure 14.

Table 12: Probability of group membership for cores GC12B, GC13A, GC13B, GC14B, GC15A, and GC16B. Values of probability for the second highest group membership classification were only included when they were greater than 0.0009.

Sample ID	Highest Probability Group Membership	Probability of Membership	Second Highest Probability Group Membership	Probability of Membership
GC12B 48.5	5	1.000	4	
GC12B 67.5	5	.997	4	.003
GC12B 87.5	1	.997	3	.003
GC12B 107.5	1	1.000	3	
GC12B 127.5	3	1.000	4	
GC12B 147.5	4	1.000	1	
GC12B 167.5	1	1.000	3	
GC12B 181.5	5	.871	4	.129
GC13A 43.5	5	1.000	4	
GC13A 63.5	3	1.000	4	
GC13A 83.5	5	.996	4	.004
GC13A 103.5	1	1.000	3	
GC13A 123.5	1	1.000	5	
GC13A 143.5	1	1.000	3	
GC13A 163.5	3	1.000	4	
GC13A 183.5	3	1.000	1	
GC13A 192.5	1	1.000	4	
GC13B 36.5	4	.526	1	.444
GC13B 55.5	5	1.000	1	
GC13B 75.5	5	1.000	1	
GC13B 95.5	3	1.000	1	
GC13B 115.5	1	1.000	3	
GC13B 135.5	3	1.000	1	
GC13B 155.5	3	1.000	1	
GC13B 175.5	1	1.000	3	
GC13B 189.5	3	1.000	5	
GC14B 26.5	3	1.000	4	
GC14B 45.5	5	1.000	4	
GC14B 65.5	3	1.000	4	
GC14B 85.5	5	1.000	2	
GC14B 105.5	5	1.000	1	
GC14B 125.5	5	1.000	3	
GC14B 134.5	3	1.000	4	
GC15A 26.5	4	.999	5	.001
GC15A 45.5	3	1.000	4	
GC15A 65.5	4	1.000	5	
GC15A 85.5	5	1.000	3	
GC15A 105.5	4	.991	5	.009
GC15A 125.5	1	1.000	5	
GC15A 145.5	5	1.000	1	
GC15A 165.5	3	1.000	4	
GC15A 185.5	1	1.000	3	
GC15A 205.5	3	1.000	1	
GC15A 221.5	3	1.000	1	
GC16B 46.5	3	.976	4	.023
GC16B 65.5	5	1.000	3	
GC16B 85.5	1	1.000	4	
GC16B 105.5	5	1.000	2	
GC16B 125.5	1	1.000	2	
GC16B 145.5	1	1.000	2	
GC16B 165.5	2	1.000	1	
GC16B 185.5	2	1.000	1	
GC16B 205.5	2	1.000	1	
GC16B 213.5	1	1.000	3	

Samples from cores GC10A and GC9A plotted in the same location on discriminant graphs (Fig. 17). They plotted farther to the right on CV1 and closer to *a priori* groups (biofacies) 3 and 4 than samples from cores GC12B, GC13A, GC13B, and GC15A (Fig. 15–17). This is supported by predicted group membership (Table 13). The distribution of samples from core GC11B (Fig. 18) was similar to that of core GC14B (Fig. 16), between *a priori* groups 1, 2, and 4. Generally, samples deeper within the core classified with shallower *a priori* groups.

Sediments in core GC8A were radiocarbon dated as late Pleistocene in age (45,090–50,000 cal yr BP) and thus, are much older than the sediments in all other cores used in this study (Table 4; Fig. 14). Discriminant plots (Fig. 18) indicate that samples from this core plotted between *a priori* groups 3, 4, and 5 (as did samples from GC12B, GC13A, GC13B and GC15A) but somewhat closer to *a priori* group (biofacies) 4 (Fig. 18). This is supported by predicted group membership (Table 13).

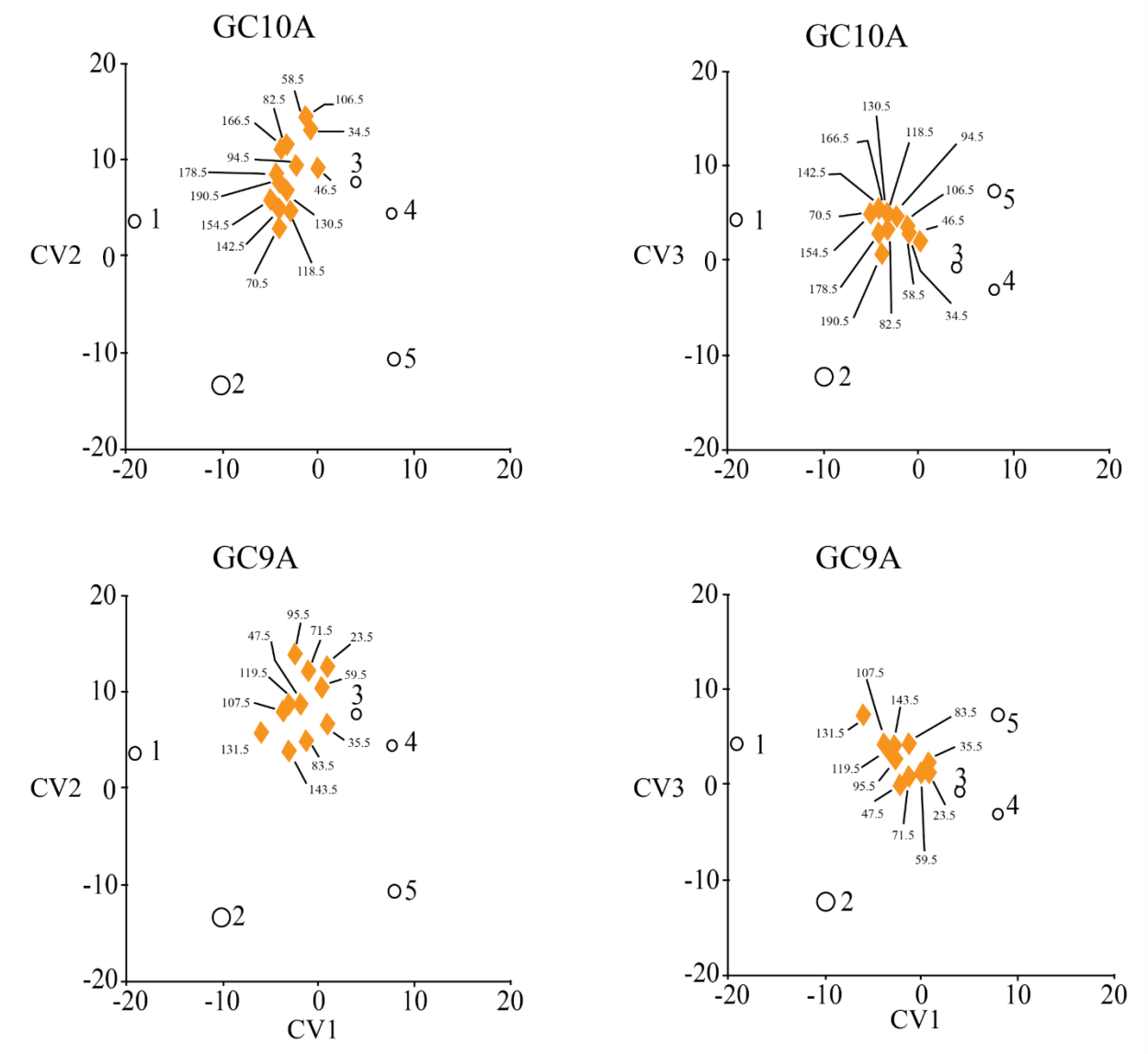

Figure 17: Results from the discrimant analysis between gravity core samples (diamonds) of Harrison (2017) and the biofacies (CGT 1–5, open circles) of Martin et al. (2018). The area within the circles represents the area of 95% confidence around group centroids. Sample colors are those of cluster groups of Figure 14.

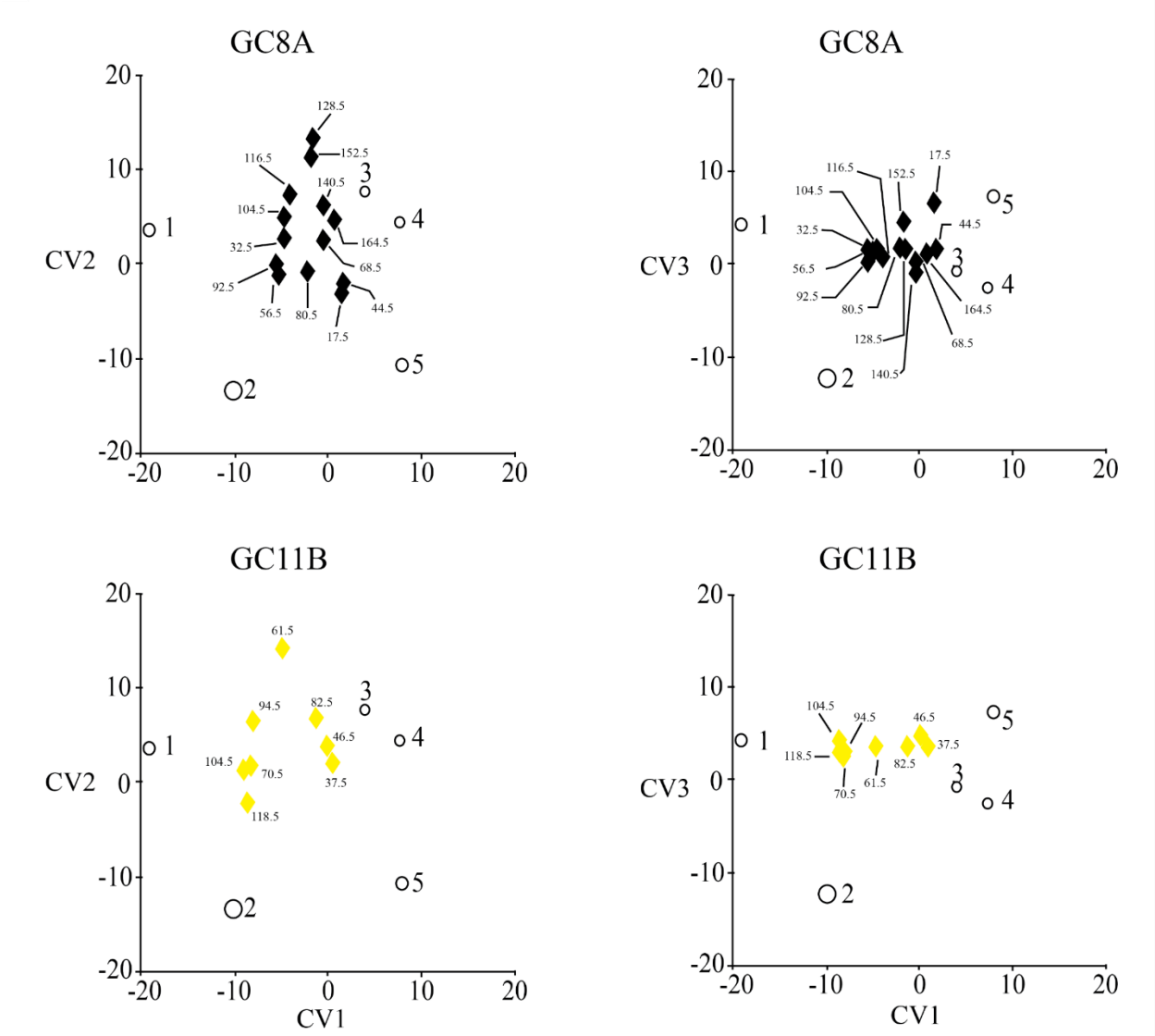

Figure 18: Results from the discrimant analysis between gravity core samples (diamonds) of Donovan (2017) and the biofacies (CGT 1–5, open circles) of Martin et al. (2018); the area within the circles represents the area of 95% confidence around group centroids. Samples from GC8A were dated to the Pleistocene. This core is not included in Figure 14. Sample colors are those of cluster groups of Figure 14.

Table 13: Probability of group membership for cores GC9A, GC10A, GC11B, and GC8A. Values of probability for the second highest group membership classification were only included when they were greater than 0.0009.

Sample ID	Highest Probability Group Membership	Probability of membership	Second Highest Probability Group Membership	Probability of membership
GC9A 23.5	3	1.000	4	
GC9A 35.5	3	1.000	4	
GC9A 47.5	4	1.000	3	
GC9A 59.5	3	1.000	4	
GC9A 71.5	3	1.000	4	
GC9A 83.5	3	1.000	5	
GC9A 95.5	3	1.000	4	
GC9A 107.5	3	1.000	5	
GC9A 119.5	3	1.000	5	
GC9A 131.5	1	.999	5	.001
GC9A 143.5	3	1.000	5	
GC10A 34.5	3	1.000	4	
GC10A 46.5	4	1.000	3	
GC10A 58.5	3	1.000	4	
GC10A 70.5	4	1.000	1	
GC10A 82.5	3	1.000	4	
GC10A 94.5	3	1.000	4	
GC10A 106.5	3	1.000	4	
GC10A 118.5	4	.756	3	.244
GC10A 130.5	3	1.000	4	
GC10A 142.5	3	1.000	4	
GC10A 154.5	3	1.000	1	
GC10A 166.5	3	1.000	4	
GC10A 178.5	3	1.000	4	
GC10A 190.5	3	1.000	4	
GC11B 37.5	4	1.000	3	
GC11B 46.5	4	1.000	3	
GC11B 61.5	3	1.000	4	
GC11B 70.5	1	1.000	3	
GC11B 82.5	4	1.000	3	
GC11B 94.5	1	1.000	3	
GC11B 104.5	1	1.000	3	
GC11B 118.5	1	1.000	4	
GC8A 17.5	5	1.000	4	
GC8A 32.5	4	1.000	1	
GC8A 44.5	4	1.000	5	
GC8A 56.5	4	.990	1	.010
-GC8A 68.5	4	1.000	3	
GC8A 80.5	4	1.000	3	
GC8A 92.5	4	1.000	1	
GC8A 104.5	4	1.000	1	
GC8A 116.5	4	1.000	3	
GC8A 128.5	4	1.000	3	
GC8A 140.5	4	1.000	3	
GC8A 152.5	3	1.000	4	
GC8A 164.5	4	1.000	3	

Discussion

Discriminant Analysis

In contrast to the results of cluster analysis of down-core foarminiferal assemblages, results of the comparison of down-core assemblages to surficial assemblages (Martin et al., 2018) using discriminant analysis generally do not conform with BMS, elemental results, geochronology and regional sea-level curves. For example, deep water group classifications are commonly overlain by shallower ones (Tables 12, 13), although regional sea-level curves predict a deepening upwards trend (Fig. 2 A, B). Furthermore, cluster analysis of foraminiferal assemblages, as well as elemental, BMS and planktonic foraminiferal data, confirm up-core deepening, i.e., greater marine influence during deposition. Differences in the treatment of foraminiferal assemblages between Martin et al. (2018) and this study could help explain this discrepency. If species recorded in Martin et al. (2018) were also found in this study, their abundances in core samples were entered into the discriminant analysis file whether or not they comprised greater than 2% or more of the assemblage in any one core sample. In addition, several species important for the discrimination of the five surface sample groups of Martin et al. (2018) did not occur in down-core samples. Indeed, the results indicate that no down-core samples contained assemblages that characterized the three shallowest biofacies (CGT1, CGT2, CGT3) of Martin et al. (2018) (Fig. 4), dominated by the larger foraminifera *Amphistegina lessonii, Amphistegina radiata,* and *Assilina ammonoides.* Had the two data sets been more similar, a more accurate classification of down-core samples would likely be possible.

Sample classification was as expected in core GC16B. The bottom six samples classified with groups 1 (8–14 m water depth) and 2 (21–22 m) of Martin et al. (2018). Three of four samples above 110 cm were classifed in groups 3 (32– 41 m water depth) and 5 (60 m) of Martin

et al. (2018). This deepening upward trend is consistent with radiocarbon age estimates and sea-level curves (Figs. 2A, 5). However, the samples that were classified in groups 1 and 2 differed from all samples in Martin et al. (2018). These samples generally contained few specimens, most of which were *Ammonia tepida* (G1A, Table 7). Some of the remaining species were also present in groups 1 and 2 of Martin et al. (2018) and thus these taxa resulted in the shallow water group classification.

Interpretation of cores GC16B and GC14B

Core GC16B is composed almost entirely of mud with an upper sandy mud unit from 30–45 cm (Fig. 5). Bulk sediment magnetic susceptibility (BMS) and elemental profiles of percent Ca, Al, Fe, and Ti show a slightly serrated profile near the bottom of the core which becomes smoother towards the top of the studied interval, except for a slight increase in percent Ca and decrease in percent Al at ca. 45 cm (Fig. 5). Foraminiferal assemblages are indicative of change at ca. 110 cm. From the bottom of the core (excluding the bottom sample) to ca 110 cm, the ubiquitous shallow water species *Ammonia tepida* dominates the benthic assemblage (Fig. 5). Planktonic foraminifera, *Heterolepa dutemplei*, and *Textularia* sp. A all appear in the core at ca. 105 cm and are relatively abundant up-core (Fig. 5). Discriminant analysis of foraminiferal assemblages indicates a deepening upward trend. Samples beneath 110 cm in core GC16B were classified with groups 1 (8–14 m water depth) and 2 (21–22 m) of Martin et al. (2018). Samples above 110 cm generally classifed with groups 3 (32– 41 m water depth) and 5 (60 m) of Martin et al. (2018). The deepening upwards trend is predicted from radiocarbon age estimates and regional sea-level curves. Given the age estimate (12,577–12,814 cal yr BP) from 167–168 cm in core GC16B, the present water depth of the core (ca. 71 m), and the position of RSL at that time (ca. -60 m), sediments in that section of core were likely deposited in water depths of ca. 10 m

(Hanebuth et al., 2011; Figs. 2, 5). An age estimate of 5,562–5,313 cal yr BP at 49–50 cm indicates deposition in water depths of ca. 75 m, ca. 3 m above present sea level (Hanebuth et al., 2011; Figs. 2, 5).

The appearance of planktonic foraminifera, the increase in calculated number of specimens/1 g of sediment, the replacement of *Ammonia tepida* by *Heterolepa dutemplei,* and the increase in species richness (S) and Fisher's α indicate rapid change in the foraminiferal assemblage. This change and the resulting interpreted water depth (Fig. 5; Table 5), based off the comparison of ragional RSL curves and geochronology, indicate a cryptic discontinuity at 110 cm in core GC16B despite homogenous lithology.

The bottom sample in core GC16B contains a foraminiferal assemblage different than those immediately above and the same as assemblages at the top of the core. This disagrees with interpreted water depths derived from age estimates and regional sea-level curves. The most likely explanation for this discrepancy is contamination resulting from core-bounce during gravity core recovery.

Core GC14B contains a more obvious discontinuity—a sharp change in lithology (from burrowed organic-rich mud to a shell-rich mud; Fig. 6). BMS and elemental profiles are relatively uniform beneath the discontinuity, and display an abrupt increase in percent Ca, and decreases in percent Al, Fe, and Ti above the lithologic change (Fig. 6). Ca-profiles show inverse relationships to those of Al, Fe, K, and Ti (elements of terrestrial weathering products see Bahr et al., 2005; Wehausen and Brumsack, 2002) indicating that the Ca is marine, biogenic and authigenic (Bahr et al., 2005). BMS values have a positive correlation with percent Al values and, therefore, they are both interpreted to represent changes in the deposition of terrestrial material. Thus, the data indicate an increase in deposition of biogenic marine Ca and a decrease

in deposition of terrestrially derived material at the sharp contact. Foraminiferal assemblages in the organic-rich mud are dominated by shallow shelf species *Asterorotalia pulchella*, *Textularia haueri*, and *Assilina ammonoides* (Minhat et al., 2016; Martin et al., 2018) and show relatively low numbers of species, and calculated number of tests/1 g sediment (Fig. 6; Table 5). The shell-rich muddy unit above the discontinuity has a higher number of species and calculated number of tests/1 g sediment (Table 5). Given the current water depth where core GC14B was collected, the sediments below the burrowed disconformity were deposited at ca. 20 m water depth (indicated by an age estimate 11,051–11,332 cal yr BP at 70–71 cm) and the sediments above in water depths ca. 71 m, 3 m above present (age estimate 3,590–3,880 cal yr BP at 35–36 cm; Figs. 2, 6).

Cores GC16B and GC14B both contain discontinuities (Figs. 4, 5). Sediments below the disconformities have foraminiferal assemblages that are dominated by *Ammonia tepida* in the former and *Asterorotalia pulchella* in the latter. *Asterorotalia pulchella* is abundant in water depths of 0 to 40 m off southeastern peninsular Malaysia (Minhat et al., 2016; Fig. 12; Table 1, 7). The increases above the contacts in marine Ca, percent planktonic foraminifera, decrease in *Ammonia tepida* and *Asterorotalia pulchella* and increase in *Heterolepa dutemplei* and *Textularia* sp. A are interpreted to represent significantly greater water depths/marine influence above the discontinuities (Figs. 5, 6; Table 1). The geological data of Alqahtani et al. (2015) indicate that cores GC16B and GC14B were collected near the western and eastern margins, respectively, of the paleo-Chao Phraya river incised valley (Fig. 1). The data from the lower parts of these cores indicate shallow, nearshore shelf environments on the margins of the flooded river valley (during late Pleistocene/early Holocene rising sea-level). The discontinuities (erosional in GC14B) were likely caused by transgression and are overlain by open shelf

foraminifera-rich mud deposited during the highstand of sea level on the Sunda Shelf ca. 6,500 cal yr BP (Hanebuth et al., 2009).

Interpretation of cores GC12B, GC13A, GC13B, and GC15A

GC12B, GC13A, GC13B, and GC15A are grouped together due to similar lithologic and foraminiferal characteristics and geochronology. The entirety of these cores is Holocene in age. Two units are distinguishable.

Unit 1 is characterized by the following values: (averaged among the cored sediments of this unit) BMS values of 5.99E-05 SI, Al 16.51 wt. %, Fe 4.94 wt. %, Ti 0.78 wt. %, and Ca 3.47 wt. % (Table 6). Unit 1 contains 3.94% planktonic foraminifera and 11.46% *Heterolepa dutemplei* (11.46%; Figs. 7–10; Table 6). Radiocarbon age estimates from Unit 1 range from 9,490 cal yr BP to 7,770 cal yr BP, indicating deposition in increasing water depth from ca. 20 m below present sea level to just prior to the highstand on the shelf (present sea level) ca. 6,500 cal yr BP (Fig. 2 A, B; Figs. 7–10). Unit 1 was deposited with significant terrestrial influence as indicated by greater values of BMS and greater percent Al, Fe, and Ti (terrestrial weathering products; Bahr et al., 2005; Wehausen and Brumsack, 2002), during an episode of sea-level rise.

Unit 2 is characterized by lower averaged values (than Unit 1): of BMS (5.32E-05 SI), Al (12.73 wt. %), Fe (3.27 wt. %), Ti (0.63 wt. %), and increased averaged values of Ca (8.75 wt. %) (Table 6). Unit 2 has significantly increased planktonic foraminifera (14.33%), increased *Heterolepa dutemplei* (14.73%) (Figs. 7–10; Table 6). Martin et al. (2018) found percent planktonic foraminifera and percent *Heterolepa dutemplei* to increase with both distance from shore and water depth. Thus, sediments of Unit 2 accumulated at greater water depths and with less terrestrial influence than Unit 1. Radiocarbon age estimates from Unit 2 range from ca.

6,610 cal yr BP to 1,130 cal yr BP indicating deposition in generally stable water depths of ca. +3 m (highstand on the Sunda Shelf ca. 6,500 cal yr BP; Hesp et al., 1998; Bird et al., 2007; Mallinson et al., 2014; Parham et al., 2014; Hanebuth et al., 2011) to present sea level (Figs. 2A, B, 7–10).

Cluster analysis also distinguished Unit 1 (group G2B) and Unit 2 (group G2A) (Fig. 12; Table 7). These units were similar (clustering together at Euclidean distance 0.5; Fig. 12) and both dominated by *Heterolepa dutemplei* (11.31% in G2B/Unit 1 and 14.65% in G2A/Unit 2) (Table 7). *Textularia* sp. A co-dominated Unit 2 (13–26%) whereas the assemblage of Unit 1 showed less dominance (seven species with mean percent greater than 5% compared to two species in Unit 2). Discriminant analysis plots illustrate cluster groups G2A (Unit 2) mixed those of G2B (Unit 1) and G2B (except for GC13B) indicating the compositional similarity of the assemblages of these groups (Figs. 15, 16; Table 7).

Cores GC12B, GC13A, GC13B, and GC15A were collected within the margins of the paleo-Chao Phraya River incised valley (Fig. 1). These cores recovered 2–3 meters of Holocene sediment within the margins of the river valley complex compared to the ca. 50 cm found on the shelf to the west, between the paleo-Terengganu and paleo-Marang core transects (indicated by the lithology of several short gravity cores, not selected for analysis, collected in this area) (Fig. 1B) and in the vicinity of the paleo-North Sunda River incised valley (Hanebuth and Stattegger, 2003; Hanebuth et al., 2011; Figs. 1A). Sediments above the discontinuities in cores GC16B and GC14B are environmentally equivalent to those of Unit 2 in the four cores taken within the paleo-Chao Phraya incised valley.

Comparison of paleo-Chao Phraya transect to paleo-Marang and paleo-Terengganu tributary transects

Nine cores were collected along the trend of the tributary paleo-Terengganu River and paleo-Marang River incised valleys (Fig. 1B). Cores GC9A, GC10A, and GC11B (Terengganu tributary; Fig. 1B) display trends in BMS and elemental data (Harrison, 2017 and Donovan, 2017) similar to those found in Unit 1 and Unit 2 in cores GC12B, GC13A, GC13B, and GC15A. BMS, Al, Fe, and Ti values are greater near the bottoms of the cores and represent greater terrestrial sediment deposition than in the overlying unit (Harrison, 2017 and Donovan, 2017), similar to Unit 1 in this study. Increased percent Ca, percent planktonic foraminifera and *Heterolepa dutemplei* are also seen in GC9A, GC10A, and GC11B beginning ca. 6,500 cal yr BP (Harrison, 2017; Donovan, 2017), similar to Unit 2 (Fig. 19). Geochronology in these cores corroborates the correlation of Units 1 and 2 to the tributary paleo-Terengganu transects (Fig. 19).

Cluster analysis of benthic foraminiferal assemblages (Fig. 13; Table 8) indicate that core GC11B (G1C; Donovan, 2017) clusters closest with GC14B, the easternmost core collected in this study, indicating similar depositional environments to the east and west of the paleo-Chao Phraya River valley margins. Cores GC10A and GC9A (G3; Harrison, 2017) clustered together and separately from the rest of core samples, however, they clustered more closely with G1A, G1B, and G1C indicating similarity to these assemblages. Primary productivity, sediment grain size, calcium carbonate content, salinity and total organic carbon are some of the factors influencing the distribution of foraminiferal assemblages (Szarek et al., 2006, Minhat et al., 2016, and Martin et al., 2018). It is likely that changes in these factors, with both increasing distance from shore and water depth, are responsible for the similarity of samples of GC9A and

GC10A, and dissimilarity to the rest of the core samples (Fig. 13, 14; Table 8). When foraminiferal samples from cores GC9A, GC10A, and GC11B were analyzed (cluster analysis) separately from the cores collected in this study, similar transitions from a lower Unit 1 to an upper Unit 2 were recognized in the foraminiferal assemblages ca. 6,500 cal yr BP (Harrison, 2017 and Donovan, 2017). These are indicated on Figure 19.

Tributary paleo-Marang River cores GC1, GC2, GC3, and GC4 (Fig. 1) were collected in water depths ranging 52 to 56 m (Reed, 2016). The base of the cores contained a late Pleistocene peaty mud dated to 12,411–12,012 cal yr BP (identified as a coastal wetland material) which ends at a sharp contact, overlain by a foraminiferal rich, green to brown shelly sandy mud dated at 5,262–4963 cal yr BP to 421–254 cal yr BP. The shelly sandy mud is of open marine origin as indicated by the presence of planktonic foraminifera (Reed, 2017). The lower coastal wetland unit in these cores was deposited penecontemporaneously with the lower sections of cores GC16B and GC14B which exhibit similar age estimates and represent shallower-water depth (nearer shore) depositional environments. The overlying foraminiferal-rich marine mud in the paleo-Marang River tributary cores, as supported by BMS, geochronology, elemental data, and the presence of planktonic foraminifera, was deposited coevally and in similar environments as the upper Holocene muds of the paleo-Chao Phraya River cores. Cores GC5 and GC7, collected farther east along the trend of the tributary paleo-Marang River incised valley (Fig. 1; Hindes, 2017), exhibit two units similar to those found in GC12B, GC13A, GC13B, and GC15A. Hindes (2017) described Unit 1 as having higher values of BMS, wt. % Al, wt. % Fe, and lower values of wt. % Ca, compared to the overlying unit. This was interpreted as indicating a unit with high terrestrial input during deposition. The overlying Unit 2 exhibited increases in percent marine Ca and percent planktonic foraminifera (Hindes,

2017), similar to Unit 2 of this study. Unit 1 transitioned to Unit 2 ca. 6,500 cal yr BP (Hindes, 2017), as it did in cores GC9A, GC10A, (Harrison, 2017), and GC11B (Donovan, 2017) and the cores collected in this study within the margins of the paleo-Chao Phraya incised river valley (Fig. 19).

Core GC8A is a paleo-Terengganu tributary core containing sediments dated to the Pleistocene (45,090– 50,000 cal yr BP). BMS and elemental data show no major patterns possibly due to post-depositional diagenesis of foraminiferal tests (Donovan, 2017). Percent planktonic foraminifera increase up-core, indicating a deepening upwards trend. The geochronology of this core and increase in planktonic foraminifera suggest an open marine, neritic depositional environment, from a previous interglacial period. *Asterorotalia pulchella* and *Hanzawaia nipponica* are the most dominant benthic foraminifera in GC8A, similar to core samples from GC11B (Donovan, 2017). High abundance of these species is also found in samples from GC14B and GC16B, indicating late-Pleistocene depositional environments of GC8A were similar to the transgressional environments of GC11B, GC16B, and GC14B.

Regional Comparison and Sequence Stratigraphy

Cores GC12B, GC13A, GC13B, and GC15A were collected within the margins of the paleo-Chao Phraya river incised valley and show greater accumulation of Holocene sediment (Fig. 19) compared to the thin (ca. 1 m) veneer of Holocene sediment elsewhere on the shelf (Hanebuth et al., 2011). Holocene sediment collected over the paleo-Marang River, paleo-Terengganu River and paleo-Chao Phraya River incised valleys can be divided into Unit 1 and Unit 2. The boundary between these units correlates with the onset of the 6,500 cal yr BP highstand on the shelf but is variable due to sediment deposition rate and range in radiocarbon age estimation. The cores collected near the margins of the paleo-Chao Phraya River incised

valley, core GC16B and GC14B, contain less than 1 m of Holocene sediment, separated by discontinuities from underlying late Pleistocene/early Holocene shallow marine deposits that also correlate with the 6,500 cal yr BP highstand. Cores collected along the tributary incised valleys of the paleo-Marang and paleo-Terengganu Rivers, by Hindes (2016), Reed (2016), Harrison (2017) and Donovan (2017) (Fig. 1B), indicate units similar to Unit 1 and Unit 2 found in this study, underlain disconformably by late Pleistocene coastal plain material in the four cores taken closest to shore (Fig. 19).

The ca. 16 m thick Holocene sediment record interpreted to lie within the margins of the paleo-Chao Phraya River incised valley by Alqahtani et al. (2015) has not been found. Holocene sediment accumulation within the margins of the paleo-Chao Phraya is only ca. 2 to 3 m (Fig. 19), similar to that recorded by Hanebuth and Stattegger (2003) and Hanebuth et al. (2011) in the paleo-North Sunda River incised valley.

The stratigraphic record of this study closely resembles that of the upper units offshore of peninsular Malaysia in the Malacca Strait (Emmel and Curray, 1982), the seismic interpretations of Evans et al. (1995) between Borneo and SE peninsular Malaysia, and the suite of cores collected within the incised valley of the paleo-North Sunda River by Hanebuth and Stattegger (2003). The late Pleistocene/early Holocene marine deposits (Unit 1) are likely an upper part of their transgressive unit, formed during the marine transgression on the Sunda Shelf (Fig 2). Unit 2 of this study and the Holocene foraminiferal-rich muds found in the tributary river valleys (Hindes, 2016; Reed, 2016; Harrison, 2017; Donovan, 2017; Fig 1B) are part of the surficial Holocene unit of Emmel and Curray (1982), Evans et al. (1995) and Hanebuth and Stattegger (2003). Unit 1 transitions to Unit 2 ca. 6,500 cal yr BP at the onset of the highstand on the shelf.

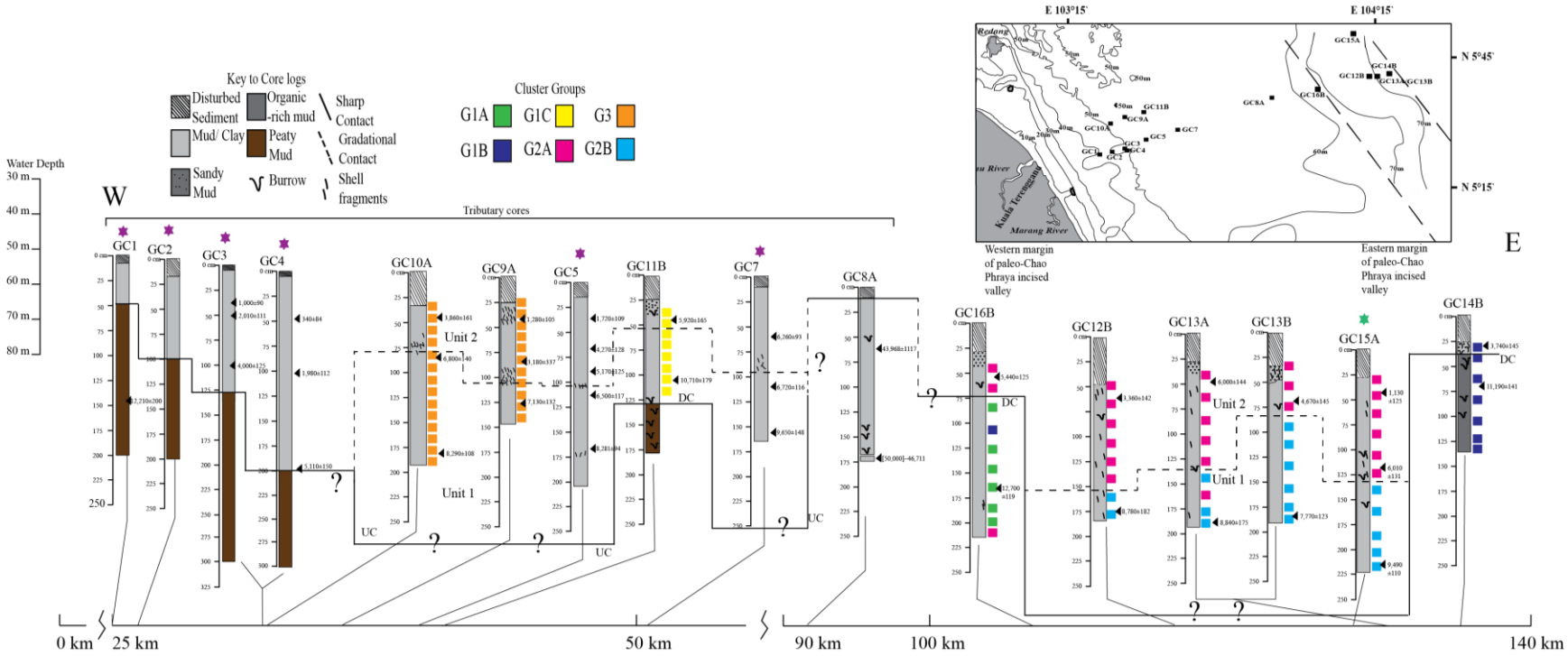

Figure 19. Cores collected in this study, and well as cores collected along the trends on the tributary incised valleys of the paleo-Terengganu and paleo-Marang rivers, plotted against water depth with distance from shore indicated. The dashed line indicates the correlation line of ca. 6,500 cal yr BP, at the start of the highstand on the shelf. Cluster groups from Figure 14 are indicated by colored boxes. Calibrated radiocarbon age range midpoints indicated by black arrowheads. The solid line with question marks indicates the subaerial to submarine discontinuity (DC) that approximates the Pleistocene/Holocene boundary. Purple stars indicate cores that were collected along the trend of the paleo-Marang incised river valley. Green star indicates a core taken off-transect in the paleo-Chao Phraya river incised valley.

A sequence stratigraphic model (Catuneanu, 2002; Loutit et al., 1988; Allan and Posamentier, 1993; Hunt and Tucker, 1992) can be applied to the cores collected in this study and the tributary paleo-Marang and paleo-Terengganu incised valley core transects. The cores collected by Reed (2017) contain a peaty mud near the base of the cores that was interpreted to be coastal mangrove swamp sediments, dated to the late Pleistocene (12,411–12,012 cal yr BP), that likely represents deposition during transgression (Fig. 20). The discontinuity on top of the coastal plain material represents a transgressive ravinement surface (TRS; Loutit et al., 1988; Catuneanu, 2002). The TRS was also recovered in Terengganu transect cores GC11B and GC8A, the latter containing part of a Pleistocene sequence as indicated by radiocarbon age estimates, but was not penetrated in the other cores (Fig. 19A, 20). This surface is overlain, basinward, by the transgressive systems tract (TST) which was deposited as sea-level rose ca. 21,000 cal yr BP–6,500 cal yr BP, flooding the exposed shelf and incised valleys. The TST is thicker (2 to 3 m versus <1 m) where incised valleys provided increased accommodation space. It is composed of the sediments found beneath the discontinuities in cores GC16B and GC14B and by Unit 1 (Fig. 19A, 20). The deposits correlate with the transgressive unit described by Evans et al. (1995) and Hanebuth and Stattegger (2003), i.e., a succession of terrestrial to shoreline to marine deposits underlain by a subaerial to submarine discontinuity. The dashed surface (Fig. 19) overlying the TST is the maximum flooding surface (MFS), which separates the TST from the highstand systems tract at ca. 6,500 cal yr BP (Loutit et al., 1988; Allan and Posamentier, 1993). The highstand systems tract (HST) is the surficial unit exposed on the shelf, between the MFS and seabed, containing Unit 2 and the surficial sediments of GC1, GC2, GC3, and GC4. It was deposited from ca. 6,500 cal yr BP, consistent with the regional sea-level highstand, to present as sea-level fell 1.3–3 m to 5 m (Hesp et al., 1998; Bird et al., 2007; Hanebuth et al., 2011;

Mallinson et al., 2014; Parham et al., 2014; Fig. 2). The HST is part of the surficial Holocene unit described by Emmel and Curray (1982), Evans et al. (1995), Hanebuth and Stattegger (2003), and Hanebuth et al. (2011), i.e., a thin, foraminiferal-rich, flat-lying sedimentary cover susceptible to reworking.

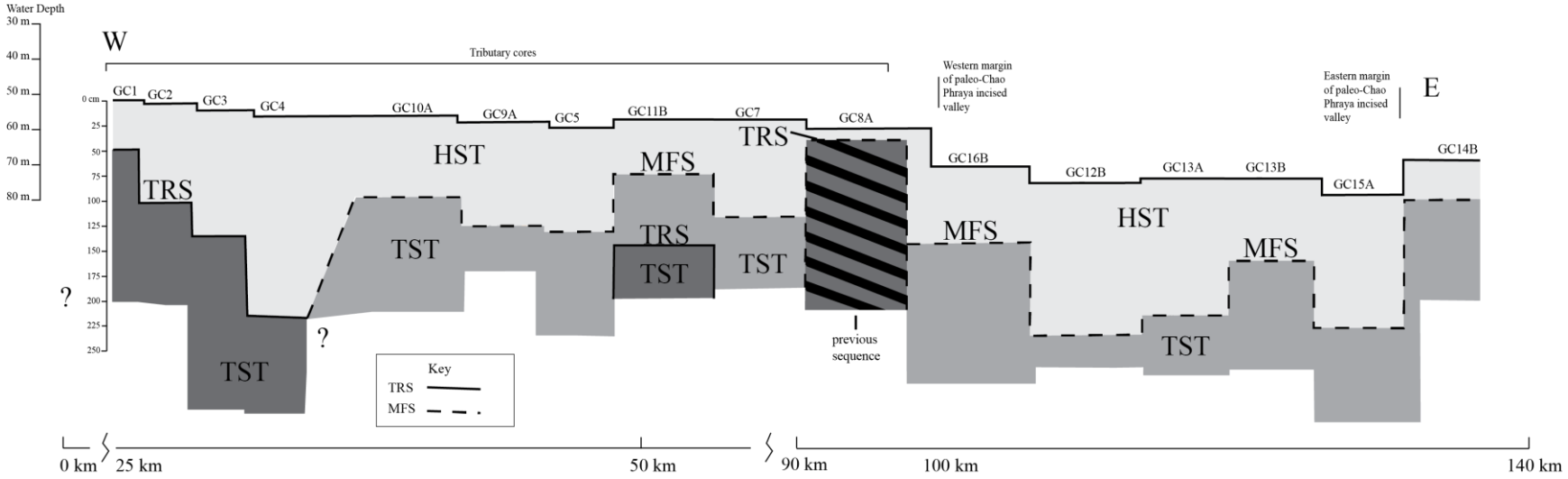

Figure 20. A sequence stratigraphic interpretation of Fig. 19, showing the transgressive ravinement surface (TRS), transgressive systems tract (TST), the maximum flooding surface (MFS), and the highstand systems tract (HST).

Conclusions

The cores collected in the paleo-Chao Phraya River incised valley (this study), and those collected in the incised river valleys of paleo-Terengganu and paleo-Marang incised valleys, are geologically consistent with the findings of Hanebuth and Stattegger (2003) and Hanebuth et al. (2011) and exhibit a Holocene foraminiferal-rich mud, 2 to 3 meters thick in channel structures, that is generally <1m thick over the Sunda Shelf.

Two Holocene units, Unit 1 and Unit 2, are distinguished in the cores collected within the paleo-Chao Phraya incised valley and tributary incised valleys on the basis of geochronology, bulk sediment magnetic susceptibility data, elemental analysis, and changes in foraminiferal assemblages. Unit 1 was deposited during late stage transgression on the Sunda Shelf (oldest date 12,814–12,577) and Unit 2 was deposited ca. 6,500 cal yr BP (the onset of the regional highstand) to present.

A sequence stratigraphic model applied to the cores collected on the Sunda shelf and, with comparison to regional sea-level curves, supports the following:

1. As RSL rose and the shelf was inundated (post-LGM; ca. 21,000 cal yr BP to 6,500 cal yr BP), coastal wetland deposits (peaty mud) transitioned upward and seaward to open shelf deposits, still with significant terrestrial influence. This represents the transgressive systems tract.
2. The maximum flooding surface occurs 6,500 cal yr BP. It is overlain by the highstand systems tract (ca. 1 m thick) and is characterized by greater marine influence during deposition.

References

Allen, G., Posamentier, H., 1993, Sequence stratigraphy and facies model of an incised valley fill: The Gironde Estuary, France: Journal of Sedimentary Petrology, v. 63, p. 378–391.

Alqahtani, F., Johnson, H., Jackson, C., Som, R., 2015, Nature, origin and evolution of a Late Pleistocene incised valley-fill, Sunda Shelf, Southeast Asia: Sedimentology, v. 62, p. 1198–1232.

Bahr, A., Lamy, F., Arz, H., Kuhlmann, H., Wefer, G., 2005, Late glacial to Holocene climate and sedimentation history in the NW Black Sea: Marine Geology, v. 214, p. 309–322.

Biswas, B., 1976, Bathymetry of Holocene Foraminifera and Quaternary sea-level changes on the Sunda Shelf: Journal of Foraminiferal Research, v. 6, p. 107–133.

Bird, M., Fifield, L., The, T., Chang, C., Shirlaw, N., Lambeck, K., 2007, An inflection in the rate of early mid-Holocene eustatic sea-level rise: a new sea-level curve from Singapore: Estuarine, Earth and Planetary Science letters, Coastal and Shelf Science, v. 71. p. 523–536.

Bradley, S., Milne, G., Horton, B., Zong, Y., 2016, Modelling sea level data from China and Malay-Thailand to estimate Holocene ice-volume equivalent sea level change: Quaternary Science Reviews, v. 137, p. 54–68.

Brijker, J. M., Jung, S. J. A., Ganssen, G. M., Bickert, T., Kroon, D., ENSO related decadal scale climate variability from the Indo-Pacific Warm Pool: Earth and Planetary Science Letters, v. 253, p. 67–82.

Buzas, M., 1979, The measurement of species analyses of unispecies and multispecies populations of foraminifera: Ecology, v. 51, p. 874–879.

Catuneanu, O., 2002, Sequence stratigraphy of clastic systems: concepts, merits, and pitfalls: Journal of African Earth Sciences, v. 35/1, p. 1–43.

Cearreta, A., Garcia-Artola, A., Leorri, E., Irabien, M., Masque, P., 2013, Recent environmental evolution of regenerated salt marshes in the southern Bay of Biscay: anthropogenic evidences in their sedimentary record: Journal of Marine Systems, v. 109–110, p. 203–212.

Clark, J. A., Farrell, W. E., Peltier, W. R., 1978, Global changes in postglacial sea level: a numerical calculation: Quaternary Research, v. 9, p. 265–287.

Culver, S., Leorri, E., Mallinson, D., Corbett, D., Shazili, N. A. M., 2015, Recent coastal evolution and sea-level rise, Setiu wetland, peninsular Malaysia: Paleogeography, Paleoclimatology, Paleoecology, v. 417, p. 406–421.

Culver, S., Mallinson, D., Corbett, D., Leorri, E., Rouf, A., Shazili, N., Yaacob, R., Whittaker, J., Buzas, M., Parham, P., 2012, Distribution of foraminifera in the Setiu estuary and lagoon Terengganu, Malaysia: Journal of Foraminiferal Research, v. 42, p. 109–133.

Dickerson, R.E., 1941. Molengraaff River: a drowned Pleistocene stream and other Asian evidences bearing upon the lowering of sea level during the Ice Age. In: Bowen, N.L., Cushman, J.A., Dickerson, R.E. (Eds.), Shiftings of Sea Floors and Coast Lines: University of Pennsylvania, Bicentennial Conference, Philadelphia.

Donovan, B., 2016, A Multiproxy Paleoenvironmental Reconstruction of Marine Sediments from Two Interglacials: Sunda Shelf, southern South China Sea: Unpublished Master's Thesis, East Carolina University, p. 1–48.

Emmel, F.J., and Curray, J.R., 1982, A Submerged Late Pleistocene delta and other features related to sea level changes in the Malacca Strait: Marine Geology, v. 47, p. 192–216.

Evans, C.D.R., Brett, C.P., James, J.W.C., and Holmes, R., 1995, Shallow seismic reflection profiles from the waters of East and Southeast Asia: an interpretation manual and atlas: British Geological Survey, Technical Report WC/94/60, p. 66–67.

Fairbanks, R., 1989, A 17,000-year glacio-eustatic sea level record: influence of glacial melting rates on the Younger Dryas event and deep-ocean circulation: Nature, v. 342, p. 637–642.

Fang, W., Guo, Z., Huang, Y., 1998, Observational study of the circulation in the southern South China Sea: Chinese Science Bulletin, v. 43, p. 898–905.

Fang, G., Wang, G., Fang, Y., Fang, W., 2012, A review on the South China Sea western boundary current: Acta Oceanologica Sinica, v. 31, p. 1–10.

Geyh, M., Kudrass, H., Streif, H., 1979, Sea-level changes during the late Pleistocene and Holocene in the Strait of Malacca: Nature, v. 278, p. 441–443.

Graham, J.J. and Militante, P.J., 1959, Recent foraminifera form the Puerto Galera area, northern Mindoro, Philippines: Stanford University Publications, Geological Sciences, v. 6, p. 1-171.

Haig, D. W., 1988, Miliolid foraminifera from inner neritic sand and mud facies of the Papuan Lagoon, New Guinea: Journal of Foraminiferal Research, v. 18, p. 203–236.

Hanebuth, T. J. J., Stattegger, K., 2003, The stratigraphic evolution of the Sunda Shelf during the past fifty thousand years: Tropical Deltas of Southeast Asia: Sedimentology, Stratigraphy, and Petroleum Geology, v. 76, p. 189 –200.

Hanebuth, T., Stattegger, K., Bojanowski, A., 2009, Termination of the Last Glacial Maximum sea-level lowstand: the Sunda-Shelf data revisited: Global and Planetary Change, v. 66, p. 76–84.

Hanebuth, T., Stattegger, K., Grootes, P.M., 2000, Rapid flooding of the Sunda Shelf: A late-glacial sea-level record: Science, v. 288, p. 1033–1035.

Hanebuth, T., Voris, H., Yokoyama, Y., Saito, Y., Okuno, J., 2011, Formation and fate of sedimentary depocentres on Southeast Asia's Sunda Shelf over the past sea-level cycle and biogeographic implications: Earth-Science Reviews, v. 204, p. 92–110.

Harrison, E.I., 2017, Holocene Paleoenvironmental Reconstruction of the Sunda Shelf, off Northeastern Peninsular Malaysia. Unpublished Master's thesis, East Carolina University, p. 1–51.

Hesp, P., Hung, C., Hilton, M., Ming, C., Turner, I., 1998, A first tentative Holocene sea-level curve for Singapore: Journal of Coastal Research, v. 14, p. 308–314.

Hindes, H., 2016, Holocene Sedimentary Record from the Sunda Shelf off Peninsular Malaysia: Insights from Elemental, Isotopic and Bulk Sediment Magnetic Susceptibility Analyses: Unpublished Master's Thesis, East Carolina University, p. 1–36.

Horton, B., Gibbard, P., Milne, G., Morley, R., Purintavaragual, C., Stargardt, J., 2005, Holocene sea levels and paleoenvironments, Malay-Thai Peninsula southeast Asia: The Holocene, v. 15, p. 1199–1213.

Jones, R. W., 1994, The Challenger Foraminifera: Oxford University Press, London, 149 p.

Ke, Z., Tan, Y., Ma, Y., Huang, L., Wang, S., 2014, Effects of surface current patterns on spatial variations of phytoplankton communities and environmental factors in Sunda Shelf, Continental Shelf Research, v. 82, p. 119–127.

Leorri, E., Cearreta, A., Irabien., M. J., Garcia-artola, A., Corbett, D. R., Horsman, E., Blake, W. H., Sanchez-Cabeza, J.A., 2014, Anthropogenic disruptions of the sedimentary record in coastal marshes: Examples from the southern Bay of Biscay (N. Spain): Continental Shelf Research, v. 86, p. 132–140.

Liu, Q., Jiang, X., Xie, S-P, Liu, W.T., 2004, A gap in the Indo-Pacific warm pool over the South China Sea in boreal winter: seasonal development and interannual variability: Journal of Geophysical Research, v. 109, p. 1–10.

Loeblich, A. R., Tappan, H., 1987, Foraminiferal Genera and their Classification: Van Nostrand Reinhold Company, New York, 1182 p.

Loeblich, A. R., Tappan, H., 1994, Foraminifera of the Sahul Shelf and Timor Sea: Cushman Foundation for Foraminiferal Research, Special Publication, no. 31, 638 p.

Loutit, T. S., Harbenbol, J., Vail, P. R., Baum, G.R., 1988, Condensed Sections: The Key to Age Determination and Correlation of Continental Margin Sequences: The Society of Economic Paleontologists and Mineralogists, Special Publication, no. 42, p. 118–213.

Luu, Q. H., Tkalich, P., Tay, T. W., 2015, Sea level trend and variability around Peninsular Malaysia: Ocean Science, v. 11, p. 617–628.

Mallinson, D.J., Culver, S.J., Corbett, D.R., Parham, P.R., Shazili, N.A.M., and Yaacob, R., 2014, Holocene coastal response to monsoons and relative sea-level changes in northeast peninsular Malaysia: Journal of Asian Earth Sciences, v. 91, p. 194–205.

Martin, S.Q., Culver, S.J., Leorri, E., Mallinson, D.J., Buzas, M.A., Hayek, L.A.C., and Shazili, N.A.M., 2018. Distribution and Taxonomy of Modern Benthic Foraminifera of the Western Sunda Shelf (South China Sea) off Peninsular Malaysia: Cushman Foundation for Foraminiferal Research, Special Publication, no. 31, 112 p.

Mello, J., Buzas, M., 1968, An application of cluster analysis as a method of determining biofacies: Journal of Paleontology, v. 42, p. 747–758.

Minhat, F., Satyanarayana, B., Husain, M., Rajan, V., 2016, Modern benthic foraminifera in subtidal waters of Johor: implications for Holocene sea-level change on the east coast of peninsular Malaysia: Journal of Foraminiferal Research, v. 46, p. 347–357.

Molengraaff, G.A.F., 1921, Modern deep-sea research in the East Indian archipelago: Geographic Journal, v. 57, p. 95–121.

Molengraaff, G. A. F., Weber, M., 1921, On the relation between the Pleistocene glacial period and the origin of the Sunda Sea (Java– and South China– Sea), and its influence on the distribution of coral reefs and on the land and freshwater fauna: Proceedings, Royal Academy of Amsterdam. Vol XXIII, Communicated at the meeting of Nov. 29, 1919, p. 395-439.

Parham, P., Saito, Y., Sapon, N., Suriadi, R., Mohtar, N., Evidence for ca. 7-ka maximum Holocene transgression on the peninsular Malaysia east coast: Journal of Quaternary Science. v. 29, p. 414–422.

Pelejero, C., Kienast, M., Wang, L., Grimalt, J., 1999, The flooding of Sundaland during the last deglaciation: imprints in hemipelagic sediments from the southern South China Sea: Earth and Planetary Science Letters, v. 171, p. 661–671.

Reed, D., 2016. Mid-to-Late Holocene Environmental Change on the Sunda Shelf off NE Peninsular Malaysia: Unpublished Master's paper, East Carolina University, p. 1–49.

Skowronek, F., Sagemann, J., Stenzel, F., Schulz, H., 1994, Evolution of heavy-metal profiles in River Weser estuary sediments, Germany: Environmental Geology, v. 24, p. 223–232.

Southon, J., Kashgarian, M., Fontugne, M., Metivier, B., Yim, W., 2002, Marine reservoir corrections for the Indian Ocean and Southeast Asia: Radiocarbon, v. 44, p. 167–180.

Stuiver, M., Grootes, P.M., 2000, GISP2 oxygen isotope ratios: Quaternary Research, v. 53, p. 277–284.

Suriadi, R.B. 2016. Distribution Patterns of Modern Benthic Foraminifera and Late Quaternary Geologic History of the Inner Shelf of the South China Sea, Peninsular Malaysia. Unpublished PhD dissertation, Universiti Malaysia Terengganu, 326 p.

Szarek, R., 2001, Biodiversity and Biogeography of Recent Benthic Foraminiferal Assemblages in the South-Western South China Sea (Sunda Shelf): PhD dissertation, University of Kiel, 273 p.

Szarek, R., Kuhnt, W., Kawamura, H., Kitazato, H., 2006, Distribution of recent benthic foraminifera on the Sunda Shelf (South China Sea): Marine Micropaleontology, v. 61, p. 171–195.

Wehausen, R. and Brumsack, H., 2002, Astronomical forcing of the East Asian monsoon mirrored by the composition of Pliocene South China Sea sediments: Earth and Planetary Science Letters, v. 201, p. 621–636.

Whittaker, J. E, Hodgkinson, R. L., 1979, Foraminifera of the Togopi Formation, eastern Sabah, Malaysia: Bulletin of the British Museum (Natural History), Geology v. 31, p. 1–120.

Woodson, A.L., Leorri, E., Culver, S.J., Mallinson, D.J., Parham, P.R., Thunell, R.C., Vijayan, V.R., Curtis, S., 2017, Sea-surface temperatures for the last 7200 years from the eastern Sunda Shelf, South China Sea: climatic inferences from planktonic foraminiferal Mg/Ca ratios: Quaternary Science Reviews, v. 165, p. 13–24.

Yu, K., and Chen, T., 2009, Beach sediments from Northern South China Sea suggest high and oscillating sea levels during the late Holocene: Earth Science Frontiers, v. 16 (6), p. 138–145.

Appendix A.

Bulk sediment magnetic susceptibility data showing all five replicates.

Sample ID	KRe[SI]	KVol[SI]
GC15A-26-27C	4.99E-05	9.08E-05
GC15A-26-27C	5.03E-05	9.15E-05
GC15A-26-27C	4.99E-05	9.07E-05
GC15A-26-27C	5.01E-05	9.10E-05
GC15A-26-27C	5.04E-05	9.15E-05
GC15A-35-36C	5.54E-05	1.01E-04
GC15A-35-36C	5.60E-05	1.02E-04
GC15A-35-36C	5.59E-05	1.02E-04
GC15A-35-36C	5.60E-05	1.02E-04
GC15A-35-36C	5.62E-05	1.02E-04
GC15A-40-41C	4.56E-05	8.30E-05
GC15A-40-41C	4.69E-05	8.53E-05
GC15A-40-41C	4.67E-05	8.49E-05
GC15A-40-41C	4.69E-05	8.52E-05
GC15A-40-41C	4.70E-05	8.55E-05
GC15A-45-46C	5.85E-05	1.06E-04
GC15A-45-46C	5.95E-05	1.08E-04
GC15A-45-46C	5.92E-05	1.08E-04
GC15A-45-46C	5.95E-05	1.08E-04
GC15A-45-46C	5.95E-05	1.08E-04
GC15A-55-56C	5.05E-05	9.19E-05
GC15A-55-56C	5.02E-05	9.13E-05
GC15A-55-56C	5.11E-05	9.29E-05
GC15A-55-56C	5.11E-05	9.30E-05
GC15A-55-56C	5.11E-05	9.30E-05
GC15A-65-66C	5.23E-05	9.51E-05
GC15A-65-66C	5.35E-05	9.73E-05
GC15A-65-66C	5.35E-05	9.72E-05
GC15A-65-66C	5.38E-05	9.78E-05
GC15A-65-66C	5.37E-05	9.77E-05
GC15A-70-71C	6.45E-05	1.17E-04
GC15A-70-71C	6.51E-05	1.18E-04
GC15A-70-71C	6.53E-05	1.19E-04
GC15A-70-71C	6.56E-05	1.19E-04
GC15A-70-71C	6.58E-05	1.20E-04
GC15A-75-76C	5.23E-05	9.50E-05
GC15A-75-76C	5.30E-05	9.63E-05
GC15A-75-76C	5.27E-05	9.59E-05
GC15A-75-76C	5.35E-05	9.73E-05

GC15A-75-76C	5.35E-05	9.72E-05
GC15A-85-86C	4.84E-05	8.80E-05
GC15A-85-86C	4.85E-05	8.82E-05
GC15A-85-86C	4.95E-05	9.00E-05
GC15A-85-86C	4.96E-05	9.01E-05
GC15A-85-86C	4.97E-05	9.04E-05
GC15A-95-96C	5.28E-05	9.59E-05
GC15A-95-96C	5.34E-05	9.71E-05
GC15A-95-96C	5.32E-05	9.66E-05
GC15A-95-96C	5.38E-05	9.79E-05
GC15A-95-96C	5.34E-05	9.71E-05
GC15A100-101	5.84E-05	1.06E-04
GC15A100-101	5.86E-05	1.07E-04
GC15A100-101	5.86E-05	1.07E-04
GC15A100-101	5.88E-05	1.07E-04
GC15A100-101	5.86E-05	1.07E-04
GC15A105-106	4.57E-05	8.31E-05
GC15A105-106	4.62E-05	8.40E-05
GC15A105-106	4.63E-05	8.42E-05
GC15A105-106	4.64E-05	8.44E-05
GC15A105-106	4.64E-05	8.43E-05
GC15A115-116	6.00E-05	1.09E-04
GC15A115-116	6.06E-05	1.10E-04
GC15A115-116	6.10E-05	1.11E-04
GC15A115-116	6.07E-05	1.10E-04
GC15A115-116	6.11E-05	1.11E-04
GC15A125-126	6.83E-05	1.24E-04
GC15A125-126	6.84E-05	1.24E-04
GC15A125-126	6.92E-05	1.26E-04
GC15A125-126	6.89E-05	1.25E-04
GC15A125-126	6.90E-05	1.26E-04
GC15A130-131	7.26E-05	1.32E-04
GC15A130-131	7.31E-05	1.33E-04
GC15A130-131	7.27E-05	1.32E-04
GC15A130-131	7.34E-05	1.33E-04
GC15A130-131	7.37E-05	1.34E-04
GC15A135-136	7.46E-05	1.36E-04
GC15A135-136	7.51E-05	1.37E-04
GC15A135-136	7.52E-05	1.37E-04
GC15A135-136	7.52E-05	1.37E-04
GC15A135-136	7.52E-05	1.37E-04
GC15A145-146	7.81E-05	1.42E-04
GC15A145-146	7.92E-05	1.44E-04

GC15A145-146	7.92E-05	1.44E-04
GC15A145-146	7.95E-05	1.45E-04
GC15A145-146	7.93E-05	1.44E-04
GC15A155-156	7.92E-05	1.44E-04
GC15A155-156	7.98E-05	1.45E-04
GC15A155-156	7.97E-05	1.45E-04
GC15A155-156	7.98E-05	1.45E-04
GC15A155-156	7.98E-05	1.45E-04
GC15A160-161	7.47E-05	1.36E-04
GC15A160-161	7.48E-05	1.36E-04
GC15A160-161	7.51E-05	1.36E-04
GC15A160-161	7.50E-05	1.36E-04
GC15A160-161	7.50E-05	1.36E-04
GC15A165-166	8.19E-05	1.49E-04
GC15A165-166	8.25E-05	1.50E-04
GC15A165-166	8.29E-05	1.51E-04
GC15A165-166	8.27E-05	1.50E-04
GC15A165-166	8.26E-05	1.50E-04
GC15A175-176	8.97E-05	1.63E-04
GC15A175-176	9.11E-05	1.66E-04
GC15A175-176	9.13E-05	1.66E-04
GC15A175-176	9.11E-05	1.66E-04
GC15A175-176	9.14E-05	1.66E-04
GC15A185-186	7.95E-05	1.45E-04
GC15A185-186	8.04E-05	1.46E-04
GC15A185-186	8.05E-05	1.46E-04
GC15A185-186	8.05E-05	1.46E-04
GC15A185-186	8.05E-05	1.46E-04
GC15A190-191	8.01E-05	1.46E-04
GC15A190-191	8.05E-05	1.46E-04
GC15A190-191	8.02E-05	1.46E-04
GC15A190-191	8.07E-05	1.47E-04
GC15A190-191	8.07E-05	1.47E-04
GC15A195-196	7.69E-05	1.40E-04
GC15A195-196	7.70E-05	1.40E-04
GC15A195-196	7.70E-05	1.40E-04
GC15A195-196	7.71E-05	1.40E-04
GC15A195-196	7.71E-05	1.40E-04
GC15A205-206	7.84E-05	1.43E-04
GC15A205-206	7.87E-05	1.43E-04
GC15A205-206	7.88E-05	1.43E-04
GC15A205-206	7.87E-05	1.43E-04
GC15A205-206	7.87E-05	1.43E-04

GC15A215-216	8.80E-05	1.60E-04
GC15A215-216	8.80E-05	1.60E-04
GC15A215-216	8.80E-05	1.60E-04
GC15A215-216	8.83E-05	1.61E-04
GC15A215-216	8.80E-05	1.60E-04
GC15A219-220	8.01E-05	1.46E-04
GC15A219-220	8.06E-05	1.47E-04
GC15A219-220	8.06E-05	1.47E-04
GC15A219-220	8.05E-05	1.46E-04
GC15A219-220	8.06E-05	1.47E-04
GC15A221-222	7.85E-05	1.43E-04
GC15A221-222	7.85E-05	1.43E-04
GC15A221-222	7.86E-05	1.43E-04
GC15A221-222	7.86E-05	1.43E-04
GC15A221-222	7.88E-05	1.43E-04
GC15A221-222	8.17E-05	1.49E-04
GC15A221-222	8.19E-05	1.49E-04
GC15A221-222	8.21E-05	1.49E-04
GC15A221-222	8.20E-05	1.49E-04
GC15A221-222	8.21E-05	1.49E-04
GC13A43-44CM	5.83E-05	1.06E-04
GC13A43-44CM	5.84E-05	1.06E-04
GC13A43-44CM	5.82E-05	1.06E-04
GC13A43-44CM	5.82E-05	1.06E-04
GC13A43-44CM	5.84E-05	1.06E-04
GC13A53-54CM	5.92E-05	1.08E-04
GC13A53-54CM	5.97E-05	1.09E-04
GC13A53-54CM	5.98E-05	1.09E-04
GC13A53-54CM	5.95E-05	1.08E-04
GC13A53-54CM	5.98E-05	1.09E-04
GC13A58-59CM	6.38E-05	1.16E-04
GC13A58-59CM	6.43E-05	1.17E-04
GC13A58-59CM	6.43E-05	1.17E-04
GC13A58-59CM	6.44E-05	1.17E-04
GC13A58-59CM	6.44E-05	1.17E-04
GC13A63-64CM	5.41E-05	9.84E-05
GC13A63-64CM	5.42E-05	9.86E-05
GC13A63-64CM	5.41E-05	9.84E-05
GC13A63-64CM	5.43E-05	9.86E-05
GC13A63-64CM	5.43E-05	9.87E-05
GC13A73-74CM	5.00E-05	9.10E-05
GC13A73-74CM	5.05E-05	9.18E-05
GC13A73-74CM	5.06E-05	9.21E-05

GC13A73-74CM	5.06E-05	9.20E-05
GC13A73-74CM	5.07E-05	9.21E-05
GC13A83-84CM	4.40E-05	7.99E-05
GC13A83-84CM	4.45E-05	8.08E-05
GC13A83-84CM	4.43E-05	8.05E-05
GC13A83-84CM	4.46E-05	8.10E-05
GC13A83-84CM	4.46E-05	8.10E-05
GC13A88-89CM	4.67E-05	8.49E-05
GC13A88-89CM	4.71E-05	8.56E-05
GC13A88-89CM	4.70E-05	8.54E-05
GC13A88-89CM	4.71E-05	8.56E-05
GC13A88-89CM	4.71E-05	8.57E-05
GC13A93-94CM	4.58E-05	8.34E-05
GC13A93-94CM	4.64E-05	8.44E-05
GC13A93-94CM	4.63E-05	8.41E-05
GC13A93-94CM	4.65E-05	8.45E-05
GC13A93-94CM	4.65E-05	8.46E-05
GC13A103-104	5.48E-05	9.96E-05
GC13A103-104	5.51E-05	1.00E-04
GC13A103-104	5.50E-05	1.00E-04
GC13A103-104	5.50E-05	1.00E-04
GC13A103-104	5.50E-05	1.00E-04
GC13A113-114	5.67E-05	1.03E-04
GC13A113-114	5.71E-05	1.04E-04
GC13A113-114	5.73E-05	1.04E-04
GC13A113-114	5.73E-05	1.04E-04
GC13A113-114	5.73E-05	1.04E-04
GC13A118-119	5.64E-05	1.03E-04
GC13A118-119	5.67E-05	1.03E-04
GC13A118-119	5.67E-05	1.03E-04
GC13A118-119	5.69E-05	1.04E-04
GC13A118-119	5.71E-05	1.04E-04
GC13A123-124	4.98E-05	9.06E-05
GC13A123-124	5.02E-05	9.13E-05
GC13A123-124	5.03E-05	9.15E-05
GC13A123-124	5.01E-05	9.12E-05
GC13A123-124	5.05E-05	9.17E-05
GC13A133-134	5.67E-05	1.03E-04
GC13A133-134	5.69E-05	1.03E-04
GC13A133-134	5.69E-05	1.03E-04
GC13A133-134	5.68E-05	1.03E-04
GC13A133-134	5.69E-05	1.03E-04
GC13A143-144	5.90E-05	1.07E-04

GC13A143-144	5.92E-05	1.08E-04
GC13A143-144	5.95E-05	1.08E-04
GC13A143-144	5.95E-05	1.08E-04
GC13A143-144	5.96E-05	1.08E-04
GC13A148-149	5.49E-05	9.98E-05
GC13A148-149	5.53E-05	1.00E-04
GC13A148-149	5.53E-05	1.01E-04
GC13A148-149	5.55E-05	1.01E-04
GC13A148-149	5.54E-05	1.01E-04
GC13A153-154	5.25E-05	9.55E-05
GC13A153-154	5.27E-05	9.57E-05
GC13A153-154	5.26E-05	9.56E-05
GC13A153-154	5.29E-05	9.61E-05
GC13A153-154	5.29E-05	9.62E-05
GC13A163-164	5.87E-05	1.07E-04
GC13A163-164	5.90E-05	1.07E-04
GC13A163-164	5.89E-05	1.07E-04
GC13A163-164	5.91E-05	1.07E-04
GC13A163-164	5.90E-05	1.07E-04
GC13A173-174	5.09E-05	9.25E-05
GC13A173-174	5.11E-05	9.29E-05
GC13A173-174	5.12E-05	9.32E-05
GC13A173-174	5.13E-05	9.33E-05
GC13A173-174	5.13E-05	9.33E-05
GC13A178-179	6.04E-05	1.10E-04
GC13A178-179	6.06E-05	1.10E-04
GC13A178-179	6.03E-05	1.10E-04
GC13A178-179	6.07E-05	1.10E-04
GC13A178-179	6.07E-05	1.10E-04
GC13A183-184	5.12E-05	9.31E-05
GC13A183-184	5.16E-05	9.38E-05
GC13A183-184	5.19E-05	9.43E-05
GC13A183-184	5.16E-05	9.39E-05
GC13A183-184	5.18E-05	9.43E-05
GC13A192-193	5.64E-05	1.03E-04
GC13A192-193	5.69E-05	1.04E-04
GC13A192-193	5.71E-05	1.04E-04
GC13A192-193	5.71E-05	1.04E-04
GC13A192-193	5.71E-05	1.04E-04
GC14B26-27CM	3.16E-05	5.75E-05
GC14B26-27CM	3.17E-05	5.77E-05
GC14B26-27CM	3.20E-05	5.81E-05
GC14B26-27CM	3.20E-05	5.83E-05

GC14B26-27CM	3.23E-05	5.86E-05
GC14B35-36CM	2.71E-05	4.93E-05
GC14B35-36CM	2.70E-05	4.91E-05
GC14B35-36CM	2.77E-05	5.04E-05
GC14B35-36CM	2.75E-05	4.99E-05
GC14B35-36CM	2.78E-05	5.05E-05
GC14B40-41CM	3.00E-05	5.45E-05
GC14B40-41CM	3.03E-05	5.51E-05
GC14B40-41CM	3.08E-05	5.60E-05
GC14B40-41CM	3.08E-05	5.60E-05
GC14B40-41CM	3.09E-05	5.62E-05
GC14B45-46CM	2.01E-05	3.66E-05
GC14B45-46CM	2.06E-05	3.75E-05
GC14B45-46CM	2.07E-05	3.76E-05
GC14B45-46CM	2.10E-05	3.82E-05
GC14B45-46CM	2.08E-05	3.79E-05
GC14B55-56CM	1.90E-05	3.46E-05
GC14B55-56CM	1.87E-05	3.40E-05
GC14B55-56CM	1.96E-05	3.57E-05
GC14B55-56CM	1.99E-05	3.62E-05
GC14B55-56CM	1.99E-05	3.61E-05
GC14B65-66CM	2.06E-05	3.74E-05
GC14B65-66CM	2.09E-05	3.80E-05
GC14B65-66CM	2.11E-05	3.84E-05
GC14B65-66CM	2.13E-05	3.88E-05
GC14B65-66CM	2.16E-05	3.92E-05
GC14B70-71CM	2.33E-05	4.24E-05
GC14B70-71CM	2.40E-05	4.36E-05
GC14B70-71CM	2.38E-05	4.33E-05
GC14B70-71CM	2.40E-05	4.36E-05
GC14B70-71CM	2.39E-05	4.34E-05
GC14B75-76CM	2.38E-05	4.33E-05
GC14B75-76CM	2.39E-05	4.35E-05
GC14B75-76CM	2.40E-05	4.36E-05
GC14B75-76CM	2.39E-05	4.35E-05
GC14B75-76CM	2.41E-05	4.39E-05
GC14B85-86CM	2.40E-05	4.37E-05
GC14B85-86CM	2.42E-05	4.40E-05
GC14B85-86CM	2.46E-05	4.47E-05
GC14B85-86CM	2.45E-05	4.45E-05
GC14B85-86CM	2.43E-05	4.43E-05
GC14B95-96CM	2.79E-05	5.08E-05
GC14B95-96CM	2.83E-05	5.15E-05

GC14B95-96CM	2.83E-05	5.14E-05
GC14B95-96CM	2.81E-05	5.11E-05
GC14B95-96CM	2.86E-05	5.19E-05
GC14B100-101	2.73E-05	4.96E-05
GC14B100-101	2.80E-05	5.08E-05
GC14B100-101	2.77E-05	5.04E-05
GC14B100-101	2.82E-05	5.12E-05
GC14B100-101	2.80E-05	5.10E-05
GC14B105-106	2.65E-05	4.82E-05
GC14B105-106	2.67E-05	4.86E-05
GC14B105-106	2.69E-05	4.90E-05
GC14B105-106	2.69E-05	4.89E-05
GC14B105-106	2.70E-05	4.92E-05
GC14B115-116	2.86E-05	5.19E-05
GC14B115-116	2.87E-05	5.21E-05
GC14B115-116	2.86E-05	5.20E-05
GC14B115-116	2.87E-05	5.23E-05
GC14B115-116	2.88E-05	5.24E-05
GC14B125-126	2.75E-05	5.00E-05
GC14B125-126	2.78E-05	5.05E-05
GC14B125-126	2.82E-05	5.12E-05
GC14B125-126	2.86E-05	5.19E-05
GC14B125-126	2.81E-05	5.11E-05
GC14B130-131	2.46E-05	4.47E-05
GC14B130-131	2.53E-05	4.61E-05
GC14B130-131	2.52E-05	4.59E-05
GC14B130-131	2.53E-05	4.60E-05
GC14B130-131	2.55E-05	4.64E-05
GC14B134-135	2.90E-05	5.28E-05
GC14B134-135	3.02E-05	5.48E-05
GC14B134-135	3.03E-05	5.52E-05
GC14B134-135	3.05E-05	5.55E-05
GC14B134-135	3.03E-05	5.51E-05
GC16B46-47CM	5.79E-05	1.05E-04
GC16B46-47CM	5.86E-05	1.07E-04
GC16B46-47CM	5.86E-05	1.07E-04
GC16B46-47CM	5.88E-05	1.07E-04
GC16B46-47CM	5.87E-05	1.07E-04
GC16B55-56CM	5.55E-05	1.01E-04
GC16B55-56CM	5.59E-05	1.02E-04
GC16B55-56CM	5.68E-05	1.03E-04
GC16B55-56CM	5.74E-05	1.04E-04
GC16B55-56CM	5.69E-05	1.04E-04

GC16B60-61CM	6.35E-05	1.15E-04
GC16B60-61CM	6.38E-05	1.16E-04
GC16B60-61CM	6.42E-05	1.17E-04
GC16B60-61CM	6.39E-05	1.16E-04
GC16B60-61CM	6.41E-05	1.17E-04
GC16B65-66CM	6.33E-05	1.15E-04
GC16B65-66CM	6.33E-05	1.15E-04
GC16B65-66CM	6.34E-05	1.15E-04
GC16B65-66CM	6.34E-05	1.15E-04
GC16B65-66CM	6.34E-05	1.15E-04
GC16B75-76CM	6.32E-05	1.15E-04
GC16B75-76CM	6.35E-05	1.16E-04
GC16B75-76CM	6.37E-05	1.16E-04
GC16B75-76CM	6.34E-05	1.15E-04
GC16B75-76CM	6.32E-05	1.15E-04
GC16B85-86CM	6.19E-05	1.13E-04
GC16B85-86CM	6.21E-05	1.13E-04
GC16B85-86CM	6.28E-05	1.14E-04
GC16B85-86CM	6.31E-05	1.15E-04
GC16B85-86CM	6.31E-05	1.15E-04
GC16B90-91CM	6.41E-05	1.16E-04
GC16B90-91CM	6.47E-05	1.18E-04
GC16B90-91CM	6.47E-05	1.18E-04
GC16B90-91CM	6.48E-05	1.18E-04
GC16B90-91CM	6.50E-05	1.18E-04
GC16B95-96CM	6.07E-05	1.10E-04
GC16B95-96CM	6.05E-05	1.10E-04
GC16B95-96CM	6.05E-05	1.10E-04
GC16B95-96CM	6.09E-05	1.11E-04
GC16B95-96CM	6.07E-05	1.10E-04
GC16B105-106	6.64E-05	1.21E-04
GC16B105-106	6.65E-05	1.21E-04
GC16B105-106	6.66E-05	1.21E-04
GC16B105-106	6.70E-05	1.22E-04
GC16B105-106	6.69E-05	1.22E-04
GC16B115-116	6.15E-05	1.12E-04
GC16B115-116	6.15E-05	1.12E-04
GC16B115-116	6.28E-05	1.14E-04
GC16B115-116	6.26E-05	1.14E-04
GC16B115-116	6.26E-05	1.14E-04
GC16B120-121	6.21E-05	1.13E-04
GC16B120-121	6.31E-05	1.15E-04
GC16B120-121	6.28E-05	1.14E-04

GC16B120-121	6.26E-05	1.14E-04
GC16B120-121	6.32E-05	1.15E-04
GC16B125-126	5.81E-05	1.06E-04
GC16B125-126	5.79E-05	1.05E-04
GC16B125-126	5.85E-05	1.06E-04
GC16B125-126	5.86E-05	1.07E-04
GC16B125-126	5.88E-05	1.07E-04
GC16B135-136	6.11E-05	1.11E-04
GC16B135-136	6.15E-05	1.12E-04
GC16B135-136	6.10E-05	1.11E-04
GC16B135-136	6.16E-05	1.12E-04
GC16B135-136	6.17E-05	1.12E-04
GC16B145-146	5.26E-05	9.56E-05
GC16B145-146	5.30E-05	9.64E-05
GC16B145-146	5.31E-05	9.66E-05
GC16B145-146	5.29E-05	9.62E-05
GC16B145-146	5.30E-05	9.63E-05
GC16B150-151	5.85E-05	1.06E-04
GC16B150-151	5.93E-05	1.08E-04
GC16B150-151	5.95E-05	1.08E-04
GC16B150-151	6.01E-05	1.09E-04
GC16B150-151	6.02E-05	1.09E-04
GC16B155-156	4.73E-05	8.60E-05
GC16B155-156	4.72E-05	8.58E-05
GC16B155-156	4.74E-05	8.62E-05
GC16B155-156	4.72E-05	8.59E-05
GC16B155-156	4.79E-05	8.71E-05
GC16B165-166	3.72E-05	6.76E-05
GC16B165-166	3.84E-05	6.98E-05
GC16B165-166	3.87E-05	7.04E-05
GC16B165-166	3.85E-05	6.99E-05
GC16B165-166	3.85E-05	7.00E-05
GC16B175-176	4.43E-05	8.05E-05
GC16B175-176	4.43E-05	8.05E-05
GC16B175-176	4.47E-05	8.12E-05
GC16B175-176	4.47E-05	8.13E-05
GC16B175-176	4.49E-05	8.16E-05
GC16B180-181	4.83E-05	8.78E-05
GC16B180-181	5.00E-05	9.09E-05
GC16B180-181	5.00E-05	9.10E-05
GC16B180-181	4.95E-05	9.00E-05
GC16B180-181	4.97E-05	9.04E-05
GC16B185-186	3.31E-05	6.01E-05

GC16B185-186	3.31E-05	6.01E-05
GC16B185-186	3.38E-05	6.15E-05
GC16B185-186	3.41E-05	6.19E-05
GC16B185-186	3.39E-05	6.17E-05
GC16B195-196	3.42E-05	6.22E-05
GC16B195-196	3.45E-05	6.27E-05
GC16B195-196	3.47E-05	6.30E-05
GC16B195-196	3.45E-05	6.28E-05
GC16B195-196	3.51E-05	6.38E-05
GC16B205-206	7.41E-05	1.35E-04
GC16B205-206	7.50E-05	1.36E-04
GC16B205-206	7.51E-05	1.37E-04
GC16B205-206	7.54E-05	1.37E-04
GC16B205-206	7.56E-05	1.38E-04
GC16B210-211	2.83E-05	5.15E-05
GC16B210-211	2.82E-05	5.14E-05
GC16B210-211	2.82E-05	5.13E-05
GC16B210-211	2.87E-05	5.21E-05
GC16B210-211	2.85E-05	5.18E-05
GC16B213-214	3.11E-05	5.65E-05
GC16B213-214	3.19E-05	5.80E-05
GC16B213-214	3.19E-05	5.80E-05
GC16B213-214	3.20E-05	5.81E-05
GC16B213-214	3.19E-05	5.80E-05
GC12B48-49CM	4.00E-05	7.27E-05
GC12B48-49CM	4.18E-05	7.60E-05
GC12B48-49CM	4.15E-05	7.55E-05
GC12B48-49CM	4.12E-05	7.50E-05
GC12B48-49CM	4.19E-05	7.62E-05
GC12B57-58CM	4.97E-05	9.04E-05
GC12B57-58CM	4.99E-05	9.07E-05
GC12B57-58CM	5.06E-05	9.20E-05
GC12B57-58CM	5.08E-05	9.23E-05
GC12B57-58CM	5.05E-05	9.19E-05
GC12B62-63CM	4.94E-05	8.97E-05
GC12B62-63CM	5.02E-05	9.14E-05
GC12B62-63CM	5.02E-05	9.13E-05
GC12B62-63CM	5.03E-05	9.14E-05
GC12B62-63CM	5.02E-05	9.13E-05
GC12B67-68CM	4.99E-05	9.06E-05
GC12B67-68CM	5.14E-05	9.35E-05
GC12B67-68CM	5.22E-05	9.49E-05
GC12B67-68CM	5.20E-05	9.46E-05

GC12B67-68CM	5.23E-05	9.50E-05
GC12B77-78CM	5.30E-05	9.63E-05
GC12B77-78CM	5.33E-05	9.69E-05
GC12B77-78CM	5.36E-05	9.74E-05
GC12B77-78CM	5.41E-05	9.84E-05
GC12B77-78CM	5.37E-05	9.76E-05
GC12B87-88CM	6.44E-05	1.17E-04
GC12B87-88CM	6.47E-05	1.18E-04
GC12B87-88CM	6.47E-05	1.18E-04
GC12B87-88CM	6.52E-05	1.19E-04
GC12B87-88CM	6.52E-05	1.19E-04
GC12B92-93CM	6.14E-05	1.12E-04
GC12B92-93CM	6.09E-05	1.11E-04
GC12B92-93CM	6.17E-05	1.12E-04
GC12B92-93CM	6.18E-05	1.12E-04
GC12B92-93CM	6.11E-05	1.11E-04
GC12B97-98CM	6.71E-05	1.22E-04
GC12B97-98CM	6.74E-05	1.23E-04
GC12B97-98CM	6.75E-05	1.23E-04
GC12B97-98CM	6.77E-05	1.23E-04
GC12B97-98CM	6.78E-05	1.23E-04
GC12B107-108	6.01E-05	1.09E-04
GC12B107-108	6.00E-05	1.09E-04
GC12B107-108	6.01E-05	1.09E-04
GC12B107-108	6.05E-05	1.10E-04
GC12B107-108	6.05E-05	1.10E-04
GC12B117-118	5.77E-05	1.05E-04
GC12B117-118	5.83E-05	1.06E-04
GC12B117-118	5.86E-05	1.07E-04
GC12B117-118	5.88E-05	1.07E-04
GC12B117-118	5.87E-05	1.07E-04
GC12B122-123	5.27E-05	9.57E-05
GC12B122-123	5.23E-05	9.51E-05
GC12B122-123	5.28E-05	9.60E-05
GC12B122-123	5.31E-05	9.65E-05
GC12B122-123	5.36E-05	9.74E-05
GC12B127-128	5.52E-05	1.00E-04
GC12B127-128	5.68E-05	1.03E-04
GC12B127-128	5.65E-05	1.03E-04
GC12B127-128	5.65E-05	1.03E-04
GC12B127-128	5.69E-05	1.03E-04
GC12B137-138	5.83E-05	1.06E-04
GC12B137-138	5.80E-05	1.06E-04

GC12B137-138	5.90E-05	1.07E-04
GC12B137-138	5.88E-05	1.07E-04
GC12B137-138	5.93E-05	1.08E-04
GC12B147-148	6.28E-05	1.14E-04
GC12B147-148	6.29E-05	1.14E-04
GC12B147-148	6.33E-05	1.15E-04
GC12B147-148	6.32E-05	1.15E-04
GC12B147-148	6.32E-05	1.15E-04
GC12B152-153	7.10E-05	1.29E-04
GC12B152-153	7.24E-05	1.32E-04
GC12B152-153	7.27E-05	1.32E-04
GC12B152-153	7.27E-05	1.32E-04
GC12B152-153	7.24E-05	1.32E-04
GC12B157-158	7.03E-05	1.28E-04
GC12B157-158	7.06E-05	1.28E-04
GC12B157-158	7.05E-05	1.28E-04
GC12B157-158	7.07E-05	1.29E-04
GC12B157-158	7.10E-05	1.29E-04
GC12B167-168	7.28E-05	1.32E-04
GC12B167-168	7.43E-05	1.35E-04
GC12B167-168	7.39E-05	1.34E-04
GC12B167-168	7.44E-05	1.35E-04
GC12B167-168	7.51E-05	1.37E-04
GC12B177-178	7.88E-05	1.43E-04
GC12B177-178	7.88E-05	1.43E-04
GC12B177-178	7.92E-05	1.44E-04
GC12B177-178	7.95E-05	1.45E-04
GC12B177-178	7.93E-05	1.44E-04
GC12B181-182	8.48E-05	1.54E-04
GC12B181-182	8.52E-05	1.55E-04
GC12B181-182	8.59E-05	1.56E-04
GC12B181-182	8.58E-05	1.56E-04
GC12B181-182	8.62E-05	1.57E-04
GC13B36-37CM	4.03E-05	7.32E-05
GC13B36-37CM	4.16E-05	7.56E-05
GC13B36-37CM	4.13E-05	7.52E-05
GC13B36-37CM	4.14E-05	7.52E-05
GC13B36-37CM	4.12E-05	7.48E-05
GC13B45-46CM	3.04E-05	5.53E-05
GC13B45-46CM	3.08E-05	5.60E-05
GC13B45-46CM	3.06E-05	5.56E-05
GC13B45-46CM	3.12E-05	5.68E-05
GC13B45-46CM	3.09E-05	5.61E-05

GC13B50-51CM	2.82E-05	5.12E-05
GC13B50-51CM	2.93E-05	5.33E-05
GC13B50-51CM	2.89E-05	5.26E-05
GC13B50-51CM	2.94E-05	5.34E-05
GC13B50-51CM	2.95E-05	5.36E-05
GC13B55-56CM	3.38E-05	6.15E-05
GC13B55-56CM	3.47E-05	6.31E-05
GC13B55-56CM	3.52E-05	6.40E-05
GC13B55-56CM	3.46E-05	6.29E-05
GC13B55-56CM	3.46E-05	6.29E-05
GC13B65-66CM	3.74E-05	6.80E-05
GC13B65-66CM	3.79E-05	6.89E-05
GC13B65-66CM	3.77E-05	6.85E-05
GC13B65-66CM	3.77E-05	6.86E-05
GC13B65-66CM	3.80E-05	6.92E-05
GC13B75-76CM	3.76E-05	6.84E-05
GC13B75-76CM	3.83E-05	6.97E-05
GC13B75-76CM	3.87E-05	7.03E-05
GC13B75-76CM	3.83E-05	6.96E-05
GC13B75-76CM	3.84E-05	6.98E-05
GC13B80-81CM	3.89E-05	7.08E-05
GC13B80-81CM	3.94E-05	7.16E-05
GC13B80-81CM	3.93E-05	7.14E-05
GC13B80-81CM	3.97E-05	7.22E-05
GC13B80-81CM	3.95E-05	7.18E-05
GC13B85-86CM	3.90E-05	7.10E-05
GC13B85-86CM	3.97E-05	7.21E-05
GC13B85-86CM	4.05E-05	7.36E-05
GC13B85-86CM	3.98E-05	7.24E-05
GC13B85-86CM	3.91E-05	7.11E-05
GC13B95-96CM	4.28E-05	7.78E-05
GC13B95-96CM	4.50E-05	8.18E-05
GC13B95-96CM	4.46E-05	8.11E-05
GC13B95-96CM	4.43E-05	8.06E-05
GC13B95-96CM	4.47E-05	8.13E-05
GC13B105-106	3.88E-05	7.05E-05
GC13B105-106	4.02E-05	7.31E-05
GC13B105-106	4.03E-05	7.32E-05
GC13B105-106	4.01E-05	7.29E-05
GC13B105-106	4.00E-05	7.28E-05
GC13B110-111	4.44E-05	8.07E-05
GC13B110-111	4.56E-05	8.28E-05
GC13B110-111	4.58E-05	8.33E-05

GC13B110-111	4.50E-05	8.19E-05
GC13B110-111	4.51E-05	8.20E-05
GC13B115-116	3.92E-05	7.12E-05
GC13B115-116	4.10E-05	7.46E-05
GC13B115-116	4.14E-05	7.52E-05
GC13B115-116	4.09E-05	7.43E-05
GC13B115-116	4.14E-05	7.52E-05
GC13B125-126	4.52E-05	8.22E-05
GC13B125-126	4.68E-05	8.51E-05
GC13B125-126	4.58E-05	8.33E-05
GC13B125-126	4.63E-05	8.42E-05
GC13B125-126	4.59E-05	8.35E-05
GC13B135-136	3.99E-05	7.26E-05
GC13B135-136	4.18E-05	7.59E-05
GC13B135-136	4.19E-05	7.62E-05
GC13B135-136	4.14E-05	7.53E-05
GC13B135-136	4.10E-05	7.45E-05
GC13B140-141	4.28E-05	7.79E-05
GC13B140-141	4.32E-05	7.85E-05
GC13B140-141	4.25E-05	7.73E-05
GC13B140-141	4.31E-05	7.84E-05
GC13B140-141	4.27E-05	7.77E-05
GC13B145-146	3.90E-05	7.09E-05
GC13B145-146	3.97E-05	7.22E-05
GC13B145-146	4.18E-05	7.59E-05
GC13B145-146	4.05E-05	7.37E-05
GC13B145-146	4.08E-05	7.42E-05
GC13B155-156	4.38E-05	7.96E-05
GC13B155-156	4.52E-05	8.22E-05
GC13B155-156	4.45E-05	8.08E-05
GC13B155-156	4.44E-05	8.07E-05
GC13B155-156	4.50E-05	8.19E-05
GC13B165-166	4.20E-05	7.64E-05
GC13B165-166	4.21E-05	7.65E-05
GC13B165-166	4.23E-05	7.68E-05
GC13B165-166	4.22E-05	7.68E-05
GC13B165-166	4.23E-05	7.69E-05
GC13B170-171	4.15E-05	7.55E-05
GC13B170-171	4.24E-05	7.72E-05
GC13B170-171	4.22E-05	7.67E-05
GC13B170-171	4.25E-05	7.72E-05
GC13B170-171	4.24E-05	7.71E-05
GC13B175-176	4.04E-05	7.34E-05

GC13B175-176	4.11E-05	7.47E-05
GC13B175-176	4.11E-05	7.47E-05
GC13B175-176	4.07E-05	7.40E-05
GC13B175-176	4.09E-05	7.43E-05
GC13B185-186	3.92E-05	7.13E-05
GC13B185-186	3.88E-05	7.06E-05
GC13B185-186	3.98E-05	7.24E-05
GC13B185-186	3.99E-05	7.26E-05
GC13B185-186	4.10E-05	7.45E-05
GC13B189-190	4.24E-05	7.71E-05
GC13B189-190	4.31E-05	7.83E-05
GC13B189-190	4.31E-05	7.84E-05
GC13B189-190	4.35E-05	7.91E-05
GC13B189-190	4.35E-05	7.91E-05

Appendix B.

X-ray fluorescence spectrometry data for 19 elements.

	Sum of conc. (%)	Al2O3 Al (%)	Br Br (ppm)	CaO Ca (%)	Cu Cu3 (ppm)	FeO Fe (%)	K2O K (%)	MgO Mg (%)	MnO Mn (%)	Na2O Na (%)	Ni Ni (ppm)	P2O5 P (%)	S S (%)	SiO2 Si (%)	TiO2 Ti (%)	Zn Zn (ppm)	Zr Zr4 (ppm)	Sr Sr (ppm)	Pb Pb (ppm)	As As (ppm)
TER16-GC15A 221-222CM	95.24	16.51	80.98	2.43	23.63	5.808	2.401	2.913	0.105	7.108	49.63	0.087	0.2	56.81	0.793	91.15	205.9	185.9	30.2	8.123
TER16-GC15A 205-206CM	97.33	16.16	76.55	2.332	21.47	5.897	2.367	2.838	0.12	10.54	51.03	0.089	0.198	55.92	0.801	93.43	206.1	181.7	31.32	8.775
TER16-GC15A 190-191CM	96.97	16.37	75.91	2.915	18.99	5.756	2.382	2.955	0.117	9.185	51.33	0.102	0.174	56.16	0.783	90.64	206.7	207.5	27.87	2.274
TER16-GC15A 175-176CM	95.52	16.64	77.53	2.76	19.81	5.739	2.425	2.994	0.091	6.698	49.22	0.085	0.149	57.08	0.797	92.32	206.4	190.7	32.35	10.15
TER16-GC15A 160-161CM	96.62	16.18	78.89	3.089	20.64	5.682	2.369	2.95	0.086	9.302	48.56	0.087	0.182	55.85	0.775	90.61	205.6	204.6	25.63	7.852
TER16-GC15A 145-146CM	97.13	15.93	82.85	3.081	20.6	5.615	2.341	2.924	0.08	10.32	48.98	0.085	0.18	55.73	0.777	90.01	205	205.9	29.44	9.737
TER16-GC15A 130-131CM	93.13	16.38	78.58	4.192	19.01	5.366	2.414	2.997	0.075	3.095	47.21	0.098	0.214	57.44	0.792	83.27	212.2	236.2	30.51	8.447
TER16-GC15A 115-116CM	93.4	14.6	64.6	8.143	7.363	3.856	2.094	2.966	0.055	2.425	33.89	0.119	0.17	58.22	0.668	58.58	234.2	357.5	19.5	6.823
TER16-GC15A 100-101CM	91.76	13.47	74.57	9.207	13.57	3.723	2.02	3.025	0.051	1.558	32.52	0.125	0.143	57.7	0.66	56.16	249.9	399.6	22.73	3.146
TER16-GC15A 85-86CM	92.07	12.9	72	9.188	14.84	3.342	1.883	2.961	0.046	1.924	30.54	0.127	0.15	58.83	0.636	49.78	265.1	382.9	21.6	2.577
TER16-GC15A 70-71CM	92.05	13.25	75.76	8.922	14.64	3.62	1.978	3.003	0.048	1.855	31.66	0.125	0.16	58.36	0.647	54.79	252.6	377.6	18.78	5.11
TER16-GC15A 55-56CM	91.47	12.75	75.76	9.22	13.58	3.346	1.891	2.899	0.045	1.812	29.63	0.124	0.132	58.54	0.633	49.59	263.9	381.8	15.94	6.603
TER16-GC15A 40-41CM	91.74	12.88	81.68	9.189	14.25	3.432	1.92	2.932	0.047	1.746	30.24	0.126	0.14	58.61	0.63	52.21	252	378.1	18.03	5.505
TER16-GC15A 26-27CM	91.64	12.75	98.12	9.111	14.88	3.281	1.889	2.917	0.047	2.044	27.71	0.13	0.132	58.64	0.62	50.36	259.3	371	16.13	5.731
TER16-GC13A 192-193CM	93.47	15.95	62.7	3.689	18.88	4.712	2.273	2.827	0.058	1.98	40.67	0.095	0.171	60.88	0.769	73.96	232.6	215.2	25.94	7.979
TER16-GC13A 183-184CM	93.98	15.58	55.63	3.869	18.38	4.439	2.197	2.736	0.053	1.712	40.65	0.098	0.182	62.29	0.757	67.98	250.1	223.1	22.83	7.977
TER16-GC13A 163-164CM	94.23	15.65	61.45	4.356	16.13	4.418	2.211	2.783	0.051	1.907	38.28	0.098	0.185	61.75	0.745	68.31	238.9	237.6	26.95	7.373
TER16-GC13A 148-149CM	93.61	15.49	57.81	4.498	17.97	4.409	2.206	2.752	0.052	1.841	38.56	0.1	0.151	61.29	0.749	66.63	236.8	241.6	28.41	1.505
TER16-GC13A 133-134CM	93.43	15.15	58.23	4.48	15.31	4.178	2.147	2.709	0.048	1.761	37.23	0.105	0.147	61.9	0.742	65.21	243.9	236.3	27.8	2.279
TER16-GC13A 118-119CM	92.63	14.83	62.69	4.942	17.55	4.01	2.124	2.74	0.047	1.616	35.42	0.103	0.213	61.21	0.72	58.19	253	251.7	24.01	7.634
TER16-GC13A 103-104CM	92.42	13.67	53.7	5.997	16.82	3.569	1.988	2.679	0.043	1.693	30.64	0.105	0.224	61.71	0.674	50.95	254.1	273.3	22.56	6.862
TER16-GC13A 88-89CM	90.58	12.47	50.6	6.369	14.64	3.111	1.831	2.488	0.039	1.544	26.95	0.109	0.195	61.72	0.636	41.31	266.5	308.3	18.95	6.506
TER16-GC13A 73-74CM	89.27	12.33	50.27	7.825	14.91	3.231	1.887	2.686	0.04	1.79	25.29	0.116	0.222	58.46	0.618	44.93	254.5	312.7	21.34	2.257
TER16-GC13A 58-59CM	90.07	13.11	58.18	7.852	14.4	3.583	2.049	2.816	0.045	1.523	29.31	0.122	0.245	57.99	0.669	52.14	253.3	315.1	20.88	4.391
TER16-GC13A 43-44CM	89.62	12.18	50.88	8.242	9.761	3.276	1.929	2.652	0.041	1.33	26.1	0.116	0.179	58.98	0.635	45.76	252.5	331.5	17.4	4.216
TER16-GC16B 210-211CM	94.14	17.23	49.16	0.179	19.07	3.818	1.96	1.483	0.015	1.344	36.29	0.057	1.052	66.05	0.906	56.15	266.7	79.41	34.02	4.457
TER16-GC16B 195-196CM	96.34	18.27	47.49	0.225	18.18	4.577	2.155	1.71	0.017	1.461	34.04	0.055	1.034	65.91	0.874	61.68	241.5	82.69	27.61	9.089
TER16-GC16B 180-181CM	94.69	17.38	46.16	0.32	16.01	4.589	2.304	1.774	0.022	1.349	34.26	0.068	0.629	65.31	0.889	63.67	245	90.76	32.37	5.869

TER16-GC16B 165-166CM	96.42	18.56	47.32	0.275	21.07	4.884	2.462	1.849	0.02	1.389	38.33	0.058	0.751	65.19	0.932	72.22	228.2	96.43	31.36	8.31
TER16-GC16B 150-151CM	97.83	18.94	50.14	0.311	20.39	5.209	2.493	1.988	0.026	1.859	39.14	0.061	0.465	65.48	0.931	75.64	222.7	99.43	30.27	9.64
TER16-GC16B 135-136CM	97.24	18.82	58.65	0.313	17.74	5.659	2.504	2.049	0.028	1.596	39.77	0.062	0.52	64.71	0.936	74.88	213.3	99.3	31.8	10.55
TER16-GC16B 120-121CM	97.09	18.6	53.23	0.292	19.11	5.69	2.554	2.049	0.03	1.55	41.03	0.063	0.455	64.79	0.967	79.17	215.2	99.14	40.83	10.71
TER16-GC16B 105-106CM	96.96	18.46	55.83	0.333	15.43	5.796	2.557	2.079	0.031	1.395	40.33	0.069	0.492	64.75	0.948	76.95	213.3	102	35.23	5.61
TER16-GC16B 90-91CM	95.72	17.67	55.96	0.644	17.53	5.954	2.534	2.045	0.034	1.349	38.74	0.271	0.474	63.75	0.933	76.11	213.9	116.1	30.9	8.322
TER16-GC16B 75-76CM	96.93	18.07	55.46	0.353	17.45	5.563	2.539	2.119	0.031	1.776	39.58	0.064	0.409	65.02	0.934	77.92	216	102.4	28.92	10.5
TER16-GC16B 60-61CM	97.59	18.38	62.94	0.27	18.14	5.422	2.577	2.186	0.03	1.81	39.8	0.061	0.421	65.44	0.936	78.43	216	100.6	32.28	11.31
TER16-GC16B 46-47CM	95.81	16.92	62.15	1.724	15.45	4.88	2.469	2.155	0.033	1.411	34.73	0.064	0.437	64.79	0.866	67.36	218.1	175.6	29.84	11.01
TER16-GC13B-185-186CM	96.68	17.17	55.3	3.398	23.23	4.681	2.461	3.944	0.069	1.548	40.14	0.074	0.553	61.92	0.786	76.14	219.5	257	25.85	10.73
TER16-GC13B-170-171CM	97.28	17.01	63.51	3.818	14.96	4.557	2.436	3.944	0.068	1.618	40.22	0.087	0.582	62.31	0.768	73.44	222.8	327.7	28.7	10.52
TER16-GC13B-155-156CM	96.81	17	61.05	3.216	17.93	4.653	2.453	3.92	0.068	1.709	39.18	0.078	0.57	62.3	0.781	76.5	218.3	244.7	20.63	10.38
TER16-GC13B-140-141CM	96.92	17	63.43	3.062	15.68	4.622	2.437	3.953	0.065	1.601	38.24	0.082	0.583	62.67	0.784	73.43	220	210.4	28.42	6.699
TER16-GC13B-125-126CM	97.08	17.17	63.48	3.053	15.76	4.677	2.446	4.019	0.066	1.597	39.73	0.079	0.598	62.53	0.785	75.74	218	211.1	25.27	7.786
TER16-GC13B-110-111CM	97.19	16.93	69.33	3.249	15.5	4.572	2.407	4.03	0.064	2.133	38.47	0.084	0.563	62.32	0.776	74.83	218.1	222.6	22.29	7.126
TER16-GC13B-95-96CM	98.26	17.43	65.35	3.256	13.32	4.622	2.45	4.139	0.062	2.207	39.9	0.083	0.568	62.6	0.781	75.25	218.2	220.8	20.55	9.139
TER16-GC13B-80-81CM	97.1	17.18	71.09	3.403	17.56	4.818	2.498	4.111	0.064	2.657	40.95	0.09	0.662	60.73	0.808	76.17	218.5	235.8	21.78	7.972
TER16-GC13B-65-66CM	97.76	16.53	62.57	3.733	15.45	4.303	2.32	3.948	0.057	2.544	35.43	0.085	0.609	62.81	0.757	66.34	224.8	233.4	25.81	7.709
TER16-GC13B-50-51CM	91.41	9.906	47.82	13.29	8.882	2.297	1.528	2.625	0.034	1.743	14.45	0.127	0.334	58.94	0.498	22.61	235.1	507.8	12.42	5.37
TER16-GC13B-36-37CM	88.55	10.48	59.6	10.69	14.72	2.598	1.698	2.495	0.035	1.651	19.17	0.136	0.177	57.96	0.552	32.64	253.1	409.6	15.24	4.019
TER16-GC12B-181-182CM	94.88	17.29	67.39	3.328	17.6	5.308	2.587	2.995	0.074	1.387	44.07	0.105	0.175	60.74	0.824	83.51	210	200	23.69	6.237
TER16-GC12B 167-168CM	95.63	17.18	62.46	3.537	20.68	5.16	2.535	2.951	0.067	1.569	43.47	0.105	0.188	61.45	0.815	80.76	213.8	204.2	28.03	6.11
TER16-GC12B 152-153CM	95.23	16.41	82.28	4.539	17.4	4.614	2.401	3.009	0.059	1.775	38.69	0.105	0.185	61.3	0.768	69.93	223.4	227.8	30.01	5.151
TER16-GC12B 137-138CM	93.44	13.33	53.09	8.813	11.05	3.227	1.982	2.758	0.046	1.664	25.59	0.126	0.217	60.56	0.637	45.11	244.9	357.7	18.7	4.398
TER16-GC12B 122-123CM	93.3	12.83	54.56	9.258	15.06	3.046	1.909	2.799	0.043	1.638	23.59	0.131	0.223	60.74	0.612	41.8	250.3	366.8	16.95	4.751
TER16-GC12B 107-108CM	93.7	13.41	58.29	8.922	13.56	3.403	2.033	2.925	0.045	1.374	28.34	0.129	0.239	60.5	0.648	48.78	244.8	350.5	18.33	11.23
TER16-GC12B 92-93CM	94.37	13.9	57.06	9.447	12.82	3.449	2.082	3.065	0.047	1.391	27.54	0.13	0.205	59.93	0.644	50.47	241.2	369.2	19.93	4.976
TER16-GC12B 77-78CM	92.52	12.39	55.58	8.989	13.31	2.958	1.874	2.792	0.039	1.507	23.14	0.12	0.192	60.97	0.612	41.46	254.5	346	13.21	4.807
TER16-GC12B 62-63CM	90.68	12.23	58.92	9.463	13.95	3.121	1.924	2.785	0.041	1.571	25.5	0.124	0.207	58.52	0.62	43.63	250.9	352.1	23.94	1.492
TER16-GC12B 48-49CM	90.54	10.31	50.54	9.347	14.86	2.435	1.611	2.434	0.032	1.609	18.92	0.117	0.157	61.86	0.55	31.66	270.7	343.9	12.25	8.651
TER16-GC14B 134-135CM	93.42	15	88.64	0.514	18.59	3.912	2.159	2.4	0.043	3.843	29.59	0.054	1.341	63.32	0.775	57.65	236.8	109.4	28.86	12.54

TER16-GC14B 130-131CM	93.39	14.33	78.36	0.711	18.64	3.667	2.013	2.309	0.041	3.178	29.54	0.056	1.378	64.89	0.759	53.07	254.4	113.8	24.69	9.91
TER16-GC14B 115-116CM	91.98	15.07	86.33	0.569	22.61	4.218	2.156	2.418	0.047	2.362	33.31	0.055	1.602	62.6	0.823	60.6	241.2	109.7	31.56	9.806
TER16-GC14B 100-101CM	90.67	14.3	104.3	0.526	18.27	3.981	2.051	2.353	0.046	2.472	31.52	0.053	1.597	62.41	0.821	54.02	265.5	108	23.32	11.31
TER16-GC14B 85-86CM	91.33	13.63	92.63	0.521	18.12	3.537	1.843	2.164	0.039	2.497	28.19	0.048	1.666	64.57	0.764	47.68	255.7	105.2	24.83	9.907
TER16-GC14B 70-71CM	89.68	12.72	70.64	0.722	15.9	3.262	1.732	2.046	0.033	1.9	26.11	0.049	1.47	64.9	0.782	39.42	306.3	105.8	20.9	11.01
TER16-GC14B 55-56CM	87.36	11.78	89.28	0.732	17.33	3.087	1.524	1.985	0.028	1.989	22.86	0.046	1.762	63.63	0.73	35.34	299	103.9	25.2	10.05
TER16-GC14B 40-41CM	84.92	7.947	41.63	10.07	10.39	2.024	1.326	1.942	0.024	1.421	13.29	0.134	0.277	59.19	0.492	18.02	297.2	421.2	6.22	6.351
TER16-GC14B 26-27CM	85.83	8.339	46.41	11.9	10.3	2.09	1.411	2.168	0.026	1.71	13.22	0.109	0.23	57.29	0.467	20.27	261.3	419.8	19.49	1.539

Appendix C.

Foraminiferal data for core samples collected in this study.

Species	TER16-GC15A 26-27	TER16-GC15A 45-46	TER16-GC15A 65-66	TER16-GC15A 85-86	TER16-GC15A 105-106	TER16-GC15A 125-126	TER16-GC15A 145-146	TER16-GC15A 165-166	TER16-GC15A 185-186	TER16-GC15A 205-206	TER16-GC15A 221-222	TER16-GC14B 26-27	TER16-GC14B 45-46	TER16-GC14B 65-66	TER16-GC14B 85-86	TER16-GC14B 105-106	TER16-GC14B 125-126	TER16-GC14B 134-135	TER16-GC13B 36-37	TER16-GC13B 55-56	TER16-GC13B 75-76	TER16-GC13B 95-96	TER16-GC13B 115-116	TER16-GC13B 135-136	TER16-GC13B 155-156	TER16-GC13B 175-176	TER16-GC13B 189-190	TER16-GC13A 43-44	TER16-GC13A 63-64	TER16-GC13A 83-84	TER16-GC13A 103-104
Adelosina bicornis																															
Adelosina laevigata				1											1																
Adelosina littoralis		1	1	2	3	5	6	4	1	3		1	1	1					1		3	3	2			3		3			4
Agglutinella agglutinans	4	7	5	5	8	11	8	6	4	8	5	4	6	4	1		1	4	10	7	3	2	5	2	2	4	15	11	14	12	8
Agglutinella arenata																			1												
Alassoida virgula								1	1										1	1									1		
Alliatina variabilis																												1			
Alliatinella differens	1																			1											
Ammobaculites reophaciformis	1		1											1							1							1			
Ammobaculites sp.																															
Ammonia cf. *A. takanabensis*			1		2	8			2	1	2		1	4						1	1			2		2					
Ammonia convexa	4		1	1		1	2	3	2	1	2	7	1			1	2	1	3	4	2	2	1	2	1	3	2	1	2	3	2
Ammonia sp.																			1	3											
Ammonia supera	10	10	9	7	9		16	24	12	14	5	7	7	3		3	4	3	17	3	8	12	18	11	19	13	7	7	8	10	6
Ammonia tepida										1	1	1		4		1		3					1		1	1					
Amphicoryna sublineata												2																			
Anomalinoides globulosus																			1							1					
Articulina alticostata																												3			
Articulina mayori																									1						
Assiliina ammonoides												25	13	1	1	1	9	1	1					1				2			
Asterorotalia gaimardi	7	19	17	11	12	4		10	6	12	14	1	7			1	3	2	14	15	17	12	11	5	14	19	20	10	7	14	13
Asterorotalia milletti	4	3	2	3	1	5	4	5	5	2		23	2	12				5		1		5	1	4	3	5	1	1	12		
Asterorotalia pulchella									1				10	52	28	14	3	63					2		1	2	4				
Astrononion novozealandium	2	2	2	1		1			1										1												
Astrononion stelligerum																															
Bigenerina nodosaria	2	3	7	5	3	9	10	4	10	10	5	8	3	5				4	4	15	6		7	11	12	6	3	8	4	5	4
Biloculinella inflata																						1							1		
Biloculinella lunata		1																													
Bolivina sabahensis		1	1	1			3		1		1								1	1	1		1		1	1			4	1
Bolivina striatula												2													2						
Bolivina vadescens						1			1		1	2							4												
Bombulina echinata				1					1	1												1	1	3	2		2				
Bulimina marginata		1			1																								1		
Cancris auriculus	1	1	4	5		1	1	8	3	16	5								2	1	1	1	5	1	5	1	3		2	1	2
Caribeanella philippinensis	3																														
Cassidelina subcapitata				2		2				1	1					1					1										
Cavarotalia annectens													2		1				2										1		
Cellanthus craticulatus																		1	1		4										
Cibicides refulgens																	2														
Cibicides sp.	1	5			2									1			1					8	1					1			1
Cornuspira planorbis				1																										1	
Cornuspira sp.							1																						1		
Cribroelphidium cf. *C. detense*													1	6																	
Cylindroclavulina bradyi	11	2	10	16	11	35	21	6	25	7	5	7	3		1				6	12	12	8	7	7	13	4	17	6	11	5	7
Cymbaloporetta squammosa		2																													
Discorbea candeiana	1	5	3		2	1				1	1	8										1	1	1	2	2	1		4	1	4
Discorbea sp.																			3												
Discorbinella bertheloti									2	2							1														
Discorbinella bodjongensis	2			1	3	1							1				1		6		1	1	3	1	3	4		3			
Edentostomina cultrata																							2	3						1	1
Edentostomina milletti																			1												
Ehrenbergina undulata											1																				
Elphidium cf. *E. advenum*			2	1	2	4	8	2		1					1			7			3	3	1	6	3		2	1	3	2	3
Elphidium cf. *E. neosimplex*														2																	
Elphidium crispum																	1														
Elphidium indicum										3			3			3				1		1	2	5	3	1	4			2	

Species	TER16-GC13A 123-124	TER16-GC13A 143-144	TER16-GC13A 163-164	TER16-GC13A 183-184	TER16-GC13A 192-193	TER16-GC12B 48-49	TER16-GC12B 67-68	TER16-GC12B 87-88	TER16-GC12B 107-108	TER16-GC12B 127-128	TER16-GC12B 147-148	TER16-GC12B 167-168	TER16-GC12B 181-182	TER16-GC16B 46-47	TER16-GC16B 65-66	TER16-GC16B 85-86	TER16-GC16B 105-106	TER16-GC16B 126-126	TER16-GC16B 145-146	TER16-GC16B 165-166	TER16-GC16B 185-186	TER16-GC16B 205-206	TER16-GC16B 213-214
Adelosina bicornis																							1
Adelosina laevigata																							
Adelosina littoralis	2	2	1	5	3	1			2	3	1	4				1							
Agglutinella agglutinans	4	8	8	7	1	12	9	15	8	7		4	20	7	18	5	2	4					14
Agglutinella arenata																							
Alassoida virgula	1			1	3							1											
Alliatina variabilis			1								1	1											
Alliatinella differens				1								1											
Ammobaculites reophaciformis									1						2								
Ammobaculites sp.																							1
Ammonia cf. *A. takanabensis*	1	4		7									1										
Ammonia convexa		2	1	5	3	2	1	7	3	3	3	4	2	2	1								1
Ammonia sp.																1					1		
Ammonia supera	10	9	9	15	15	8	9	2	9	9	9	22	11	9	12	1							2
Ammonia tepida													1		1	4	2	10	11	30	127	1	
Amphicoryna sublineata																							
Anomalinoides globulosus							1					1											
Articulina alticostata																							
Articulina mayori					3																		
Assiliina ammonoides														6	2		2						3
Asterorotalia gaimardi	11	12	16	9			7	3	15	3	8			11	14		1	1					8
Asterorotalia milletti		2	8	4	3	15	9	6	4	8	7	6	5	3	3								
Asterorotalia pulchella															1	10	4	11					1
Astrononion novozealandium								1															
Astrononion stelligerum	1	1																					
Bigenerina nodosaria	3	3	8	7	5	9	8	9	9	6	5	7	1	10	3	1	2						10
Biloculinella inflata	1																						
Biloculinella lunata																							
Bolivina sabahensis	4			1	1		1	1	2	2	2	3		1									
Bolivina striatula																							
Bolivina vadescens							1		1														
Bombulina echinata	1	1	1																				
Bulimina marginata						1			2	2	1												
Cancris auriculus	4		1	6	5	1		3	2	2	2	5	4		2								
Caribeanella philippinensis			1						1														
Cassidelina subcapitata	2	1					1			1	1	3											
Cavarotalia annectens																1							
Cellanthus craticulatus															1	1							
Cibicides refulgens				1				1		1	1												
Cibicides sp.		4			1		1							2	2								
Cornuspira planorbis																							
Cornuspira sp.																							
Cribroelphidium cf. *C. detense*															1	16							
Cylindroclavulina bradyi	7	11	15	8	8	19	22	22	18	8	4	7	7	5	2								5
Cymbaloporetta squammosa																							
Discorbea candeiana	12	1	3	1	2				2	3	2	1	2										
Discorbea sp.																							
Discorbinella bertheloti								1															
Discorbinella bodjongensis						5								2	5		1						
Edentostomina cultrata	2	1	2	1																			
Edentostomina milletti																							
Ehrenbergina undulata																							
Elphidium cf. *E. advenum*	1	2	3	3	5		1	2		4	2	7	1		6		1						3
Elphidium cf. *E. neosimplex*																							
Elphidium crispum						1																	
Elphidium indicum		1		7							1					1							

Species	TER16-GC15A 26-27	TER16-GC15A 45-46	TER16-GC15A 65-66	TER16-GC15A 85-86	TER16-GC15A 105-106	TER16-GC15A 125-126	TER16-GC15A 145-146	TER16-GC15A 165-166	TER16-GC15A 185-186	TER16-GC15A 205-206	TER16-GC15A 221-222	TER16-GC14B 26-27	TER16-GC14B 45-46	TER16-GC14B 65-66	TER16-GC14B 85-86	TER16-GC14B 105-106	TER16-GC14B 125-126	TER16-GC14B 134-135	TER16-GC13B 36-37	TER16-GC13B 55-56	TER16-GC13B 75-76	TER16-GC13B 95-96	TER16-GC13B 115-116	TER16-GC13B 135-136	TER16-GC13B 155-156	TER16-GC13B 175-176	TER16-GC13B 189-190	TER16-GC13A 43-44	TER16-GC13A 63-64	TER16-GC13A 83-84	TER16-GC13A 103-104
Elphidium jensoni													1	2		2	1				1				1	1					
Elphidium macellum																															
Elphidium sp.																							1								
Eponides repandus	1	3	1	2		2	1	2	1			1	4	3						1	5	3	4	1		1	1	3	2	1	1
Exsculptina glaphyraheda																								1							1
Facetocochlea pulchra			1				1							2					1									1			
Favulina melosquammosa																															
Gavelinopsis praegeri																							1								
Geminospria bradyi					1																										
Glandulina antarctica																															
Glandulina laevigata				1																											
Glandulina symmetrica	1	1						1	1		1										1				1					1	1
Globulina sp.																														1	
Hanzawaia grossepunctata		3								2	1																				
Hanzawaia nipponica	8	8	8	8	11	17	28	32	23	26	31	29	10	1	4	2	5	1	10	19	12	14	30	25	23	28	40	8	6	4	2
Hanzawaia sp.																					1										
Heterolepa dutemplei	41	45	49	49	58	45	30	39	25	33	24	36	41	17	2	5	9	7	27	57	33	26	13	31	27	32	28	53	33	58	32
Heterolepa praecincta				2											3		1			1	1						1				
Heterolepa subhaidingeri			1												2				3				1								
Hyalinea florenceae				1																											
Hyalinonetrion distomapolitum													1						1						1						1
Lachlanella compressiostoma																														1	
Laevidentalina antarctica						1				1				1							1		1		1						1
Laevidentalina bradyensis			1																												
Laevidentalina inflexa			1																								1				1
Lagena crenata		1																													
Lagena dorbignyi			1																												
Lagena semistriata																													1		
Lagena spicata			1																							1					
Lagena substriata	3		2		1	1	1						1								1		1				1	1			
Lagenosolenia bradyiformata																													2		
Lenticulina calcar																				1	1										
Lenticulina sp.												1	1																		
Lobatula lobatula												1		1					2	1											
Massilina cf. *M. planata*												3	1			1	3		1						1					1	1
Massilina granulocostata	1					1														2									1		
Melonis affinis												1																			
Miliolinella philippinensis																															1
Millettiana millettii						1		3		1	3											4	1	4	1	1				2	
Neoponides bradyi				1	1															1								2	1	1	
Nonion asanoi																						1									
Nonion sp.																													2		
Nonion subturgidium	2	2		1					1	2			2							2						1	1		1		
Nonionoides grateloupi		1																			2								1		
Nubeculina divaricata	5		1	2		3		1					3	4					1			1		1				1		8	8
Nummulites venosus																		1													
Paracibicides edomica	10	16	19	16	7			2	1									1	1	3	7	5		4	2	5		8		2	2
Parafissurina sp. A	1																														
Parrellina hispidula							1					5	4	1	1	1	1	3	1			4	5	2	3		2				
Planispirinella exigua										1		5	2					1				4	7	3	6	3	2			1	1
Proemassilina arenaria	8	10	6	5	4	5	6	3	3	1	4	1	2	1	1				1	3	4	1		2	3	4		9	1	3	6
Pseudoeponides japonicus																															
Pseudogaudriaina pacifica		3	2	2									2						3		1							4	2	4	3
Pseudorotalia indopacifica	1	2	4		5	15	8	3	9	6	1	4	2			2	1	2	7	7	4	9	5	6	8	1	6	8	5	4	1
Pseudorotalia schroeteriana			1	1	1	4		1		5	1	11	4		3	2	3		7	2	2	1	1	2	2	6	1	1	3	1	1
Pseudorotalia sp.										2																					
Pseudotriloculina lunata											1																2				
Pygmaeoseistron islandium		1		2	1		1				1						1								1				1		
Pyramidulina catesbiyi																												1		1	

Species	TER16-GC13A 123-124	TER16-GC13A 143-144	TER16-GC13A 163-164	TER16-GC13A 183-184	TER16-GC13A 192-193	TER16-GC12B 48-49	TER16-GC12B 67-68	TER16-GC12B 87-88	TER16-GC12B 107-108	TER16-GC12B 127-128	TER16-GC12B 147-148	TER16-GC12B 167-168	TER16-GC12B 181-182	TER16-GC16B 46-47	TER16-GC16B 65-66	TER16-GC16B 85-86	TER16-GC16B 105-106	TER16-GC16B 126-126	TER16-GC16B 145-146	TER16-GC16B 165-166	TER16-GC16B 185-186	TER16-GC16B 205-206	TER16-GC16B 213-214
Elphidium jensoni				1																			
Elphidium macellum		1																					
Elphidium sp.														7			1	1			1		
Eponides repandus	1		1	2		1	1		1	2	2	3	1	2	3								
Exsculptina glaphyraheda																							
Facetocochlea pulchra															1	1							
Favulina melosquammosa												1											
Gavelinopsis praegeri																							
Geminospria bradyi				1																			
Glandulina antarctica												1											
Glandulina laevigata																							
Glandulina symmetrica				2					1		1	2											
Globulina sp.																							
Hanzawaia grossepunctata																							
Hanzawaia nipponica	2	2	7	10	18	28	18	3	6	6	13	33	19	10	13		1						7
Hanzawaia sp.																							
Heterolepa dutemplei	33	34	32	50	30	45	41	33	3	38	45	35	20	50	48	2	6				1		23
Heterolepa praecincta															1								
Heterolepa subhaidingeri	1							1															1
Hyalinea florenceae										1													
Hyalinonetrion distomapolitum				2	2			1															
Lachlanella compressiostoma		1		1																			
Laevidentalina antarctica	1			1	1	1					1												
Laevidentalina bradyensis	1					1																	
Laevidentalina inflexa		1	1												1								
Lagena crenata																							
Lagena dorbignyi				1																			
Lagena semistriata																							
Lagena spicata																							
Lagena substriata	2	2		1		1	1			2	1		1	1									
Lagenosolenia bradyiformata																							
Lenticulina calcar																							1
Lenticulina sp.																							
Lobatula lobatula															1								10
Massilina cf. *M. planata*	1				2										1								
Massilina granulocostata																							
Melonis affinis																							
Miliolinella philippinensis																							
Millettiana millettii	2	2		3						1													
Neoponides bradyi			1				1	2															1
Nonion asanoi							1		1	1	1												1
Nonion sp.																							
Nonion subturgidium																							
Nonionoides grateloupi													1										
Nubeculina divaricata	1	10	10	11		1	4	2	3	12	4			3	2								
Nummulites venosus																							
Paracibicides edomica	4					2	1							8	5		2	1					1
Parafissurina sp. A																							
Parrellina hispidula				2	1										1		3						
Planispirinella exigua	4	4	2	10	4											1							1
Proemassilina arenaria	2	2	9	3	3	5	1	3	2	5	6	4	5	4	5								2
Pseudoeponides japonicus																1							
Pseudogaudriaina pacifica			2					2	3	3	2			1	1								
Pseudorotalia indopacifica	4	3	5	3	2	9	6	9	5	3	3	2	2	6	3		2						
Pseudorotalia schroeteriana	1	1	4	3	1	4		4	5	5	2	1		2	5								4
Pseudorotalia sp.																							
Pseudotriloculina lunata																							
Pygmaeoseistron islandium		2			1	1					1	1	1	1									
Pyramidulina catesbiyi																							

Species	TER16-GC15A 26-27	TER16-GC15A 45-46	TER16-GC15A 65-66	TER16-GC15A 85-86	TER16-GC15A 105-106	TER16-GC15A 125-126	TER16-GC15A 145-146	TER16-GC15A 165-166	TER16-GC15A 185-186	TER16-GC15A 205-206	TER16-GC15A 221-222	TER16-GC14B 26-27	TER16-GC14B 45-46	TER16-GC14B 65-66	TER16-GC14B 85-86	TER16-GC14B 105-106	TER16-GC14B 125-126	TER16-GC14B 134-135	TER16-GC13B 36-37	TER16-GC13B 55-56	TER16-GC13B 75-76	TER16-GC13B 95-96	TER16-GC13B 115-116	TER16-GC13B 135-136	TER16-GC13B 155-156	TER16-GC13B 175-176	TER16-GC13B 189-190	TER16-GC13A 43-44	TER16-GC13A 63-64	TER16-GC13A 83-84	TER16-GC13A 103-104
Pyramidulina cf. *P. luzonensis*				1																										1
Pyrgo pisum																													1	
Pyrgo sarsi	1			1																							1	1		
Pyrgo sp.																														
Pyrgoella sp.							1																							
Pyrgoella tenuiaperta		1	1						1	2	6										2		4		1		1			3
Quinqueloculina bubnanensis								1																						
Quinqueloculina cf. *Q. bubnanensis*																														
Quinqueloculina cf. *Q. crassicarinata*																														
Quinqueloculina cf. *Q. quinquecarinata*												4																		
Quinqueloculina adiazeta				2		7	3			3		3		2			1		3			3	1				2		1		1
Quinqueloculina bicarinata		4		1	2	1			1	1		3						2	2	1		1					3	1			3
Quinqueloculina cf. *Q. philippinensis*							4																							
Quinqueloculina cf. *Q. schwantzi*																		1												
Quinqueloculina columnosa		1		1				4	3				1									1		1	2	5	1	1		1	1
Quinqueloculina crassicarinata						2	1						1							5											
Quinqueloculina fichteliana			1	1								3	1	1	1					1				1						
Quinqueloculina incisa	15	16	17	14	15	7	17	12	18	8	12	5	4	2				1	13	8	7	16	25	20	22	21	11	19	18	17	17
Quinqueloculina laevigata	1	1	1	4		3	6	1	4	1	2		1	1					5		8	2	4	7	3	3	2	1	2	1	1
Quinqueloculina lamarckiana		1		1	1	1	1	5	2	6	1	4	1	1				1		1	2	1		1			1			4	4
Quinqueloculina latidentella						1	1			1													1								2
Quinqueloculina parvaggluta	1		2	3	2		1			1	1		1		1						4	1		1	1	2		3		5	5
Quinqueloculina philippinensis	4	3	1	4	5	8		2	1	6	5	2	1	2	1		1	2	3	9	2	4	6	4	5	1	1	3	6		3
Quinqueloculina quinquecarinata												2										1			1			1		1	
Quinqueloculina schwantzi		1	1					1	1		1		1								1										
Quinqueloculina sp.		4	3	6	4	2	3		2	3		12	6	9			3	1	10	2	6	1				1	4	1	6	2	
Quinqueloculina sp. A																															
Reophax bradyi																															
Reophax scorpiurus																		3													
Reophax sp.				1		4									2				2	2		1						1			5
Reussella pulchra										1			1									1	2						1		
Reussella spinulosa	2	1		1			2	2	3		2	9	3	2		1			2	1	3	7	10	5	8	3	9	1	3		5
Rosalina sp.																															
Sahulia barkeri		1							1	1																				1	
Sahulia conica	2													1						1											
Scutuloris sp.			1					1																							
Sigmoilopsis schlumbergeri																1															
Siphonina bradyana												1						1										1			
Spiroloculina communis	4	3	4	1	1	1			2	2									1		1	1	2		2	2	3	4	1		1
Spiroloculina depressa		1		7																											1
Spiroloculina manifesta		3																													
Spiroloculina scrobiculata		1							1											1			2	1							1
Spirophthalmidium concava	1		5	2									1											2				1			
Spirosigmoilina pusilla												1																			
Spirotextularia fistulosa				3	3	2	1	3			3		1							1		2	2	5	4			3	2		
Spirotextularia floridana	3	3	3	9	6	5	5	4			2	4	1	3					1	8		4		3	1	1		1	5	6	5
Textularia agglutinans							1																								
Textularia fistulosa																											2	1			
Textularia haueri		5		9	5	11	2	16	36	15	4	9	5	17	2	4	2		13	2	3	19	22	20	20	23	2	4	13	3	7
Textularia sp.		1								1																					
Textularia sp. A	16	15	22	28	33	33	30	53	23	38	24	13	20	14		5		11	41	73	39	1	31	13	32	34	20	57	27	50	25
Textulina subplanoides																				1											
Triloculina cf. *T. pentagonalis*																															2
Triloculina sp.																															2
Triloculina tricarinata	3	9	5	7	4	11	22	20	12	20	17						1	2	1	2	10	5	23	14	7	20	12	3	4	4	6
Triloculina trigonula							3				3		1	1											1	1					
Triloculinella cf. *T. pseudooblonga*										2																					
Triloculinella chiastocytis			2					1	2													1									
Triloculinella pilasensis																															
Triloculinella pseudooblonga	1			1	1		1	5		2											4	3	6	1	3	1	1		1	1	2
Valvulinaria minuta																															
Total no. benthics	190	234	234	265	231	283	262	291	255	278	200	271	193	185	57	51	61	135	244	285	233	210	284	246	282	274	243	259	230	254	223
Total no. planktonics	58	78	35	53	31	32	10	13	5	4	3	45	27	15	2	4	10	1	41	39	14	15	7	6	5	13	6	29	32	22	39
Total no. specimens	248	312	269	318	262	315	272	304	260	282	203	316	220	200	59	55	71	136	285	324	247	225	291	252	287	287	249	288	262	276	262

Species	TER16-GC13A 123-124	TER16-GC13A 143-144	TER16-GC13A 163-164	TER16-GC13A 183-184	TER16-GC13A 192-193	TER16-GC12B 48-49	TER16-GC12B 67-68	TER16-GC12B 87-88	TER16-GC12B 107-108	TER16-GC12B 127-128	TER16-GC12B 147-148	TER16-GC12B 167-168	TER16-GC12B 181-182	TER16-GC16B 46-47	TER16-GC16B 65-66	TER16-GC16B 85-86	TER16-GC16B 105-106	TER16-GC16B 126-126	TER16-GC16B 145-146	TER16-GC16B 165-166	TER16-GC16B 185-186	TER16-GC16B 205-206	TER16-GC16B 213-214
Pyramidulina cf. *P. luzonensis*								1			1												
Pyrgo pisum																							
Pyrgo sarsi																							
Pyrgo sp.		1																					
Pyrgoella sp.						1																	
Pyrgoella tenuiaperta	5	5	4		4		1		2				3										
Quinqueloculina bubnanensis																							
Quinqueloculina cf. *Q. bubnanensis*											1	1											
Quinqueloculina cf. *Q. crassicarinata*												1											
Quinqueloculina cf. *Q. quinquecarinata*																							
Quinqueloculina adiazeta			1	2				2			4			3	1							1	1
Quinqueloculina bicarinata			6	2	3			2		1		1		1	1								1
Quinqueloculina cf. *Q. philippinensis*																							
Quinqueloculina cf. *Q. schwantzi*																							
Quinqueloculina columnosa	4	2	1	4																			
Quinqueloculina crassicarinata						3	6				1												
Quinqueloculina fichteliana	1						2		1														2
Quinqueloculina incisa	21	26	12	26	14	7	12	13	16	11	11	34	10	7	1	1							9
Quinqueloculina laevigata	4	1		5			3	5		4	5	3			3	1							
Quinqueloculina lamarckiana	2	1	1	1				1	3	2	4			2									
Quinqueloculina latidentella	3	1										2											
Quinqueloculina parvaggluta	3	1	4	4					1		2				10								
Quinqueloculina philippinensis	1	3	4	3		1	5	9	8	3	1			5	2								5
Quinqueloculina quinquecarinata		1		2										1									
Quinqueloculina schwantzi		2	1						1														
Quinqueloculina sp.						2		1	8	7	1	3		1	8								1
Quinqueloculina sp. A													3										
Reophax bradyi					2																		
Reophax scorpiurus																							
Reophax sp.			2			1				1	2	1		1									
Reussella pulchra						2								2									
Reussella spinulosa	6	11	6	12	16	3			1	2	1	3	6		5								1
Rosalina sp.						1																	
Sahulia barkeri															1								
Sahulia conica		1						1															1
Scutuloris sp.																							
Sigmoilopsis schlumbergeri																							
Siphonina bradyana																							
Spiroloculina communis	4		3	2	1	3	5		3	4	1	1		4	6								1
Spiroloculina depressa				1																			
Spiroloculina manifesta																							
Spiroloculina scrobiculata			1	2	1					1			1										
Spirophthalmidium concava							1	2			2												
Spirosigmoilina pusilla																							
Spirotextularia fistulosa	3		1	3	10			2			2	2	5	1									2
Spirotextularia floridana	2	2	5	4	1	4	6	8	5	4	7	3	1	3	8								5
Textularia agglutinans													1										
Textularia fistulosa																							
Textularia haueri	8	42	1	29	9		5	7	3	16	10	18		7	11	3		1	1				16
Textularia sp.										1													1
Textularia sp. A	30	11	33	6	32	35	32	29	39	37	25	14	18	44	54	3	3						52
Textulina subplanoides									1														
Triloculina cf. *T. pentagonalis*			1																				
Triloculina sp.					1				1														
Triloculina tricarinata	24	2	9	15	9	3	2	3	2	3	4	16	19		1								
Triloculina trigonula	2	3		3							7				1								
Triloculinella cf. *T. pseudooblonga*																							
Triloculinella chiastocytis		1							1														
Triloculinella pilasensis										1	1												
Triloculinella pseudooblonga	3	3		2									1		1								
Valvulinaria minuta					1																		
Total no. benthics	253	250	248	324	227	239	227	218	205	239	225	263	173	235	281	55	33	29	12	30	130	2	199
Total no. planktonics	26	16	22	15	9	35	31	40	46	48	43	11	11	22	19	7	4	0	0	0	0	0	12
Total no. specimens	279	266	270	339	236	274	258	258	251	287	268	274	184	257	300	62	37	29	12	30	130	2	211

Appendix D.

List of standards used in XRF calibration.

STANDARD ID	Description	Distributor
1633	Coal fly ash	NIST
1633a	Coal fly ash	NIST
1646a	Estuarine sediment	NIST
2702	Inorganics in marine sediment	NIST
2704	River sediment	NIST
6103-91	Quartz diorite	BSCI
98a	Plastic clay	NIST
AGV-2	Andesite standard	USGS
CGL-011	CGL diorite	BSCI
GSP-2	Granodiorite standard	USGS
MAG-1	Marine sediment	USGS
MRG-1	Not available	CCRMP
DC71302	China standard diorite	BSCI
NIM-L	Lujavrite	MINTEK
NIM-N	Norite	MINTEK
NIM-P	Pyroxenite	MINTEK
NIM-S	Syenite	MINTEK
NIM-G	Granite	MINTEK
USGS SCO-1	Cody shale	USGS
SY-2	Syenite	CCRMP
SY-3	Syenite	CCRMP